AN ENERGY-BASED DAMPING EVALUATION USING BAYESIAN MODEL UPDATING FOR VIBRATION-BASED STRUCTURAL HEALTH MONITORING OF STEEL TRUSS BRIDGES

（鋼トラス橋ヘルスモニタリングのためのベイズ推定による モデルアップデートを利用したエネルギー的振動減衰評価法）

2017 年 3 月

埼玉大学大学院理工学研究科（博士後期課程）

理工学専攻（主指導教員　松本　泰尚）

SAMIM MUSTAFA

AN ENERGY-BASED DAMPING EVALUATION USING BAYESIAN MODEL UPDATING FOR VIBRATION-BASED STRUCTURAL HEALTH MONITORING OF STEEL TRUSS BRIDGES

鋼トラス橋ヘルスモニタリングのためのベイズ推定による モデルアップデートを利用したエネルギー的振動減衰評価法

Saitama University
Graduate School of Science and Engineering

A dissertation
submitted to the Saitama University
for the Degree of Doctor of Philosophy

By

Samim Mustafa

Examination Committee

Professor Yasunao Matsumoto (Chairperson)
Professor Yoshiaki Okui
Professor Hiroshi Mutsuyoshi
Professor Masato Saitoh

March, 2017

To my Parents, Sis, Aunt and Uncle

ACKNOWLEDGEMENTS

The work presented in this dissertation would not have been possible without the support that I received from numerous individuals. Foremost, I am very grateful to my supervisor Prof. Yasunao Matsumoto for his technical guidance and encouraging association throughout the period of my research work in Saitama University. Furthermore, I would like to express my gratitude to my examination committee members, Prof. Yoshiaki Okui, Prof. Hiroshi Mutsuyoshi and Prof. Masato Saitoh for their valuable comments, advices and guidance provided during this research studies. I would also like to thank Assistant Prof. Ji Dang for his interest into my research.

I would like to express my gratitude to Japanese government MEXT scholarship program for offering this valuable opportunity of full-time scholarship to pursue my research goals in Saitama University.

I am thankful to my colleagues in the Structural Mechanics and Dynamics Group of Saitama University for providing a congenial working atmosphere in the laboratory. I am particularly thankful to Dr. Dammika for providing me the experimental data conducted by the past researchers of this laboratory. Furthermore, I would like to extend my appreciation to my tutors, Mr. Tobita and Mr. Tanaka, for helping me in many ways to make my life comfortable in Japan. I would also like to thank to Ms. Kudou who gave numerous support as a secretory of the laboratory.

I also want to thank my parents, aunt and uncles for their inspiration, in spite of being far away from me. I am ever grateful to my family members, who have always emphasized the importance of a good education and have supported me through my numerous years in school. Finally, I want to thank my sis Sharmistha without her constant mental support and encouragements this work might not come into this shape.

ABSTRACT

The existing infrastructure such as bridges which are the valuable national assets for transportation and economy are required to be maintained properly to ensure the performance and condition for their continuous operation. Difficulties in practical application of vibration-based structural health monitoring (SHM) of structures include considerable amount of uncertainties in structural modeling and vibration measurement and sensitivity issues of modal parameters due to local damage in case of large structure. This dissertation proposed an analytical framework for SHM addressing the aforementioned difficulties by combining two techniques: A Bayesian based probabilistic approach for finite element model (FE-model) updating that accounts for the underlying uncertainties and an energy-based damping model for detecting damage at local level using a small number of sensors.

An efficient and robust Bayesian model updating was presented in this dissertation by introducing a new objective function and a realistic parameterization of mass and stiffness matrices. In this framework, the likelihood function for mode shapes was formulated based on the cosine of the angle between the analytical and measured mode shapes which does not require any scaling or normalization as compared to conventional Bayesian methods. Four stiffness parameters were introduced for each element considering both sectional and material properties to take into account variation in each element due to local damage. The proposed updating method was validated experimentally by updating a FE-model of existing steel truss bridge utilizing the vibration data obtained from limited number of sensors by a car running test.

It has been recognized that the damping is more sensitive to local damage and the advantage of using damping is that the damping change in global modes affected by local damage can be identified with a small number of sensors. In this dissertation, an energy-based damping model was introduced for practical and effective SHM by estimating the contribution of modal damping ratios from different structural elements utilizing the data from updated FE-model and the identification results of damping from a small number of sensors. A previous study reported that the studied bridge with damage at local diagonal member showed a significant increase in the damping of global vibration mode of the structure. The present study utilized the energy-based damping evaluation to identify possible cause of the modal damping increase by observing the change in the contribution from different structural elements on the modal damping ratios.

TABLE OF CONTENTS

LIST OF FIGURES

LIST OF TABLES

NOMENCLATURE

Chapter 3

$\boldsymbol{D_E}$	Available data from a dynamic system
$\boldsymbol{\chi}$	Uncertain model parameters
C	Model class
$p(\boldsymbol{\chi}\|C)$	Prior probability density function
$p(\boldsymbol{D_E}\|\boldsymbol{\chi}, C)$	Likelihood function of observed data $\boldsymbol{D_E}$
$p(\boldsymbol{\chi}\|\boldsymbol{D_E}, C)$	Updated or posterior probability of the model parameter $\boldsymbol{\chi}$
$p(\boldsymbol{D_E}\|C)$	Normalizing constant
N_d	Degrees of freedom of the system
$\boldsymbol{K}$	Global stiffness matrix
$\boldsymbol{\theta}$	Stiffness parameters
$\boldsymbol{K}_0$	Sub-system stiffness matrix where no parameterization was assigned
$N_{\boldsymbol{\theta}}$	Total number of stiffness parameters
$\boldsymbol{K}_i$	Sub-system stiffness matrix corresponding to $\boldsymbol{\theta}_i$
$\boldsymbol{M}$	Global mass matrix
$\boldsymbol{\vartheta}$	Mass parameters
$\boldsymbol{M}_0$	Sub-system mass matrix where no parameterization was assigned
$N_{\boldsymbol{\vartheta}}$	Total number of mass parameters
$\boldsymbol{M}_j$	Sub-system mass matrix corresponding to $\boldsymbol{\vartheta}_i$
α_r	Angle between the *r*th analytical and measured mode shapes
$\widehat{\boldsymbol{\psi}}_r$	*r*th mode shape identified from measured vibration data
$\boldsymbol{\phi}_r$	*r*th mode shape obtained from finite element model
MAC_r	Modal assurance criteria for the *r*th mode
$\varepsilon_{\boldsymbol{\psi}_r}$	Measurement error for the *r*th mode shape
$\sigma_{\boldsymbol{\psi}}^2$	Variance of measurement error for mode shapes
N_m	Number of measured modes identified from recorded vibration data
$\boldsymbol{L}$	Observation or selection matrix
N_o	Observed degrees of freedom
$\hat{\lambda}_r$	Experimentally identified eigenvalue for the *r*th mode
λ_r	Analytically obtained eigenvalue for the *r*th mode
σ_{λ}^2	Variance of measurement error for eigenvalues
$\mathbb{R}$	Space of real numbers
$\|\bullet\|$	Absolute value of (•)
$(\bullet)^T$	Matrix transpose of (•)
$\sum(\bullet)$	Summation operator
$\in$	Belongs to
$\prod(\bullet)$	Product operator
$exp(\bullet)$	Exponential of (•)
σ_e^2	Prescribed equation errors variance
$\boldsymbol{E}_{g,r}$	Eigenvalue equation error for the *r*th mode
$\boldsymbol{I}_{N_d}$	$N_d \times N_d$ identity matrix
$\boldsymbol{\theta}_n$	Nominal values of stiffness parameters
$\boldsymbol{\vartheta}_n$	Nominal values of mass parameters
$\boldsymbol{\Sigma}_{\boldsymbol{\theta}}$	Covariance matrix of stiffness parameters
$\boldsymbol{\Sigma}_{\boldsymbol{\vartheta}}$	Covariance matrix of mass parameters
Γ	Objective function

$\| \bullet \|$	Euclidean norm of (•)
$(\bullet)^{-1}$	Matrix inverse of (•)
ν_r	Auxiliary variable for the *r*th mode
γ_r	Lagrange multiplier for the *r*th mode
$\frac{\partial^2(\bullet)}{\partial(\bullet)^2}$	Second order partial derivatives
$sgn(\bullet)$	Sign or signum function of (•)
$(\bullet)^*$	Optimal value of (•)
$f_{n,i}$	*i*th modal frequency corresponding to system order *n*
ε_f	Tolerance limit for frequencies
$\boldsymbol{\phi}_{n,i}$	*i*th mode shape corresponding to system order *n*
ε_{MAC}	Tolerance limit for mode shapes
$\xi_{n,i}$	*i*th modal damping ratio corresponding to system order *n*
ε_ξ	Tolerance limit for modal damping ratios
E	Modulus of elasticity
G	Modulus of rigidity
A	Cross-sectional area
I_z	Moment of inertia about *z*-axis
I_y	Moment of inertia about *y*-axis
J	Polar moment of inertia

Chapter 4

ξ_n	nth modal damping ratio
D_n	nth modal dissipating energy per unit cycle
U_n	nth modal potential energy per unit cycle
$\equiv$	Equality sign by definition
$\eta_{(\bullet)}$	Equivalent loss factor of (•) sub-structure
D	Diagonal members
G	Girders
UC	Upper chord members
TLB	Top lateral bracings
BLB	Bottom lateral bracings
S	Supports
$D_{i,n}$	Internal energy dissipation for the nth mode
$D_{s,n}$	Frictional energy dissipation at support for the nth mode
$V_{(\bullet),n}$	nth modal strain energy of (•) sub-structure
$A_{s,n}$	nth modal amplitude at the movable support
μ_s	Dynamic friction coefficient
R	Support's reaction due to vertical load
$\boldsymbol{\phi}_n^*$	nth updated mode shape
$\boldsymbol{K}_e^*$	Updated elastic stiffness matrix
$\boldsymbol{K}_G$	Geometric stiffness matrix
$\boldsymbol{K}_T$	Total stiffness matrix
N_l	Number of elements in the FE-model

ABBREVIATIONS

SHM	Structural health monitoring
FE-model	Finite element model
FD	Fractal dimension
FRF	Frequency response function
DOF	Degrees of freedom
PDF	Probability density functions
FV	Free vibration
SSI	Stochastic Subspace Identification
ERA	Eigensystem Realization Algorithm
PSD	Power spectral density
MAC	Modal assurance criteria
EMAC	Extended modal amplitude coherence
NNLS	Non-negative least-squares method
MER	Modal energy ratio
SD	Standard deviation
AR	After reinforcement
BR	Before reinforcement
CB	Cross beams
St	Stringers
LC	Lower chords
OSP	Optimal sensor placement

CHAPTER 1
INTRODUCTION

1.1 Research Background and Motivation

As most of the current civil infrastructures such as bridges are aging and structurally deteriorating due to reaching of their theoretical design life, the need for vibration-based structural health monitoring (SHM) has gained significant amount of interest in recent years. In Japan, a large number of bridges constructed during the rapid economic growth period from 1950's are having aging problem. There were serious incidents due to deterioration or damage for steel truss bridges found in rigorous inspections conducted after the tragic collapse of I-35W Bridge in Minneapolis, USA on August, 2007. Some damages in the steel bridges in Japan were also reported in the same year [1]. In all these cases, the damage in early stage were not detected by a periodic visual inspection which may imply the limitations of visual inspection.

In the current standard bridge management strategy in Japan, primary periodic inspections rely on visual inspection, although various nondestructive test methods have been used in second step detailed inspections [2]. The current scheduled visual inspections are often time consuming, costly and require the components to be readily accessible. Furthermore, the results of visual inspection are subjective, and vary with the knowledge and experience of the inspectors. To address these issues, damage detection based on physical behaviors through measurements of deformations, stresses, vibrations are required.

The goal is to detect damage in a structure if damage occurs to prevent catastrophic failure of such infrastructures or to evaluate the condition and performance of the same to ensure public safety. The basic idea for vibration-based damage detection is that the damage induced changes in the physical properties will result in detectable changes in modal properties. Therefore, it is intuitive that damage can be identified by analyzing the changes in vibration features of the structure. These vibration-based damage detection techniques can be classified into two categories: non-model based and model based inverse methods. The main drawback of non-model based methods is that they cannot quantify the structural damage severity which is

critical information for the evaluation of structural performance [3,4]. On the other hand, model based inverse methods have been used to detect damage location and its severity as well [5−7].

However, there are some inherent difficulties in the model based SHM due to the underlying uncertainties in the initial finite element model (FE-model). These sources of uncertainties can be classified into three categories: the measurement error representing the uncertainties in the measured vibration data; the modelling errors due to idealization and assumptions while constructing FE-model; and lastly the statistical uncertainties in the model parameters. Therefore, an effective method for FE-model updating is needed to be established to treat these uncertainties explicitly [8−10].

Out of the wide array of available uncertainty quantification approaches, the Bayesian statistical framework is considered to be most efficient one as it is capable of incorporating all types of available information, all types of uncertainties and incomplete experimental data [11−13]. Several model updating approaches have been proposed based on identified modal parameters using Bayesian statistical frameworks [14−18]. Though these were validated by small scale simulated structures, practical applications of Bayesian approaches for structural model updating utilizing incomplete identified modal data sets are yet to be explored. Secondly, so far the Bayesian based model updating approaches proposed in the literature are based on forming objective function by direct correlating the experimentally identified mode shapes with the corresponding components of analytical ones [17,19−23]. However, relating mode shapes directly to get the optimal values required proper scaling or normalization of mode shape components as the mass distribution of the FE-model and the actual structure are usually different, hence, the mode shapes may not be scaled consistently. To address these issues, an advanced Bayesian statistical framework was proposed in this study by introducing a new objective function. In this framework, the likelihood function for mode shapes was formulated based on the cosine of the angle between the analytical and measured mode shapes which does not require any scaling or normalization.

After getting the updated FE-model which is supposed to be free from all the underlying uncertainties mentioned above, the next step is to use that for structural analysis and SHM. There are many vibration-based damage detection approaches have been proposed in the literature and an extensive review of those can be found in Doebling et al. [24] and Fan and Qiao [25]. Most of these studies for damage detection have been mainly based on change in modal frequencies and/or change in mode shape related indices. However, the problem related

to low sensitivity of damage features due to local damages remains a concern for the practical application of these methodologies. On the other hand, it has been recognized that the damping is more sensitive to the local damages especially due to crack or some internal changes in the structural property [26−28]. However, there is some inherent difficulties in accurately identifying the experimental modal damping ratios.

There are very few examples of analytical damping evaluation in the literature [29−32] using energy-based approach which initiated research in this field. The evaluation of analytical modal damping has an advantage that the contribution of energy dissipations in sub-structures on modal damping ratios can be estimated which could be useful knowledge in the field of vibration-based SHM. In this study, an energy-based damping model was introduced for practical and effective SHM based on vibration measurement by estimating the contribution of modal damping ratios from different structural elements utilizing the data from updated FE-model and the identification results of damping from a small number of sensors. As an application of proposed Bayesian based model updating and energy-based damping model for SHM, an existing steel truss bridge was considered and vibration data measured by car running test were used in the analysis.

1.2 Objectives of the Study

The main objective of the research presented in this thesis is to develop a practical and effective vibration-based SHM approach for steel truss bridges. Difficulties in practical application of vibration-based SHM of structures include considerable amount of uncertainties in structural modeling and vibration measurement and sensitivity issues of modal parameters due to local damage in case of large structure. In realistic scenarios, usually there are limited number of sensors available to perform SHM practically. Therefore, it would be worthy to develop a method to detect damage or evaluate structural state with less number of sensors. This dissertation proposes an analytical framework for SHM addressing the aforementioned difficulties by combining two techniques: a Bayesian based probabilistic approach for FE-model updating that accounts for the underlying uncertainties, and an energy-based damping evaluation for detecting damage at local level using a small number of sensors. Fig. 1.1 schematically illustrates the methodology proposed in this dissertation for SHM of steel truss bridges.

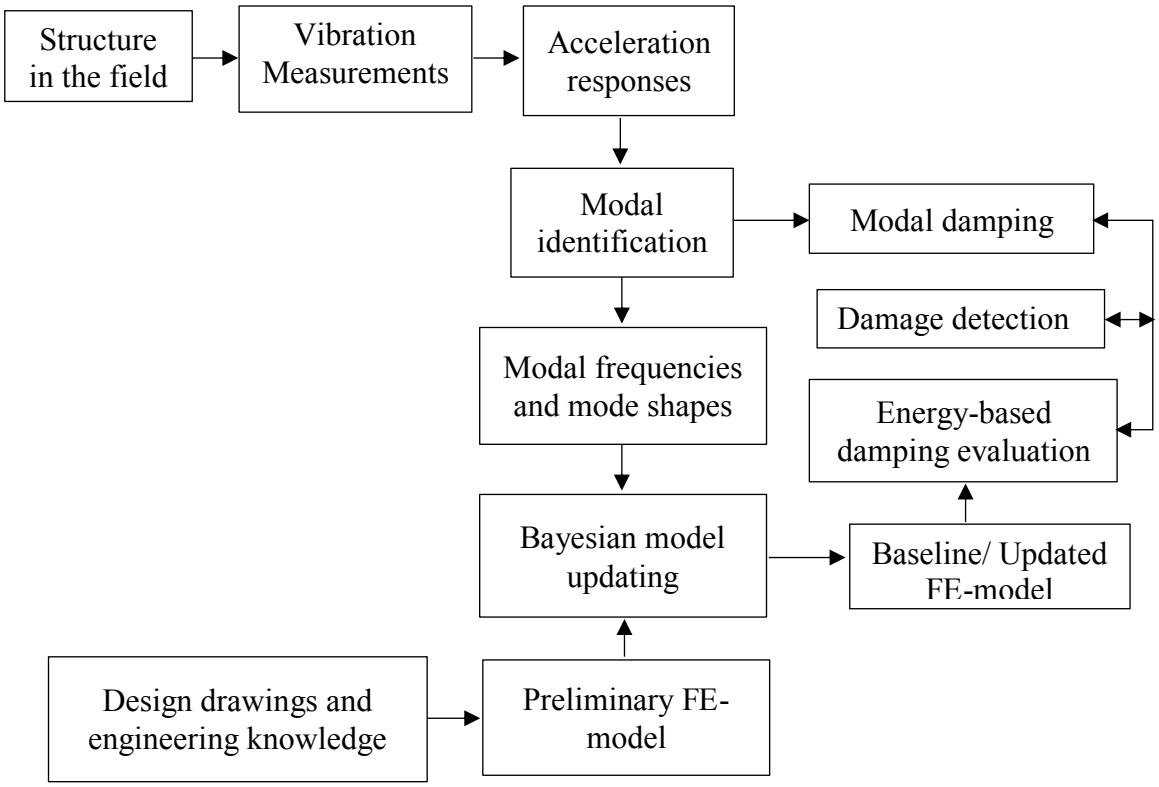

Fig. 1.1. Schematic diagram of proposed methodology for SHM

1.3 Outline of the Dissertation

Motivated by the existing gaps and open problems identified in section 1.1, a systematic study on vibration-based SHM of an existing steel truss bridge has been carried out in this dissertation. The dissertation is divided into six chapters and two Appendices.

Chapter 2 provides an overview of vibration-based SHM approaches. Then, brief summary of reviewed literatures related to two vibration-based SHM techniques categorized by the utilization of FE-model is included and the difficulties in practical application of these methodologies to detect local damages are discussed. Possible solutions to overcome these difficulties faced by the past researchers in this field are also provided.

Chapter 3 is aimed at developing a Bayesian probabilistic approach for FE-model updating using limited sensor data and treating all the underlying uncertainties. Practical difficulties in updating an initial FE-model of real-life structures are addressed in this proposed framework by introducing a new objective function and a realistic parameterization of mass and stiffness matrices. The proposed updating method was validated experimentally by updating a FE-model of existing steel truss bridge.

Chapter 4 introduces an energy-based damping framework for SHM by estimating the contributions to modal damping ratios from different structural elements utilizing the data from updated FE-model. Model updating using only global modes identified with a limited number of sensors may not be able to trace the damaged stiffness parameters as the changes in the frequencies for the global modes due to local damage are not significant. Therefore, damping is considered in this research work for SHM as the advantage of using the damping is that the damping change in global modes affected by local damage can be identified with a small number of sensors. An equivalent viscous damping model is considered in this dissertation and the contributions to modal damping ratios from different sub-structures of the studied truss bridge are evaluated by relevant damping analysis.

In Chapter 5, experimental verification of the proposed vibration-based SHM framework developed in this dissertation is considered. A previous study by Yoshioka, et al. reported that the studied bridge with damage at local diagonal member showed a significant increase in the damping of global vibration mode of the structure. The present study utilized the energy-based damping evaluation to identify the cause of the modal damping increase by observing the change in the contribution from different structural elements on the modal damping ratios.

Finally, Chapter 6 presents the conclusions emerging from the studies taken up in this dissertation and makes a few suggestions for further research.

CHAPTER 2
LITERATURE REVIEW

2.1 An Overview of Vibration-based SHM

The interest in the ability to monitor a structure and detect damage at the earliest possible stage is pervasive throughout the civil, mechanical, and aerospace engineering communities. The goal is to detect, locate and access the extent of damage in a structure if damage occurs to prevent catastrophic failure of such infrastructures or to evaluate the condition and performance of the same to ensure public safety. As an alternative to the current local inspection methods, global vibration-based methods have been widely developed over the years [5,24,25]. The basic idea for vibration-based damage detection is that the damage induced changes in the physical properties will result detectable changes in modal properties. Therefore, it is intuitive that damage can be identified by analyzing the changes in vibration features of the structure.

The global nature of the vibrational characteristics of interest to vibration-based SHM provides advantages compared to other health monitoring techniques. It allows for a relatively easy interpretation of the measured responses, have the ability to analyse complex structures and do not require the structure to be readily accessible in order to be able to identify damage. Utilization of global vibration signatures such as natural frequencies, mode shapes and damping leads to the monitoring of the entire structural system, not just each structural component, which means a large civil engineering structure can be effectively monitored with a relatively small set of sensors and equipment.

Conceptually, the general procedure of the vibration-based SHM consists of five steps namely [33-35]: (1) vibration measurement of structural dynamic response, e.g., in terms of accelerations or displacements, (2) system identification by analysing recorded vibration data to extract modal parameters, (3) characterization of an initial FE-model based on design drawings and field observations, (4) perform FE-model updating by utilizing identified modal data in order to obtain up-to-date structural model, and (5) evaluation of structural performance using the updated finite element model.

The measurement of structural dynamic responses is achieved with an instrumentation system handling the sensing, transmission and storage of dynamic response data. Various characteristics of the instrumentation system, such as sensor types, sampling rate, and storage capacity, etc., need to be customized based on each unique application. Acceleration, velocity and displacement are the most common types of measurement for dynamic response. It should be noted that in order to achieve continuous monitoring of the bridge structure, large amount of dynamic data need to be collected and processed. The instrumentation system must be designed to handle such types of data throughput.

In order to identify structural properties, raw dynamic responses of the structure such as acceleration time histories can be utilized. However, it is more common that vibrational features such as modal parameters are extracted from the raw dynamic response. Modal parameters contain important characteristics of the structural dynamic response but are highly compressed compared to raw data, easing further analysis and storage [36]. Operational modal analysis is typically used to identify the modal model in terms of modal parameters of the structure from the dynamic responses under operational conditions.

The initial characterization of the structure provides a baseline model that adequately predicts the structural behaviour in its pristine state. Through continuous monitoring, an up-to-date modal model reflecting the current dynamic characteristics of the structure can be maintained. FE-model updating can then be performed to obtain an up-to-date representative physical model of structure based on the changes in modal parameters observed [8-13]. The objective of FE-model updating is to minimize the discrepancy between the FE-model and the actual structure so that the physical model accurately represents the structure and is able to predict structural behaviour. The sources of these discrepancies are mainly due to the modelling errors, variation of material properties during manufacture and uncertainties introduced by the construction process.

Finally, by comparing the baseline model with the current state of the structure, information regarding the location and magnitude of the damage that the structure has experienced can be deduced. Current structural performance can be evaluated and a prediction regarding the remaining life of the structure can be made.

During the last three decades, extensive research has been conducted in vibration-based SHM. A broad range of techniques, algorithms, and methods are developed to solve various problems encountered in different structures, from basic structural components (e.g., beams and plates)

to complex structural systems (e.g., bridges and buildings). Doebling et al. [37] presented an extensive review of vibration-based damage detection methods up to 1996. Sohn et al. [35] then presented an updated version of this review on the literature up to 2001. In both articles, the features extracted for identification were considered to classify the damage identification methods. Following closely this classification, Carden and Fanning [38] presented a literature survey with particular emphasis on the papers and articles published from 1996 to 2003. More recently, a comprehensive review on modal parameter-based damage identification methods carried out by Fan and Qiao [25].

2.2 Vibration-based SHM Techniques

Damage detection using vibration-based damage detection techniques can be classified into two categories: non-model based methods and model-based inverse methods. In the following sub-sections, the literature review related to these two methodologies are carried out while highlighting their merits and drawbacks when implement in practical applications.

2.2.1 Non-model based Methods

Non-model based methods, also known as pattern recognition techniques, are straightforward and do not require any computer-simulated models. In a non-model based method the results are compared with the results of a reference measurement performed prior to setting the structure in service. Deviances in the damage sensitive parameters are used to identify damage.

Hadjileontiadis et al. [39] and Hadjileontiadis and Douka [40] proposed a response-based damage detection algorithm for beams and plates using fractal dimension (FD). This method calculates the localized FD of the fundamental mode shape directly. The damage features are established by employing a sliding window across the mode shape and estimating the FD at each position for the regional mode shape inside the window. Damage location and size are determined by a peak on the FD curve indicating the local irregularity of the fundamental mode shape introduced by the damage.

Recently, wavelet analysis has shown its inherent merits in damage detection over traditional methods due to its ability to closely examine the signal with multiple scales to provide various levels of detail and approximations. The use of wavelet transform to identify damage from mode shape has been one of the most popular techniques. These methods treat mode shape data as a signal in spatial domain, and they use spatial wavelet transform technique to detect the signal irregularity caused by damage. Liew and Wang [41] first used spatial wavelet

coefficients for crack detection based on the numerical solution for the deflection of a beam under oscillating excitation. Quek et al. [42] examined the sensitivity of wavelet technique in the detection of cracks in beam structures. Although their works focused on deflection under static or impact loading other than mode shape, they demonstrated the potential of using wavelet transform on mode shape for damage detection. Hong et al. [43] showed that the continuous wavelet transform (CWT) of mode shape using a Mexican hat wavelet is effective to estimate the Lipschitz exponent for damage detection of a damaged beam.

Huth et al. [44] compared several non-model based identification techniques based on test data on a progressively damaged prestressed concrete bridge. Although the bridge was severely cracked, natural frequencies as well as mode shapes display only minor changes. However, the relative changes of mode shapes are larger than those observed for natural frequencies. Therefore, the non-model based methods are capable of detecting damage location successfully, although, these methods cannot quantify the damage severity, which is critical information for evaluating the structural performance. Additionally, a sufficient coverage on various damage scenarios is needed as training data in the non-model based method, while usually such data obtained from field are limited.

2.2.2 Model-based Inverse Methods

In a model based technique the response is compared with some form of model. This can either be an analytical or a numerical (e.g. finite element) model. Advantages of model based techniques are that these could well be extended to provide information about the severity of the detected damage and can be used to account for environmental or operational variations (e.g. temperature, boundary conditions). These methods are based on features related to changes in mass, stiffness and damping matrix indices that have been correlated such that the numerical model predicts, as closely as possible, the identified dynamic properties (resonant frequencies, modal damping and mode-shape vectors) of the undamaged and damaged structures, respectively. These methods solve for the updated matrices (or perturbations to the nominal model that produce the updated matrices) by forming a constrained optimization problem based on the structural equations of motion, the nominal model and the identified modal properties [45]. Comparisons of the matrix indices that have been correlated with modal properties identified from the damaged structure to the original correlated matrix indices provide an indication of damage that can be used to quantify the location and extent of damage.

Fritzen and Bohl [46] and also Gorl and Link [47] used this approach to localize damage in an experimental steel frame structure. A reduction in cross-section of a cantilever beam structure was similarly identified in experiment in Ref. [48]. More recently, Reynders et al. [49] used this general approach to identify loss of stiffness in a full-scale bridge structure. Similarly Shang et al. [50] used FE model updating combined with ‘‘subset selection’’ (method for damage localization) to determine location and extent of delamination in a composite laminate structure. Many damage identification algorithms rely on a well correlated numerical model of the structure in its initial state. Several issues arise when creating a correlated numerical model; the measured data chosen to be matched by the model, the accuracy of the initial model, the size and complexity of the model, the number of updating parameters and the non-uniqueness of resultant model in matching the measured data [51,52].

The accuracy of the initial model of a structure used to identify damage with an updating algorithm is important. Fritzen and Jennewein [53] used sensitivity based algorithms to locate and detect damage. It was found that even the use of Bernoulli–Euler beams instead of Timoshenko theory shifted the higher Eigen frequencies, so that no reasonable results were obtainable. Gola et al. [54] examined the number of parameters identifiable in sensitivity based updating methods. The theoretical number of parameters furnished by the matching of eigenvalues is equal to the number of measured resonant frequencies. When using mode shapes, the number of parameters has an upper limit of the number of modes times the number of degrees of freedom measured. This limit is further reduced depending on the structure of the mode derivatives.

Papadopoulas [55] presented a method of model updating and damage identification, which accounted for structural variability. The statistical properties of the healthy mass and stiffness parameters and the mean healthy natural frequencies and mode shapes of the system were first determined. The mean damaged natural frequencies and mode shapes of the system were then simulated. The number of modes available was assumed to be equal to the number of damage parameters and these parameters were determined. The statistical properties of the damaged stiffness were then determined and probabilistically compared to the healthy stiffness to yield an estimate of the probability of damage.

Model updating using frequency response function (FRF) measurements directly has also been utilised for damage identification [56-58]. The initial, and obvious, advantage in using FRF

data over modal data is that it negates the need to identify the modal parameters from measurements and to perform mode-pairing exercises.

In summary, the FE-model updating determines damage as a change in the physical properties of a structure by updating the structural parameters in a FE-model to match some selected quantities that are either directly measured or derived from field measurements at two different times. The selected quantities can be modal parameters [59-61], time-domain response data [62-64], and static responses [65,66]. According to the algorithm adopted, the conventional model updating includes direct methods, indirect or iterative methods and a sensitivity approach. Most of the early model updating methods are direct and they require complete set of measured data to update the analytical model. The system matrices are either reduced to the observed degrees of freedom (DOF) or the measured incomplete mode shapes are expanded to the full FE-model DOFs [67-69]. These early methods are computationally efficient though the physical meaning of the updated system matrices are often not preserved which raises the question of their validity for SHM.

The present work in this dissertation addresses the aforementioned difficulties by introducing a Bayesian probabilistic approach for FE-model updating using incomplete modal data to update a full analytical model to identify the structural properties at the global level and energy-based damping evaluation to detect damage at local level. In this dissertation, a Bayesian model updating was used not to detect damage but to construct a probabilistic baseline using modal frequencies and mode shapes that are not sensitive to the local damage. An energy-based damping evaluation was carried out in this dissertation to detect local damage as it has been recognized that the damping is more sensitive to the local damage [26-31]. Out of the wide array of available uncertainty quantification approaches, the Bayesian statistical framework was considered in this dissertation as it is capable of incorporating all types of available information, all types of uncertainties and incomplete experimental data [11−13]. Several model updating approaches have been proposed based on identified modal parameters using Bayesian statistical frameworks [14−18]. Though these were validated by small scale simulated structures, practical applications of Bayesian approaches for structural model updating utilizing incomplete identified modal data sets are yet to be explored.

2.3 Difficulties in Practical Application of Vibration-based SHM

Although many structural health monitoring techniques have been proposed in the literature, there are still numerous difficulties in the practical application of these approaches. The most

important technical issues that need to be resolved before structural health monitoring technologies can make the transition from a research topic to actual practice are summarized in subsequent sub-sections.

2.3.1 Issues with Sensing and System Identification

There is uncertainty about the number and place to install the sensors to successfully detect and predict the location of damage of real structure [70,71]. Many techniques that appear to work well in example cases actually perform poorly when subjected to the measurement constraints imposed by actual testing [25,35,42,44]. Techniques that are to be seriously considered for implementation in the field should demonstrate that they can perform well under the limitations of a small number of measurement locations, and under the constraint that these locations be selected a priori without knowledge of the damage location.

In reality, the number of the sensors in an installation is limited; the cost of the sensors, data acquisition systems, and system installation is significant, and the available budget is always limited. Traditionally, algorithms which can achieve adequate performance with a limited number of sensors are desirable. Unfortunately, such algorithms that are effective have been elusive. Considering that damage is an intrinsically local phenomenon, deployment of more sensors throughout the structure has the potential to lead to more accurate damage detection results.

In addition, excitation methods for bridge structures need to be considered. The two main categories of excitation methods are ambient vibration and forced vibration. Ambient vibration tests are used for a long span bridge due to the difficulty in applying sufficient forces to a large bridge, while forced vibration tests are often used for a small or middle size bridges because the responses from the ambient vibration may be too small. Therefore, effective excitation schemes should be considered according to bridge size.

Accuracy in damage detection is completely dependent upon the accuracy in measurement of modal properties of the structure. It is found that the modal properties are inflicted to fluctuation due to variations in the measurement. This makes very difficult to conclude whether the observed changes are due to damage or due to variations in the measurement. This is the serious issue of sensitivity of vibration based techniques, and need to be explored further. For practical applications of the vibration based techniques on real life structures such as tall buildings, bridges, dams, and underground structures, it is needed to reduce the dependence upon

measurable excitation forces. Vibrations produced by existing loading system and ambient environmental can be used for exciting the structure.

2.3.2 Issues with Model-based SHM

For the model-based SHM methods, the credibility of a numerical model must be established through careful model verification and validation [72]. There are some inherent difficulties in the model based SHM due to the underlying uncertainties in the initial FE-model. The sources of these uncertainties can be classified into three categories: the measurement error representing the uncertainties in the measured vibration data; the modelling errors due to idealization and assumptions while constructing FE-model; and lastly the statistical uncertainties in the model parameters. Therefore, an effective method for FE-model updating is needed to be established to treat these uncertainties explicitly [8−10].

The selection of parameters is probably the most important task in model updating. Of course, the updating parameters must describe that part of the system which is thought to be inadequately modelled. The obvious candidates include the boundary conditions and joints. When the model error is at some other point than the boundaries and joints, then there are a variety of procedures which can be carried out to either eliminate the error by improved modelling, or locate the error for subsequent removal by updating.

Another issue with FE-model updating is the availability of incomplete modal data (modal frequencies and partial mode shapes). In most updating algorithms, all the co-ordinates of a given normal mode must be known. Due to physical limitations, time or cost constraints, however, the number of measured co-ordinates is generally substantially less than the degrees of freedom of the analytical model. Moreover, only a few of the lower modes of a structures can be identified with confidence. Hence, the model updating method must be efficient enough to update a full-scale analytical model by utilizing limited sensor data only.

Several model updating approaches have been proposed based on identified modal parameters using Bayesian statistical frameworks [14−18]. Though these were validated by small scale simulated structures, practical applications of Bayesian approaches for structural model updating utilizing incomplete identified modal data sets are yet to be explored. Secondly, so far the Bayesian based model updating approaches proposed in the literature are based on forming objective function by direct correlating the experimentally identified mode shapes with the corresponding components of analytical ones [17,19−23]. However, relating mode shapes directly to get the optimal values required proper scaling or normalization of mode shape

components as the mass distribution of the FE-model and the actual structure are usually different, hence, the mode shapes may not be scaled consistently.

2.3.3 Issues with Sensitivity of Modal Parameters to Local Damage

A large obstacle for the practical application of structural health monitoring technologies is the dependency of damage parameters on the operational and environmental conditions, such as temperature, humidity, loads and boundary conditions [42,44]. Changes in these conditions can mask or magnify the effects that are resulting from the damage. Methods should have the ability to separate the damage related effects from those that are coming from changes in environmental conditions. A wide variety of methods, comprising statistical techniques and model based methods, are presented in the literature to compensate for these variations, but confidence in these methods is lacking.

Another issue that is a point of controversy among many researchers is the general level of sensitivity that modal parameters have to small flaws in a structure. Much of the evidence on both sides of this disagreement is anecdotal because it is only demonstrated for specific structures or systems and not proven in a fundamental sense. This issue is important for the development of health monitoring techniques because the user of such methods needs to have confidence that the damage will be recognized while the structure still has sufficient integrity to allow repair.

In case of large structure, such as bridges, the identification of local damage is a challenging task because of the issue of low sensitivity of frequencies and mode shapes to local damage especially due to cracks or some internal changes in the structural property [27,28,63]. In such cases, model updating using only global modes identified with a limited number of sensors may not be able to trace the damaged stiffness parameters as the changes in the frequencies for the global modes due to local damage are not significant.

2.4 Proposed Framework Overcoming Aforementioned Difficulties

This dissertation introduces a practical and effective vibration-based SHM approach for steel truss bridges. An analytical framework is proposed for SHM addressing the aforementioned difficulties by combining two techniques: a Bayesian based probabilistic approach for FE-model updating that accounts for the underlying uncertainties, and an energy-based damping evaluation for detecting damage at local level using a small number of sensors.

An efficient and robust Bayesian model updating was presented in this dissertation by introducing a new objective function and a realistic parameterization of mass and stiffness matrices [73]. For the identification of damage at local level using vibration measurements, it is necessary to update stiffness matrices of all the elements to capture the variations in the stiffness due to local changes. Hence, it is more practical to consider stiffness parameters corresponding to each element of the FE-model. In this research work, four stiffness parameters were considered for each element considering both sectional and material properties. For the parameterization of mass matrix, mass density per unit length of each section was considered as uncertain parameter. It is important to note that, the variation of mass is assumed to be much smaller compared to the stiffness due to local damage. Hence, lesser number of uncertain parameters were assigned for mass matrix. Basically, the main purpose of the parameterization of mass matrix was to make the updating results more robust to the modelling errors. In this framework, the likelihood function for mode shapes was formulated based on the cosine of the angle between the analytical and measured mode shapes which does not require any scaling or normalization. The proposed updating method was validated experimentally by updating a FE-model of existing steel truss bridge utilizing the vibration data obtained from limited number of sensors by a car running test.

After getting the updated FE-model which is supposed to be free from all the underlying uncertainties mentioned above, the next step is to use that for structural analysis and SHM. It has been recognized that the damping is more sensitive to local damage and the advantage of using damping is that the damping change in global modes affected by local damage can be identified with a small number of sensors [26-28]. However, there is some inherent difficulties in accurately identifying the experimental modal damping ratios. There are very few examples of analytical damping evaluation in the literature [29−32] using energy-based approach which initiated research in this field. Dammika et al. [32] investigated the analytical modal damping evaluation as a complementary method to the experimental SHM of bridges. In that study, an energy-based damping model was introduced to estimate the damping parameters of a steel arch bridge. The objective was to provide the theoretical basis for modal damping evaluation which can improve the reliability of the experimental damping identification. However, the uncertainties associated with FE-model of the studied arch bridge were not taken into consideration in that study. Furthermore, the proposed framework by Dammika et al. [32] could not justify the substantial change in modal damping ratio of coupled global mode caused by the damage at local diagonal member as reported in doctoral dissertation by Dammika [74].

In this dissertation, an energy-based damping model was introduced for practical and effective SHM by estimating the contribution of modal damping ratios from different structural elements utilizing the data from updated FE-model and the identification results of damping from a small number of sensors. For SHM with less number of sensors, complimentary theoretical consideration is necessary which is discussed in this dissertation. A previous study by Yoshioka, et al. [28] reported that the studied bridge with damage at local diagonal member showed a significant increase in the damping of global vibration mode of the structure. The present study utilized the energy-based damping evaluation to identify possible cause of the modal damping increase by observing the change in the contribution from different structural elements on the modal damping ratios.

CHAPTER 3

BAYESIAN PROBABILISTIC APPROACH FOR MODEL UPDATING USING LIMITED SENSOR DATA

3.1 Introduction

In conventional Bayesian model updating methods which are mainly validated by small scale simulated structures, the optimal values of uncertain parameters are obtained based on formulating likelihood function as a product of two probability density functions (PDF), one relating to modal frequencies and one to mode shapes components. However, relating mode shapes directly to get the optimal values required proper scaling or normalization of mode shape components as the mass distribution of the FE-model and the actual structure are usually different, hence, the mode shapes may not be scaled consistently. Moreover, for the identification of damage at local level using vibration measurements, it is necessary to update stiffness matrices of all the elements to capture the variations in the stiffness due to local changes. To address these issues, an efficient and robust Bayesian model updating was presented in this dissertation by introducing a new objective function and a realistic parameterization of mass and stiffness matrices. In this framework, the likelihood function for mode shapes was formulated based on the cosine of the angle between the analytical and measured mode shapes which does not require any scaling or normalization. The proposed updating method was validated experimentally by updating a FE-model of existing steel truss bridge utilizing the vibration data obtained from car running test.

3.2 Application of Bayesian Probabilistic Approach to FE-model Updating

3.2.1 Bayesian Probabilistic Approach

The Bayesian probabilistic approach are used to quantify the uncertainties in the initial FE-model along with making inferential statement about the unknown quantities given some know

quantities. Let $\boldsymbol{D_E}$ denote available data from a dynamic system under consideration. By using Bayes' theorem, the updated or posterior probability of the model parameter $\boldsymbol{\chi}$ given the available data and a model class C is given by [6,11]:

$$p(\boldsymbol{\chi}|\boldsymbol{D_E}, C) = \frac{p(\boldsymbol{D_E}|\boldsymbol{\chi}, C)p(\boldsymbol{\chi}|C)}{p(\boldsymbol{D_E}|C)} \tag{3.1}$$

where $p(\boldsymbol{\chi}|C)$ is the initial or prior probability density function (PDF) of the model parameter $\boldsymbol{\chi}$; $p(\boldsymbol{D_E}|\boldsymbol{\chi}, C)$ is the likelihood function of observed data $\boldsymbol{D_E}$ and $p(\boldsymbol{\chi}|\boldsymbol{D_E}, C)$ is the posterior PDF of the model parameters given the observed data and the model class C. The denominator in Eq. (3.1) $p(\boldsymbol{D_E}|C)$ is a normalizing constant such that integrating the posterior PDF over the parameter space yields unity as required by the definition of a probability function.

3.2.2 Parameterization of Mass and Stiffness Matrices

Assuming that the structure does not exhibit highly nonlinear behavior, a linear model of the dynamics should be adequate for identification of the dynamic characteristics of structure. A convenient parameterization for the stiffness and mass matrices for a linear structural model with N_d degrees of freedom (DOF) is [17,75]:

$$\boldsymbol{K}(\boldsymbol{\theta}) = \boldsymbol{K}_0 + \sum_{i=1}^{N_{\boldsymbol{\theta}}} \boldsymbol{\theta}_i \boldsymbol{K}_i \text{ and } \boldsymbol{M}(\boldsymbol{\vartheta}) = \boldsymbol{M}_0 + \sum_{j=1}^{N_{\boldsymbol{\vartheta}}} \boldsymbol{\vartheta}_j \boldsymbol{M}_j \tag{3.2}$$

where $\boldsymbol{K}_0$, $\boldsymbol{M}_0$, $\boldsymbol{K}_i$ and $\boldsymbol{M}_j$ all are constant matrices independent of the model parameters and $\boldsymbol{\theta}_i (i = 1, \dots, N_{\boldsymbol{\theta}})$ and $\boldsymbol{\vartheta}_i (j = 1, \dots, N_{\boldsymbol{\vartheta}})$ are the stiffness and mass parameters respectively which need to be updated to make necessary adjustment in the FE-model in order to make it more consistent with the real structure. Here, $N_{\boldsymbol{\theta}}$ and $N_{\boldsymbol{\vartheta}}$ represents the total number of stiffness and mass parameters respectively. As the modelling errors are expected to be present in both the stiffness and mass matrices, it is thus more reasonable to consider the parameterization of mass matrix as well to make the updating results more robust to the modelling errors [19].

3.2.3 Formulation of Likelihood Function

The likelihood function is constructed to measure the agreement between the observed data from a dynamic system and the corresponding structural model output. It reflects how likely the measurements are observed from the model with particular set of parameters. In conventional Bayesian methods, the likelihood function is formulated based on direct correlating measured components of modal data with corresponding analytical components obtained from FE-model. However, relating mode shapes directly requires an appropriate

scaling or normalization of mode shape components obtained from the FE-model and the actual structure. To address this issue, an alternative mode shape residual, which is more sensitive to the change of mode shape and does not require such scaling, was proposed in this study [73]. The mode shape residual was formulated based on cosine of the angle between the analytical and measured mode shapes which is expressed as [76]:

$$\cos \alpha_r = \frac{\widehat{\boldsymbol{\psi}}_r^T \boldsymbol{\phi}_r}{|\widehat{\boldsymbol{\psi}}_r||\boldsymbol{\phi}_r|} = \sqrt{MAC_r} \tag{3.3}$$

where $\boldsymbol{\phi}_r$ and $\widehat{\boldsymbol{\psi}}_r$ are the rth mode shapes from FE-model and measured data respectively and MAC_r represents modal assurance criteria (MAC) for rth mode. To construct the likelihood function for mode shape, the measurement error $\varepsilon_{\psi_r} = \left(\widehat{\boldsymbol{\psi}}_r^T \boldsymbol{\phi}_r / |\widehat{\boldsymbol{\psi}}_r||\boldsymbol{\phi}_r| - 1\right)$ was introduced and a Gaussian probability model was chosen for $\varepsilon_{\boldsymbol{\psi}} \in \mathbb{R}^{N_m}$ with zero mean and variance $\sigma_{\boldsymbol{\psi}}^2 \in \mathbb{R}^{N_m}$ where, N_m is the number of measured modes identified from recorded vibration data. Hence, the likelihood function for mode shapes can be written as:

$$p\left(\widehat{\boldsymbol{\psi}}_r, \sigma_{\psi_r} | \boldsymbol{\theta}, \boldsymbol{\vartheta}\right) = \frac{1}{\sigma_{\psi_r}\sqrt{2\pi}} exp\left[-\frac{1}{2\sigma_{\psi_r}^2}\left(\frac{\widehat{\boldsymbol{\psi}}_r^T \boldsymbol{L}\boldsymbol{\phi}_r}{|\widehat{\boldsymbol{\psi}}_r||\boldsymbol{L}\boldsymbol{\phi}_r|} - 1\right)^2\right] \tag{3.4}$$

where $\boldsymbol{L} \in \mathbb{R}^{N_o \times N_d}$ is the observation or selection matrix that picks N_o observed DOF from complete mode shape vector $\boldsymbol{\phi}_r$.

Similarly, the likelihood function for eigenvalues can be expressed as:

$$p\left(\hat{\lambda}_r, \sigma_{\lambda_r} | \boldsymbol{\theta}, \boldsymbol{\vartheta}\right) = \frac{1}{\sigma_{\lambda_r}\sqrt{2\pi}} exp\left[-\frac{1}{2\sigma_{\lambda_r}^2}\left(\lambda_r - \hat{\lambda}_r\right)^2\right] \tag{3.5}$$

where σ_λ^2 is the variance matrix for eigenvalues; $\lambda_r (r = 1, \dots, N_m)$ and $\hat{\lambda}_r (r = 1, \dots, N_m)$ are analytically and experimentally identified eigenvalues respectively. The probability models conditional on the parameter vectors $\boldsymbol{\theta}$ and $\boldsymbol{\vartheta}$ were chosen to have statistical independence between the eigenvalues and eigenvectors and between different modes.

Therefore, the likelihood function of the observed data $\boldsymbol{D_E}$ can be written as:

$$p(\boldsymbol{D_E} | \boldsymbol{\theta}, \boldsymbol{\vartheta}) = \prod_{r=1}^{N_m} p\left(\widehat{\boldsymbol{\psi}}_r, \sigma_{\psi_r} | \boldsymbol{\theta}, \boldsymbol{\vartheta}\right) p\left(\hat{\lambda}_r, \sigma_{\lambda_r} | \boldsymbol{\theta}, \boldsymbol{\vartheta}\right) \tag{3.6}$$

3.2.4 Formulation of Eigenvalue Equation Errors

Because of the modelling approximations and errors, it is assumed that the identified modal properties never satisfied exactly the eigenvalue problem of any given structural system [17,75]. System eigenvalue, λ_r and eigenvector, $\boldsymbol{\phi}_r$ were introduced here to model the eigenvalue equation errors to measure the agreement between the identified modal parameters and their counterparts from the updated FE-model model. These eigenvalue equation errors were modelled by choosing a Gaussian PDF with zero mean and σ_e^2 as the prescribed equation errors variance:

$$p(\lambda_r, \boldsymbol{\phi}_r | \, \boldsymbol{\theta}, \boldsymbol{\vartheta}) = \frac{1}{\sqrt{(2\pi)^{N_d}\left|\sigma_e^2 I_{N_d}\right|}} exp\left[-\frac{1}{2}\boldsymbol{E}_{g,r}^T\left(\sigma_e^2 \boldsymbol{I}_{N_d}\right)^{-1}\boldsymbol{E}_{g,r}\right] \tag{3.7}$$

where $\boldsymbol{E}_{g,r} = [\boldsymbol{K}(\boldsymbol{\theta}) - \lambda_r \boldsymbol{M}(\boldsymbol{\vartheta})]\boldsymbol{\phi}_r \in \mathbb{R}^{N_d}$, $r = 1, \ldots, N_m$ is the eigenvalue equation errors and $\boldsymbol{I}_{N_d}$ is a $N_d \times N_d$ identity matrix. By assigning an appropriate value for σ_e^2, one can compromise the agreement between the measured modal parameters and their counterparts from the updated structural model. A smaller value for σ_e^2 can be assigned if the eigenvalue equations are nearly satisfied.

3.2.5 Formulation of Prior PDF

The prior PDF for the model parameters, $\boldsymbol{\theta}$ and $\boldsymbol{\vartheta}$ were assumed to be independent Gaussian PDFs with mean $\boldsymbol{\theta}_n \in \mathbb{R}^{N_\theta}$ and $\boldsymbol{\vartheta}_n \in \mathbb{R}^{N_\vartheta}$, representing the nominal values of stiffness and mass parameters and with covariance matrices $\boldsymbol{\Sigma}_{\boldsymbol{\theta}} \in \mathbb{R}^{N_\theta \times N_\theta}$ and $\boldsymbol{\Sigma}_{\boldsymbol{\vartheta}} \in \mathbb{R}^{N_\vartheta \times N_\vartheta}$ respectively. The prior covariance matrices $\boldsymbol{\Sigma}_{\boldsymbol{\theta}}$ and $\boldsymbol{\Sigma}_{\boldsymbol{\vartheta}}$ were taken to be diagonal and the choice of the diagonal values should reflect the level of uncertainty in the nominal model. The final form of prior PDF considering eigenvalue equation errors and model parameters can be expressed as:

$$p(\boldsymbol{\lambda}, \boldsymbol{\phi}, \boldsymbol{\theta}, \boldsymbol{\vartheta}) = p(\boldsymbol{\lambda}, \boldsymbol{\phi} | \boldsymbol{\theta}, \boldsymbol{\vartheta}) p(\boldsymbol{\theta}) p(\boldsymbol{\vartheta}) \tag{3.8}$$

where $p(\boldsymbol{\theta})$ and $p(\boldsymbol{\vartheta})$ are the prior PDFs for stiffness parameters and mass parameters respectively which are given by:

$$p(\boldsymbol{\theta}) = \frac{1}{\sqrt{(2\pi)^{N_\theta}|\boldsymbol{\Sigma}_{\boldsymbol{\theta}}|}} exp\left[-\frac{1}{2}(\boldsymbol{\theta} - \boldsymbol{\theta}_n)^T \boldsymbol{\Sigma}_{\boldsymbol{\theta}}^{-1}(\boldsymbol{\theta} - \boldsymbol{\theta}_n)\right] \tag{3.9}$$

and

$$p(\boldsymbol{\vartheta}) = \frac{1}{\sqrt{(2\pi)^{N_\vartheta}|\boldsymbol{\Sigma}_{\boldsymbol{\vartheta}}|}} exp\left[-\frac{1}{2}(\boldsymbol{\vartheta} - \boldsymbol{\vartheta}_n)^T \boldsymbol{\Sigma}_{\boldsymbol{\vartheta}}^{-1}(\boldsymbol{\vartheta} - \boldsymbol{\vartheta}_n)\right] \tag{3.10}$$

3.2.6 Formulation of Posterior PDF

Substituting Eqs. (3.6) and (3.8) into Eq. (3.1), the expression for the posterior PDF can be obtained. The most probable values (MPV) of unknown parameters can be obtained by maximizing the posterior PDF. For the ease of this optimization problem, the negative logarithm of posterior PDF was taken as the objective function which is given by:

$$\begin{aligned}\Gamma(\boldsymbol{\theta},\boldsymbol{\vartheta},\boldsymbol{\lambda},\boldsymbol{\phi}) = &\frac{1}{2}(\boldsymbol{\theta}-\boldsymbol{\theta}_n)^T\boldsymbol{\Sigma}_{\boldsymbol{\theta}}^{-1}(\boldsymbol{\theta}-\boldsymbol{\theta}_n)+\frac{1}{2}(\boldsymbol{\vartheta}-\boldsymbol{\vartheta}_n)^T\boldsymbol{\Sigma}_{\boldsymbol{\vartheta}}^{-1}(\boldsymbol{\vartheta}-\boldsymbol{\vartheta}_n)\\ &+\frac{1}{2\sigma_e^2}\sum_{r=1}^{N_m}\|(\boldsymbol{K}(\boldsymbol{\theta})-\lambda_r\boldsymbol{M}(\boldsymbol{\vartheta}))\boldsymbol{\phi}_r\|^2\\ &+\frac{1}{2}\sum_{r=1}^{N_m}\frac{1}{\sigma_{\lambda_r}^2}\left(\lambda_r-\hat{\lambda}_r\right)^2+\frac{1}{2}\sum_{r=1}^{N_m}\frac{1}{\sigma_{\widehat{\boldsymbol{\psi}}_r}^2}\left(\frac{\widehat{\boldsymbol{\psi}}_r^T\boldsymbol{L}\boldsymbol{\phi}_r}{|\widehat{\boldsymbol{\psi}}_r||\boldsymbol{L}\boldsymbol{\phi}_r|}-1\right)^2\end{aligned} \tag{3.11}$$

where $\|.\|$ denotes the Euclidean norm. The above objective function was formulated by excluding the constants which are independent of the uncertain model parameters. The MPV of unknown parameters were obtained by minimizing this objective function sequentially and iteratively until some prescribed convergence criteria was satisfied [17,77].

3.3 Optimal Parameter Vectors

A linear optimization problem was employed to minimize the above objective function [17]. However, it can be seen that the direct linear optimization of Γ with respect to $\boldsymbol{\phi}_r$ cannot be possible as the above objective function is not quadratic about $\boldsymbol{\phi}_r$. To overcome this problem, Lagrange multiplier approach [20,23] was employed by introducing auxiliary variables ν_r such that

$$\nu_r^2 = \frac{1}{|\widehat{\boldsymbol{\psi}}_r|^2|\boldsymbol{L}\boldsymbol{\phi}_r|^2} \tag{3.12}$$

By utilizing Langrange multiplier approach, the objective function in Eq. (3.11) can be re-formulated as:

$$\begin{aligned}&\Gamma(\boldsymbol{\theta},\boldsymbol{\vartheta},\boldsymbol{\lambda},\boldsymbol{\phi},\boldsymbol{\nu},\boldsymbol{\gamma})\\ &\quad=\frac{1}{2}(\boldsymbol{\theta}-\boldsymbol{\theta}_n)^T\boldsymbol{\Sigma}_{\boldsymbol{\theta}}^{-1}(\boldsymbol{\theta}-\boldsymbol{\theta}_n)+\frac{1}{2}(\boldsymbol{\vartheta}-\boldsymbol{\vartheta}_n)^T\boldsymbol{\Sigma}_{\boldsymbol{\vartheta}}^{-1}(\boldsymbol{\vartheta}-\boldsymbol{\vartheta}_n)\\ &\quad+\frac{1}{2\sigma_e^2}\sum_{r=1}^{N_m}\|(\boldsymbol{K}(\boldsymbol{\theta})-\lambda_r\boldsymbol{M}(\boldsymbol{\vartheta}))\boldsymbol{\phi}_r\|^2+\frac{1}{2}\sum_{r=1}^{N_m}\frac{1}{\sigma_{\lambda,r}^2}\left(\lambda_r-\hat{\lambda}_r\right)^2\\ &\quad+\frac{1}{2}\sum_{r=1}^{N_m}\frac{1}{\sigma_{\widehat{\boldsymbol{\psi}},r}^2}\left(\nu_r\widehat{\boldsymbol{\psi}}_r^T\boldsymbol{L}\boldsymbol{\phi}_r-1\right)^2+\sum_{r=1}^{N_m}\gamma_r\left(\nu_r^2|\widehat{\boldsymbol{\psi}}_r|^2|\boldsymbol{L}\boldsymbol{\phi}_r|^2-1\right)\end{aligned} \tag{3.13}$$

where $\gamma_r, r = 1, \ldots, N_m$ are Lagrange multipliers. Because of the added constraints, the sequence of iteration starts from computing the optimal values for Lagrange multiplier and auxiliary variables while keeping other parameters at their nominal values.

3.3.1 Optimization for Auxiliary Variables and Lagrange Multipliers

By minimizing the objective function Γ given in Eq. (3.13) with respect to ν_r, the optimal value for ν_r can be obtained. After substituting the optimal value for ν_r into Eq. (3.12) and selecting the root which satisfies $\frac{\partial^2 \Gamma}{\partial \nu_r^2} > 0$, the optimal value for γ_r can be obtained. These are expressed as:

$$\nu_r^* = \frac{\sigma_{\psi,r}^{-2} \widehat{\boldsymbol{\psi}}_r^T \boldsymbol{L} \boldsymbol{\phi}_r}{\left(\left|\sigma_{\psi,r}^{-2} \widehat{\boldsymbol{\psi}}_r^T \boldsymbol{L} \boldsymbol{\phi}_r\right| \left|\widehat{\boldsymbol{\psi}}_r\right| |\boldsymbol{L} \boldsymbol{\phi}_r|\right)} = \frac{sgn\left(\sigma_{\psi,r}^{-2} \widehat{\boldsymbol{\psi}}_r^T \boldsymbol{L} \boldsymbol{\phi}_r\right)}{\left|\widehat{\boldsymbol{\psi}}_r\right| |\boldsymbol{L} \boldsymbol{\phi}_r|} \tag{3.14}$$

$$\gamma_r^* = \frac{-\sigma_{\psi,r}^{-2} \left(\widehat{\boldsymbol{\psi}}_r^T \boldsymbol{L} \boldsymbol{\phi}_r\right)^2}{2\left|\widehat{\boldsymbol{\psi}}_r\right|^2 |\boldsymbol{L} \boldsymbol{\phi}_r|^2} + \left|\sigma_{\psi,r}^{-2} \widehat{\boldsymbol{\psi}}_r^T \boldsymbol{L} \boldsymbol{\phi}_r / \left(2\left|\widehat{\boldsymbol{\psi}}_r\right| |\boldsymbol{L} \boldsymbol{\phi}_r|\right)\right| \tag{3.15}$$

where $sgn(.)$ denotes the sign or signum function.

3.3.2 Optimization for Mode Shapes

Similarly by minimizing the objective function Γ given in Eq. (3.13) with respect to $\boldsymbol{\phi}_r$, the optimal vector for $\boldsymbol{\phi}_r$ can be obtained as:

$$\boldsymbol{\phi}_r^* = \left[\sigma_e^{-2} (\boldsymbol{K}(\boldsymbol{\theta}) - \lambda_r \boldsymbol{M}(\boldsymbol{\vartheta}))^2 + \sigma_{\psi,r}^{-2} \nu_r^2 \left(\widehat{\boldsymbol{\psi}}_r^T \boldsymbol{L}\right)^T \left(\widehat{\boldsymbol{\psi}}_r^T \boldsymbol{L}\right) + 2\gamma_r \nu_r^2 \left|\widehat{\boldsymbol{\psi}}_r\right|^2 \boldsymbol{L}^T \boldsymbol{L}\right]^{-1} \tag{3.16}$$

3.3.3 Optimization for Frequencies

By minimizing the objective function Γ given in Eq. (3.13) with respect to λ_r, the optimal vector for λ_r can be obtained as:

$$\lambda_r^* = \left[\sigma_{\lambda,r}^{-2} + \sigma_e^{-2} \boldsymbol{\phi}_r^T \boldsymbol{M}(\boldsymbol{\vartheta})^2 \boldsymbol{\phi}_r\right]^{-1} \left[\sigma_e^{-2} \boldsymbol{\phi}_r^T \boldsymbol{M}(\boldsymbol{\vartheta}) \boldsymbol{K}(\boldsymbol{\theta}) \boldsymbol{\phi}_r + \sigma_{\lambda,r}^{-2} \hat{\lambda}_r\right] \tag{3.17}$$

3.3.4 Optimization for Stiffness Parameters

By minimizing the objective function Γ given in Eq. (3.13) with respect to $\boldsymbol{\theta}$, the optimal vector for $\boldsymbol{\theta}$ can be obtained as:

$$\boldsymbol{\theta}^* = [\boldsymbol{\Sigma}_{\boldsymbol{\theta}}^{-1} + \sigma_e^{-2} \boldsymbol{W}_{\boldsymbol{K}\boldsymbol{\theta}}^T \boldsymbol{W}_{\boldsymbol{K}\boldsymbol{\theta}}]^{-1} [\boldsymbol{\Sigma}_{\boldsymbol{\theta}}^{-1} \boldsymbol{\theta}_n + \sigma_e^{-2} \boldsymbol{W}_{\boldsymbol{K}\boldsymbol{\theta}}^T \boldsymbol{Q}_{\boldsymbol{K}\boldsymbol{\theta}}] \tag{3.18}$$

where $\boldsymbol{W_{K\theta}} = [\boldsymbol{K}_1\boldsymbol{\phi}_r, \boldsymbol{K}_2\boldsymbol{\phi}_r, \dots, \boldsymbol{K}_{N_\theta}\boldsymbol{\phi}_r] \in \mathbb{R}^{N_d N_m \times N_\theta}$ and $\boldsymbol{Q_{K\theta}} = [\lambda_r \boldsymbol{M}(\boldsymbol{\vartheta}) - \boldsymbol{K}_0]\boldsymbol{\phi}_r \in \mathbb{R}^{N_d N_m}$.

3.3.5 Optimization for Mass Parameters

By minimizing the objective function Γ given in Eq. (3.13) with respect to $\boldsymbol{\vartheta}$, the optimal vector for $\boldsymbol{\vartheta}$ can be obtained as:

$$\boldsymbol{\vartheta}^* = [\boldsymbol{\Sigma}_{\boldsymbol{\vartheta}}^{-1} + \sigma_e^{-2}\boldsymbol{W}_{\boldsymbol{M\vartheta}}^T \boldsymbol{W}_{\boldsymbol{M\vartheta}}]^{-1}[\boldsymbol{\Sigma}_{\boldsymbol{\vartheta}}^{-1}\boldsymbol{\vartheta}_n + \sigma_e^{-2}\boldsymbol{W}_{\boldsymbol{M\vartheta}}^T \boldsymbol{Q}_{\boldsymbol{M\vartheta}}] \tag{3.19}$$

where $\boldsymbol{W_{M\vartheta}} = [\lambda_r \boldsymbol{M}_1\boldsymbol{\phi}_r, \lambda_r \boldsymbol{M}_2\boldsymbol{\phi}_r, \dots, \lambda_r \boldsymbol{M}_{N_\vartheta}\boldsymbol{\phi}_r] \in \mathbb{R}^{N_d N_m \times N_\vartheta}$ and $\boldsymbol{Q_{M\vartheta}} = [\boldsymbol{K}(\boldsymbol{\theta}) - \lambda_r \boldsymbol{M}_0]\boldsymbol{\phi}_r \in \mathbb{R}^{N_d N_m}$.

3.4 Studied Steel Truss Bridge

The feasibility of the proposed model updating method is illustrated through an experimental study on an existing steel truss bridge. The description of studied steel truss bridge and its FE-model are presented in the following sub-sections.

3.4.1 Test Structure Description

The bridge studied was a warren type steel truss bridge constructed in 1965 over a river for road traffic [78]. The bridge consisted of five main spans, each having length of 70.77 meters and a width of 6.0 meters as shown in Fig. 3.1. All the spans of this bridge were simply supported. The tension diagonal members were an H-section and the compression diagonal members were made of a box section as shown in Fig. 3.1(c). There were eight or nine oval openings in the web of each tension diagonal members, except those at the ends of each span, for the reduction of the weight of steel. The bridge had a composite deck of steel plate girders and reinforced concrete slab. A photographic view of the truss bridge is shown in Fig. 3.2.

3.4.2 Finite Element Model of Test Structure

An initial FE-model was developed in MATLAB for this study as shown in Fig. 3.3 by modelling only one span (approach span) of the bridge due to its geometric similarity [73]. The structural members were modelled as three-dimensional frame elements. The equivalent section concept was used in modelling the concrete deck slab with added mass and stiffness properties to the stringer beams and added stiffness to the cross beams. Six DOF were considered at each joint. The employed numerical model was a 2510 DOF FE-model consisting

of 514 frame elements and 420 nodes. Lumped masses were applied to the model for the dynamical analysis of the bridge, which were calculated by geometry and the mass density of steel and inertia corresponding to rotational DOF was considered as zero. Boundary conditions were modelled by pin and roller support conditions and spring elements were introduced in order to model the dynamic friction at bridge supports. It was assumed that a spring constant of the support in the longitudinal direction was 1.0 x 10^4 kN/m, and a spring constant in the transverse rotation was 5.0 x 10^5 kNm/rad. The first five bending modes and two torsional modes obtained from eigenvalue analysis of the initial FE-model are shown in Fig. 3.4.

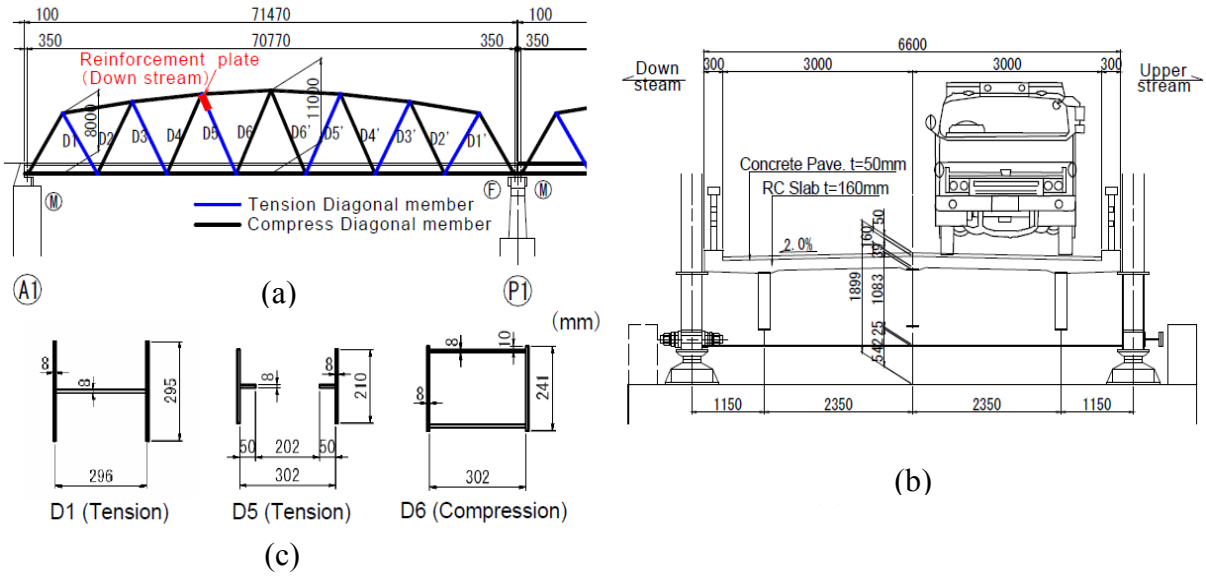

Fig. 3.1. Studied steel truss bridge; (a) Side view of the first span; (b) Cross section of bridge and (c) Cross section of diagonal members. All the units are in millimeters. [28]

Fig. 3.2. Photographic view of the studied truss bridge

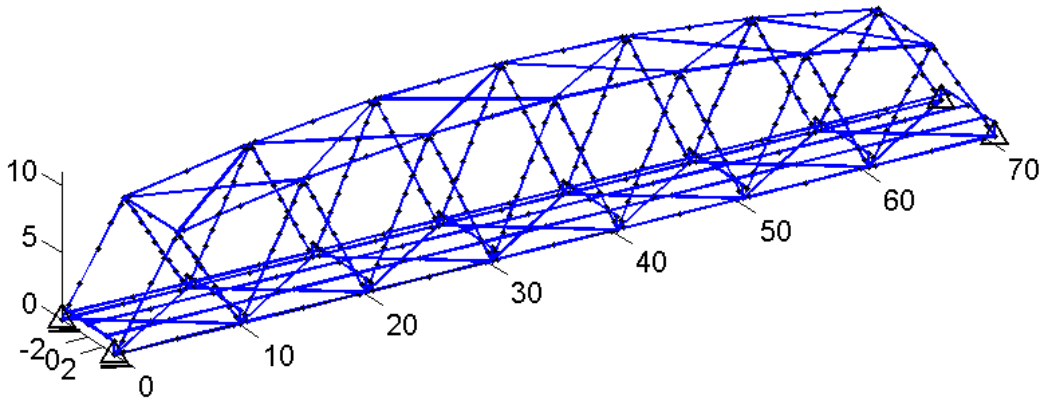

Fig. 3.3. A three dimensional FE-model developed in MATLAB

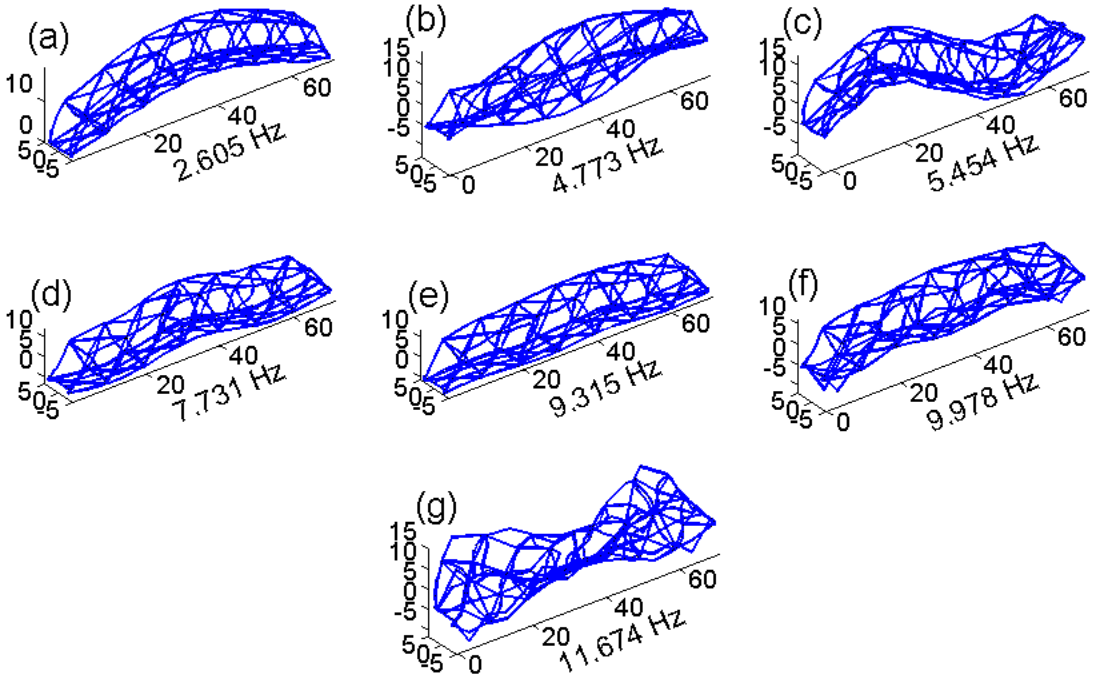

Fig. 3.4. Vibration modes obtained from the initial FE-model; (a) 1st bending, (b) 1st torsional, (c) 2nd bending, (d) 3rd bending, (e) 4th bending, (f) 5th bending and (g) 3rd torsional

3.5 Experimental Validation of Proposed Updating Framework

The feasibility of the proposed model updating method is illustrated through an experimental study on an existing steel truss bridge.

3.5.1 Vibration Measurements and System Identification

In a separate study [78], the vibration acceleration measurement was conducted by a car running test on the bridge using thirteen sensors. The measurements were made at the first span

where measurements with a wired system network were possible. Fig. 3.5 shows the layout of thirteen sensors' location along with the elevation view of the truss bridge. The measurement locations were determined for the identification of global vibration modes of the main truss. Vertical vibrations were measured at locations on the road surface close to each node in the lower chord members expect for both ends of the span where no measureable vertical vibration was expected. Additionally, vibrations were measured at the quarter point from the bottom of D5 at the upstream side, referred to as D5u. A total of five data sets of 10-min measurements were collected at a sampling rate of 100 samples per second. An example of full length recorded data measured at U5 location is shown in Fig. 3.6(a).

Free vibration (FV) responses were extracted from full length recorded data by checking the traffic free time on the bridge from the video of traffic recorded during measurements. Fig. 3.6(b) shows one such FV response extracted from full length recorded data as shown in Fig. 3.6(a). Two output-only system identification methods: Stochastic Subspace Identification (SSI) [79] and Eigensystem Realization Algorithm (ERA) [80,81] were used to identify the modal parameters from the extracted FV responses. The identification of modal parameters was done using two different techniques to ensure higher confidences against the effect of measurement noise in the recorded data as well as deviations of measured vibration from the theoretical assumption of white-noise induced vibration in case of SSI.

Stabilization diagrams were plotted corresponding to both the identification techniques as it is recognized to be the most popular tool for differentiating system modes from spurious modes. A stabilization diagram is simply a plot of various model orders versus the frequencies identified at each of these orders. The motivation is that a system mode should show up with consistent frequency, damping and mode shape at various model orders whereas the spurious ones could be expected to show a somewhat more erratic behavior. By choosing initially a high order for the state space model, system identification was performed with every model order so this procedure yields a set of modal parameters for each selected order. Parameters that belong to two different model orders were then compared according to some preset criteria such as

$$\frac{\left|f_{n,i} - f_{n+1,j}\right|}{f_{n,i}} \leq \varepsilon_f \tag{3.20}$$

$$\frac{\left|\xi_{n,i} - \xi_{n+1,j}\right|}{\xi_{n,i}} \leq \varepsilon_\xi \tag{3.21}$$

$$1 - MAC(\boldsymbol{\phi}_{n,i}, \boldsymbol{\phi}_{n+1,j}) \leq \varepsilon_{MAC} \tag{3.22}$$

where ε_f, ε_ξ and ε_{MAC} are tolerance limits to decide if mode i estimated from model order n is the same that mode j estimated from model order n+1. In the above equations, $f_{n,i}$, $\xi_{n,i}$, and $\boldsymbol{\phi}_{n,i}$ represent the ith modal frequency, modal damping ratio and mode shapes corresponding to system order n respectively. Fig. 3.7 shows the stabilization diagrams obtained from SSI an ERA by analysing data from FV1. In case of SSI, the stable modes, those verifying $\varepsilon_f = 0.01$, $\varepsilon_\xi = 0.05$, and $\varepsilon_{MAC} = 0.05$ simultaneously, had been plotted with a "⊕", while the unstable modes have been plotted with a cross "+". Fig. 3.7(a) also includes the plot of the average normalized power spectral density (PSD) of the measured data corresponding to all the measurement location. In case of ERA, the screening criteria used to extract the stable modes were $\varepsilon_f = 0.01$, $\varepsilon_\xi = 0.05$, and $\varepsilon_{MAC} = 0.1$. In addition to that extended modal amplitude coherence (EMAC) [81] was also used for further screening of the identified modes by ERA. The modes which satisfied all the above criteria simultaneously in addition to EMAC value greater than 0.3 were considered as stable modes and plotted with a "*" in Fig. 3.7(b) along with the Fourier spectra of the acceleration at U1 at the background. Fig. 3.8 shows the identified modes from both the methods and a good agreement was observed between the identified modal parameters from SSI and ERA suggesting a high level of reliability of the identified modal parameters.

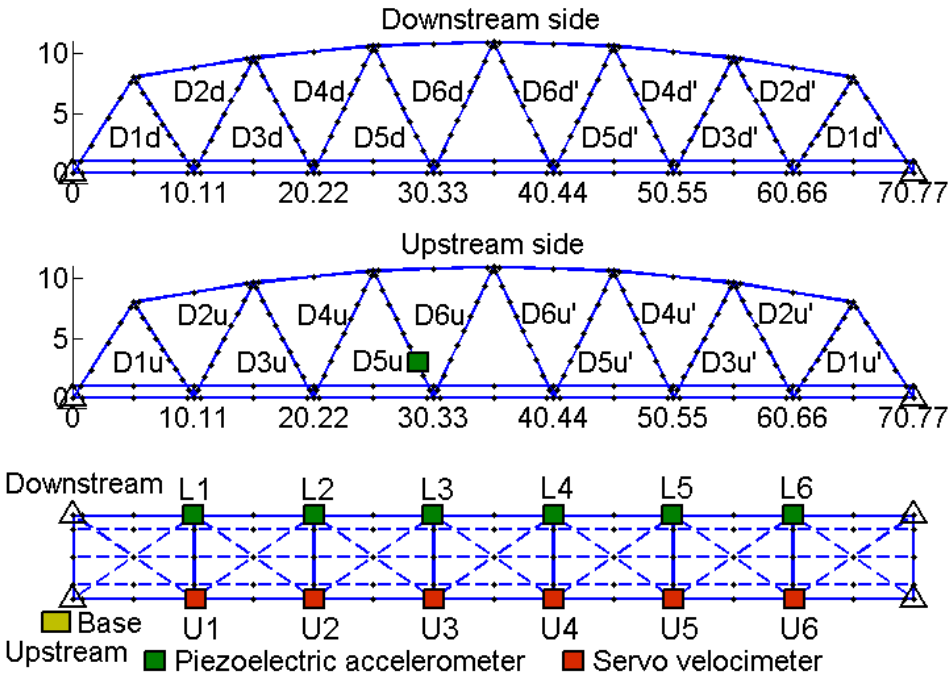

Fig. 3.5. Position of sensors during field vibration measurements at the first span

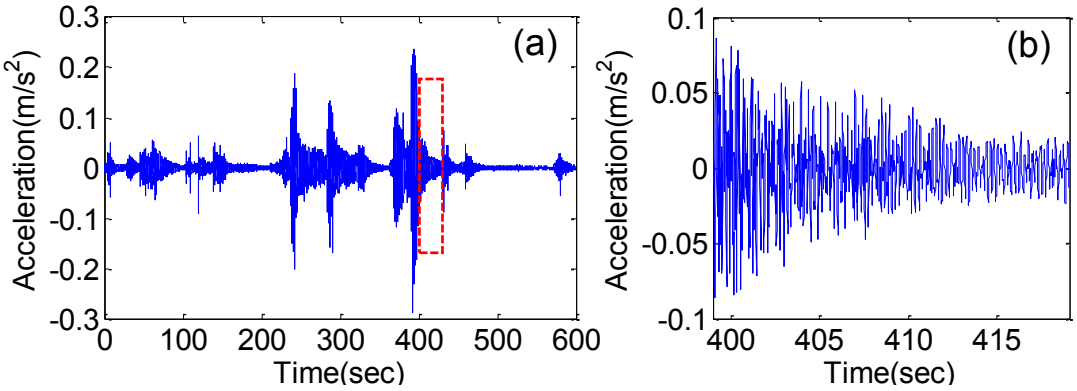

Fig. 3.6. Acceleration time history measured at U5 location; (a) Full length recorded data, (b) FV response extracted from full length recorded data

3.5.2 Parameterization of Mass and Stiffness Matrices for the Truss Bridge

For the identification of damage at local level using vibration measurements, it is necessary to update stiffness matrices of all the elements to capture the variations in the stiffness due to local changes. Also, it is evident from practical experiences that different parts of the structure are subjected to different level of deterioration due to corrosion and fatigue depending on their exposer conditions and dynamic characteristics. Hence, it is more practical to consider stiffness parameters corresponding to each element of the FE-model. In this study, four stiffness parameters were considered for each element considering both sectional and material properties resulting in a total of 2056 stiffness parameters. The stiffness parameters corresponding to the lth element are given by:

$$\boldsymbol{\theta}_{l,1} = EA_l, \boldsymbol{\theta}_{l,2} = EI_{zl}, \boldsymbol{\theta}_{l,3} = EI_{yl}, \boldsymbol{\theta}_{l,4} = GJ_l \tag{3.23}$$

where E and G are the modulus of elasticity and the modulus of rigidity of steel respectively; A_l, I_{zl}, I_{yl}, J_l are the cross-sectional area, moment of inertias about two orthogonal axes defined as z- and y-axis on cross section and polar moment of inertia of the lth element respectively.

For the parameterization of mass matrix, mass density per unit length of each section was considered as uncertain parameter. It is important to note that, the variation of mass is assumed to be much smaller compared to the stiffness due to local damage. Hence, lesser number of uncertain parameters were assigned for mass matrix. Basically, the main purpose of the parameterization of mass matrix was to make the updating results more robust to the modelling errors as explained earlier. The initial FE-model contains 46 sections which were used to assign

sectional properties of various structural members, thus, resulting in a total of 46 mass parameters. Hence, the global stiffness and mass matrices are given by:

$$\boldsymbol{K}(\boldsymbol{\theta}) = \boldsymbol{K}_0 + \sum_{i=1}^{2056} \boldsymbol{\theta}_i \boldsymbol{K}_i \text{ and } \boldsymbol{M}(\boldsymbol{\vartheta}) = \boldsymbol{M}_0 + \sum_{j=1}^{46} \boldsymbol{\vartheta}_j \boldsymbol{M}_j \tag{3.24}$$

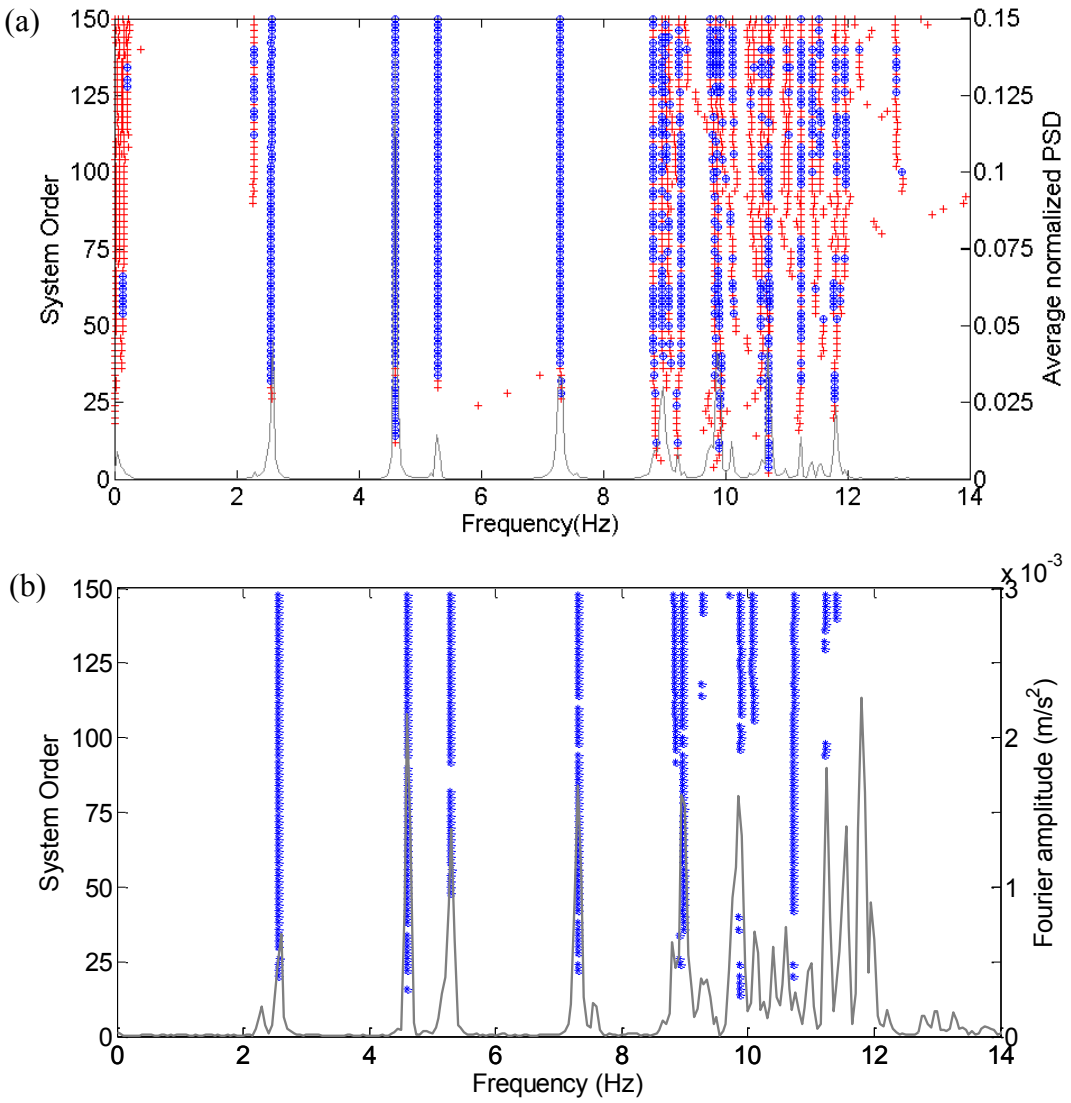

Fig. 3.7. Stabilization diagrams corresponding to FV1 obtained from; (a) SSI: ⊕, stable mode; +, unstable mode, (b) ERA: *, stable mode

3.5.3 Model Updating Results and Discussion

The model updating was carried out using proposed algorithm considering 1% coefficient of variations of the measurement error of the squared modal frequencies and mode shapes respectively for all modes. The natural frequencies and partial mode shape vectors of 12 components of the identified seven global modes were used to update the initial FE-model. The

initial model was developed with the model parameters updated manually using the modal properties identified experimentally in the previous study [78]. Table 3.1 shows the model updating results for modal frequencies and MAC values. It can be seen that the frequencies of the updated model are very close to the measured ones and MAC values are also improved, validating the proposed algorithm. Fig. 3.9 shows the comparison between the measured mode shapes (red lines) and the updated system mode shapes (green lines). The results show that the two sets of curves are almost top of each other which also suggests that the updating method is efficient in updating mode shapes though only a very few components of modes were measured. While performing the model updating, the computational time was calculated as it is one of the performance indicators for the optimization process. Total execution time was 174314.05 s for 100 iterations with a computer having Intel® Core(TM) 3.40 GHz processor and 24 GB RAM.

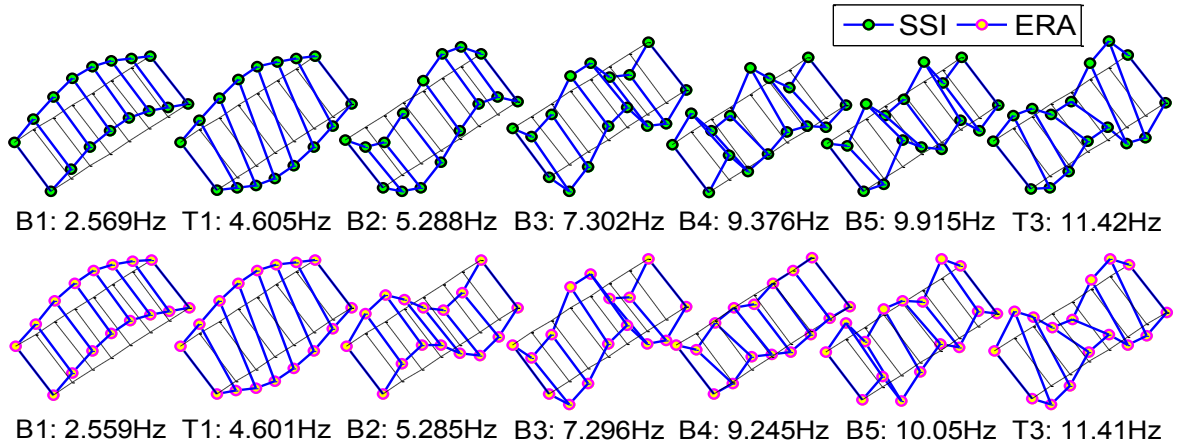

Fig. 3.8. Global modes identified by SSI and ERA from recorded data at the first span; B: Bending modes, T: Torsional modes

Table 3.1. Model updating results for frequencies and MAC values

Experimental order of Mode	Experimental f(Hz)	Initial f(Hz)	Updated f(Hz)	MAC initial	MAC Updated
1st bending	2.569	2.605	2.569	0.9956	0.9998
1st torsional	4.605	4.773	4.605	0.9987	0.9997
2nd bending	5.288	5.454	5.288	0.9917	0.9986
3rd bending	7.302	7.730	7.306	0.9502	0.9998
4th bending	9.376	9.315	9.384	0.7651	0.9983
5th bending	9.915	9.978	9.918	0.7599	0.9978
3rd torsional	11.42	11.67	11.43	0.8743	0.9998

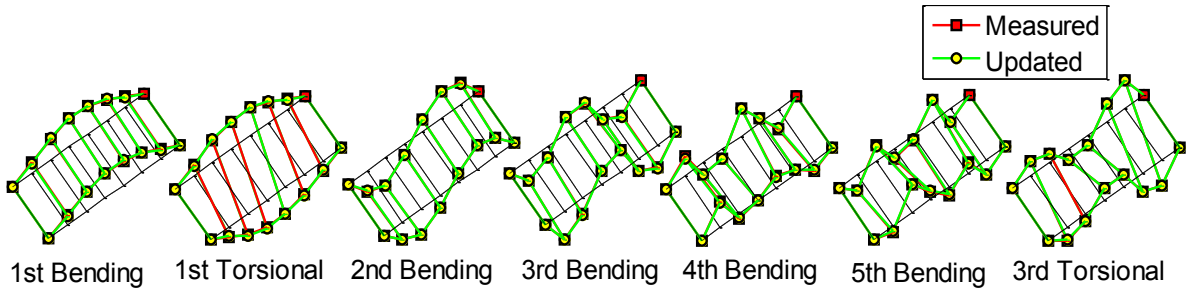

Fig. 3.9. Comparison between actual mode shapes and updated system mode shapes

It can be seen that the frequencies of the initial FE-model are close to the experimentally identified ones because the model parameters of the initial model were updated manually already in the previous study [78], as described above. Hence, to check the effectiveness of the proposed model updating framework against large discrepancy between the initial FE-model and actual structure, three different cases were considered. In case 1, the initial values of stiffness parameters were significantly overestimated by selecting the parameters from a uniform distribution over $\widetilde{\boldsymbol{\theta}}$ to $1.5\widetilde{\boldsymbol{\theta}}$ where $\widetilde{\boldsymbol{\theta}}$ is the stiffness parameters obtained by the model updating framework proposed in the present study. In case 2, the initial values of stiffness parameters were significantly underestimated by selecting the parameters from a uniform distribution over $0.5\widetilde{\boldsymbol{\theta}}$ to $\widetilde{\boldsymbol{\theta}}$. In case 3, the initial values of stiffness parameters were selected from a uniform distribution over $0.8\widetilde{\boldsymbol{\theta}}$ to $1.3\widetilde{\boldsymbol{\theta}}$ so that some parameters were overestimated and some were underestimated. The model updating was then carried out using proposed framework for each case and the results were tabulated in Tables 3.2-3.4. From these results one can conclude that the proposed model updating framework is able to update a FE-model having large discrepancy efficiently utilizing modal data that may be practically available.

Table 3.2. Model updating results for case 1

Experimental order of Mode	Experimental f(Hz)	Initial f(Hz)	Updated f(Hz)	MAC initial	MAC Updated
1st bending	2.569	2.899	2.569	0.9982	0.9987
1st torsional	4.605	5.289	4.605	0.9981	0.9970
2nd bending	5.288	6.062	5.288	0.9910	0.9998
3rd bending	7.302	8.604	7.304	0.9559	0.9998
4th bending	9.376	10.345	9.383	0.7972	0.9983
5th bending	9.915	10.896	9.916	0.7388	0.9977
3rd torsional	11.42	12.89	11.42	0.8636	0.9998

Table 3.3. Model updating results for case 2

Experimental order of Mode	Experimental f(Hz)	Initial f(Hz)	Updated f(Hz)	MAC initial	MAC Updated
1st bending	2.569	2.227	2.569	0.9992	0.9985
1st torsional	4.605	4.061	4.605	0.9975	0.9991
2nd bending	5.288	4.650	5.288	0.9896	0.9987
3rd bending	7.302	6.604	7.306	0.9589	0.9998
4th bending	9.376	7.917	9.396	0.8013	0.9983
5th bending	9.915	8.293	9.923	0.6980	0.9977
3rd torsional	11.42	9.86	11.43	0.8756	0.9998

Table 3.4. Model updating results for case 3

Experimental order of Mode	Experimental f(Hz)	Initial f(Hz)	Updated f(Hz)	MAC initial	MAC Updated
1st bending	2.569	2.652	2.569	0.9985	0.9999
1st torsional	4.605	4.838	4.605	0.9979	0.9994
2nd bending	5.288	5.544	5.288	0.9907	0.9997
3rd bending	7.302	7.870	7.303	0.9568	0.9998
4th bending	9.376	9.455	9.385	0.8000	0.9983
5th bending	9.915	9.939	9.917	0.7671	0.9978
3rd torsional	11.42	11.77	11.42	0.8768	0.9998

3.6 Conclusions

In this chapter, a Bayesian probabilistic approach for FE-model updating was presented accounting various uncertainties and utilizing incomplete modal data (modal frequencies and partial mode shapes) identified by limited number of sensors. To validate the proposed approach, an existing steel truss bridge was selected as a test-bed and modal properties were extracted from measured vibration data obtained from car running test. One new objective function was introduced for Bayesian model updating that does not require any scaling or normalization of mode shapes as the likelihood function for mode shapes was formulated based on cosine of the angle between the analytical and experimentally identified mode shapes. The initial MATLAB-based FE-model was updated using the identified modal properties by the proposed framework. It was found that the proposed updating framework is efficient enough in updating a FE-model of existing truss bridge with four stiffness parameters for each element corresponding to sectional and material properties utilizing experimental data from limited

number of sensors only. The efficiency of the proposed model updating framework against large discrepancy in the initial FE-model was also checked by significantly overestimating or underestimating the initial stiffness parameters. The model updating results confirmed the effectiveness of the proposed approach against large discrepancy in the initial FE-model as well, showing it to be both computationally efficient and robust. This makes the proposed method a deserving candidate for model updating of a large-scale structure with incomplete measured modal data.

CHAPTER 4

ENERGY-BASED DAMPING EVALUATION FOR SHM

4.1 Introduction

In this chapter, an energy-based damping model was introduced for SHM by estimating the contributions to modal damping ratios from different structural elements utilizing the data from updated FE-model. In case of large structure, such as bridges, the identification of local damage is a challenging task because of the issue of low sensitivity of frequencies and mode shapes to local damage especially due to cracks or some internal changes in the structural property. In such cases, model updating using only global modes identified with a limited number of sensors may not be able to trace the damaged stiffness parameters as the changes in the frequencies for the global modes due to local damage are not significant. On the other hand, it has been recognized that the damping is more sensitive to local damage and the advantage of using damping is that the damping change in global modes affected by local damage can be identified with a small number of sensors. These are the main motivations of considering damping for SHM of steel truss bridges in this dissertation. However, there are two major inherent difficulties in the analysis of damping for SHM: accurate identification of experimental modal damping ratios and modeling of damping to represent it analytically. In this chapter, both issues associated with damping analysis were addressed and discussed properly. The reliability in the identified modal damping ratios can be achieved by considering various FV records corresponding to different traffic conditions. An equivalent viscous damping model was considered in this study for the evaluation of analytical modal damping ratios.

4.2 Energy-based Damping Evaluation

It is common practice to express the damping of real structures in terms of equivalent viscous damping ratio which is the ratio of the given damping of an equivalent single-degree-of-freedom system to its critical damping. Using energy-based definition, this damping ratio can

be defined as the ratio of the dissipated energy per cycle to the maximum potential energy in a cycle [82,83]. Hence, the nth modal damping ratio, ξ_n can be expressed as:

$$\xi_n \equiv \frac{D_n}{4\pi U_n} \tag{4.1}$$

where D_n and U_n are the nth modal dissipating energy and nth modal potential energy per unit cycle, respectively. The nth modal dissipating energy, D_n can be expressed as the summation of dissipating energies due to different sources, such as damping capacity of materials, friction at structural connections, and energy dissipation at supports.

4.2.1 Energy-based Damping Model for Test Bridge

The studied steel truss bridge was considered to be composed of five sub-structures as shown in Fig. 4.1: diagonal members (D), girders (G), upper chord members (UC), top lateral bracings (TLB) and bottom lateral bracings (BLB). The modal energy dissipation from each sub-structure, which is referred to as the internal modal energy dissipation, $D_{i,n}$ in this dissertation, was assumed to be proportional to its modal strain energy [84,85]. Therefore, the internal modal energy dissipation of the truss bridge for the nth mode $D_{i,n}$ can be expressed as:

$$D_{i,n} = 2\pi\eta_d V_{d,n} + 2\pi\eta_g V_{g,n} + 2\pi\eta_{uc} V_{uc,n} + 2\pi\eta_{tlb} V_{tlb,n} + 2\pi\eta_{blb} V_{blb,n} \tag{4.2}$$

where $\eta_d, \eta_g, \eta_{uc}, \eta_{tlb}, \eta_{blb}$ are the equivalent loss factors of diagonal members, girders, upper chord members, top lateral bracings and bottom lateral bracings, respectively. In the present study, it was assumed that the equivalent loss factors accounted for the material damping as well as the damping at structural connection for simplicity. $V_{d,n}, V_{g,n}, V_{uc,n}, V_{tlb,n}$ and $V_{blb,n}$ are nth modal strain energies of sub-structures described above. The modal energy dissipation at supports (S), $D_{s,n}$ were expressed as

$$D_{s,n} = \sum 4A_{s,n}\mu_s R \tag{4.3}$$

where $A_{s,n}$, μ_s and R are the nth modal amplitude at the movable support, dynamic friction coefficient and support's reaction due to vertical load respectively. There may be energy dissipation at the support due to transmission of energy from supports to piers, abutments and foundations, which was assumed to be included in the energy dissipation represented by Eq. (4.3).

After calculating D_n using Eqs. (4.2) and (4.3), the nth modal damping ratio for the steel truss bridge can be evaluated using Eq. (4.1)

$$\xi_n = \frac{2\pi\eta_d V_{d,n}}{4\pi U_n} + \frac{2\pi\eta_g V_{g,n}}{4\pi U_n} + \frac{2\pi\eta_{uc} V_{uc,n}}{4\pi U_n} + \frac{2\pi\eta_{tlb} V_{tlb,n}}{4\pi U_n} + \frac{2\pi\eta_{blb} V_{blb,n}}{4\pi U_n} + \frac{8A_{s,n}\mu_s R}{4\pi U_n} \quad (4.4)$$

Therefore, as can be seen from the above equation, it is necessary to know the equivalent loss factor of each sub-structure and friction coefficient of support to evaluate the modal damping ratios of steel truss bridge. The unknown loss factors and friction coefficient can be evaluated by using experimentally identified modal damping ratios and corresponding energy ratios obtained from updated FE-model. To proceed, the Eq. (4.4) was expanded to a set of equations of m number of modes by assuming that the unknown damping parameters are independent of the vibration mode [32].

$$\begin{Bmatrix} \xi_1 \\ \vdots \\ \xi_m \end{Bmatrix} = \begin{bmatrix} \frac{2\pi V_{d,1}}{4\pi U_1} & \frac{2\pi V_{g,1}}{4\pi U_1} & \frac{2\pi V_{uc,1}}{4\pi U_1} & \frac{2\pi V_{tlb,1}}{4\pi U_1} & \frac{2\pi V_{blb,1}}{4\pi U_1} & \frac{8A_{s,1}R}{4\pi U_1} \\ \vdots & \vdots & \vdots & \vdots & \vdots & \vdots \\ \frac{2\pi V_{d,m}}{4\pi U_m} & \frac{2\pi V_{g,m}}{4\pi U_m} & \frac{2\pi V_{uc,m}}{4\pi U_m} & \frac{2\pi V_{tlb,m}}{4\pi U_m} & \frac{2\pi V_{blb,m}}{4\pi U_m} & \frac{8A_{s,m}R}{4\pi U_m} \end{bmatrix} \begin{Bmatrix} \eta_d \\ \eta_g \\ \eta_{uc} \\ \eta_{tlb} \\ \eta_{blb} \\ \mu_s \end{Bmatrix} \quad (4.5)$$

It is important to note that the number of modes considered, m should be equal to or greater than the number of unknown damping parameters in order to able to solve the above equation. The Eq. (4.5) can be solved by non-negative least-squares method (NNLS) to obtain the unknown damping parameters i.e., equivalent loss factor of each sub-structure and friction coefficient of support. After getting the loss factors and friction coefficient, the analytical modal damping ratio then can be evaluated using Eq. (4.4) and the contribution of each sub-structure to the modal damping ratio can also be evaluated.

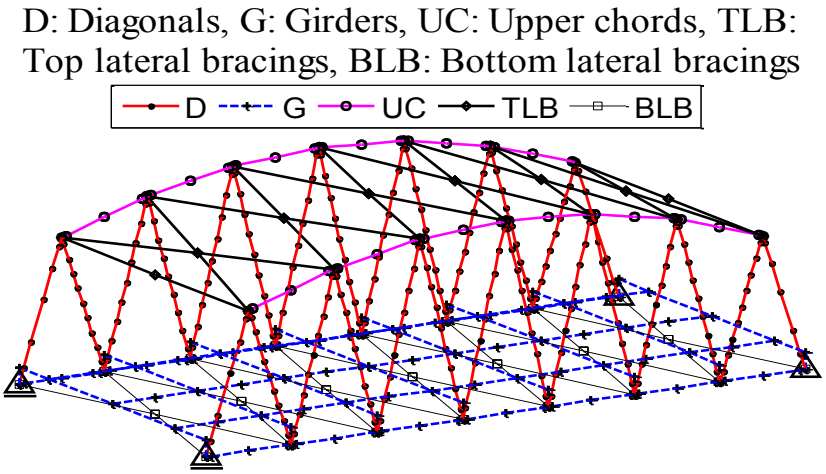

Fig. 4.1. Sub-structures considered for damping analysis

4.2.2 Elemental Damping Evaluation

In this sub-section, an extension of the above methodology to calculate the contributions from different structural elements to modal damping ratios was introduced. Using the same principle, the contribution of each internal element to the modal damping ratio, $\xi_{l,n}$ can also be obtained by using the strain energy of that element and corresponding loss factor

$$\xi_{l,n} = \frac{2\pi\eta_l V_{l,n}}{4\pi U_n} \tag{4.6}$$

where η_l and $V_{l,n}$ are the equivalent loss factor and nth modal strain energy of lth element. The equivalent loss factor of the lth element, η_l can be assumed to be the same as the loss factor of that sub-structure to which it belongs. By looking at these contributions from all the elements, one can have a clear understanding about those elements which have dominant contribution to damping for a particular mode which can be useful information from the SHM point of view. Another good aspect of this elemental damping evaluation is that it may enable one to detect damage at local level by observing the change in elemental damping parameter, such as loss factor or friction coefficient, before and after possible damage.

4.2.3 Evaluation Modal Energies

It is understood from Eq. (4.5) that the evaluation of modal potential energy and modal strain energy of each sub-structures are indispensable for the estimation of damping parameters. In order to know the contribution of each element to modal damping ratio, it is necessary to calculate strain energy of each element. The updated mode shapes and the updated stiffness matrix obtained in the previous section can be used here to evaluate the modal potential energy and modal strain energy of each element.

The nth modal potential energy, U_n and nth modal strain energy, V_n are given by

$$U_n = \frac{1}{2}\boldsymbol{\phi}_n^{*T}(\boldsymbol{K}_e^* + \boldsymbol{K}_G)\boldsymbol{\phi}_n^* = \frac{1}{2}\boldsymbol{\phi}_n^{*T}\boldsymbol{K}_T\boldsymbol{\phi}_n^* = \sum_{l=1}^{N_l}\frac{1}{2}\boldsymbol{\phi}_{l,n}^{*T}\boldsymbol{K}_{T,l}\boldsymbol{\phi}_{l,n}^* \tag{4.7}$$

$$V_n = \frac{1}{2}\boldsymbol{\phi}_n^{*T}\boldsymbol{K}_e^*\boldsymbol{\phi}_n^* = \sum_{l=1}^{N_l}\frac{1}{2}\boldsymbol{\phi}_{l,n}^{*T}\boldsymbol{K}_{e,l}^*\boldsymbol{\phi}_{l,n}^* \tag{4.8}$$

where $\boldsymbol{K}_e^*$, $\boldsymbol{K}_G$, $\boldsymbol{K}_T$ and $\boldsymbol{\phi}_n^*$ represents updated elastic stiffness matrix, geometric stiffness matrix, total stiffness matrix and nth updated mode shape of the structure; while suffix "l"

represents components of total stiffness matrix and nth updated mode shape corresponding to the lth element. N_l denotes the number of elements in the FE-model. $\boldsymbol{K}_{e,l}^{*}$ can be calculated using updated stiffness parameters for the lth element and corresponding subsystem stiffness matrices. Once the modal strain energy of each element is calculated, the contribution of each element to the modal damping ratio can be evaluated using Eq. (4.6). Here $\boldsymbol{K}_G$ was considered in the evaluation of total potential energy as the effect of $\boldsymbol{K}_G$ was found to be significant for the local modes as can be seen in Fig. 4.2.

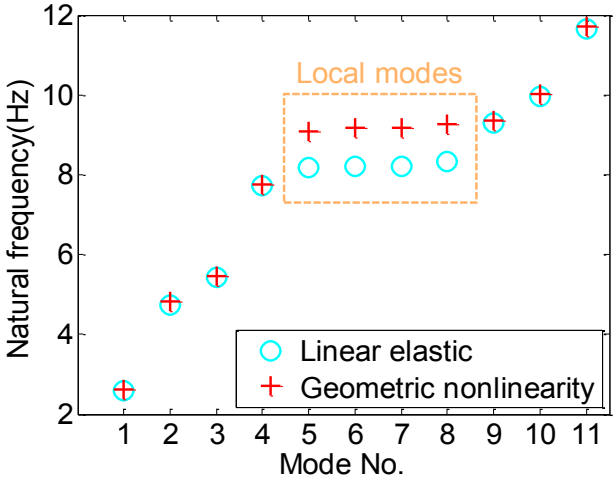

Fig. 4.2 Comparison of frequencies obtained from linear elastic and geometric nonlinear analysis

4.3 Application to Test Bridge

4.3.1 Experimental Damping Identification

The energy-based damping model requires the identification of unknown loss factors and friction coefficient which can be evaluated using experimentally identified modal damping ratios and analytically computed energy from updated FE-model. Hence, the efficiency of this method is highly dependent on the accuracy in experimental identification of damping ratios. The vibration measurements described in Section 3.5.1 enabled identification of global modes only. For the identification of diagonal modes, another two sets of measurements were carried out using the sensor setup shown in Fig. 4.3. Hence, a total of seven sets of measurements were recorded. FV records extracted from the measurement data were then processed by SSI and ERA for the identification of modal parameters. Four diagonal modes were identified as shown in Fig. 4.4 from the measurement setup shown in Fig. 4.3. Fig. 4.4 shows the bar plots of the identified mode shape vectors corresponding to sensor locations. It can be seen that the

components of mode shapes corresponding to diagonal members are dominant compared to the components corresponding to deck. Fig. 4.5 shows the modal identification results for damping and corresponding natural frequency for all the FV records by taking the average of the identified values obtained from SSI and ERA. There were slight fluctuations of the identified modal damping ratios as can be seen from Fig. 4.5. A possible source of the variation in the modal damping ratios might include the dependence of the modal damping on vibration amplitude [86].

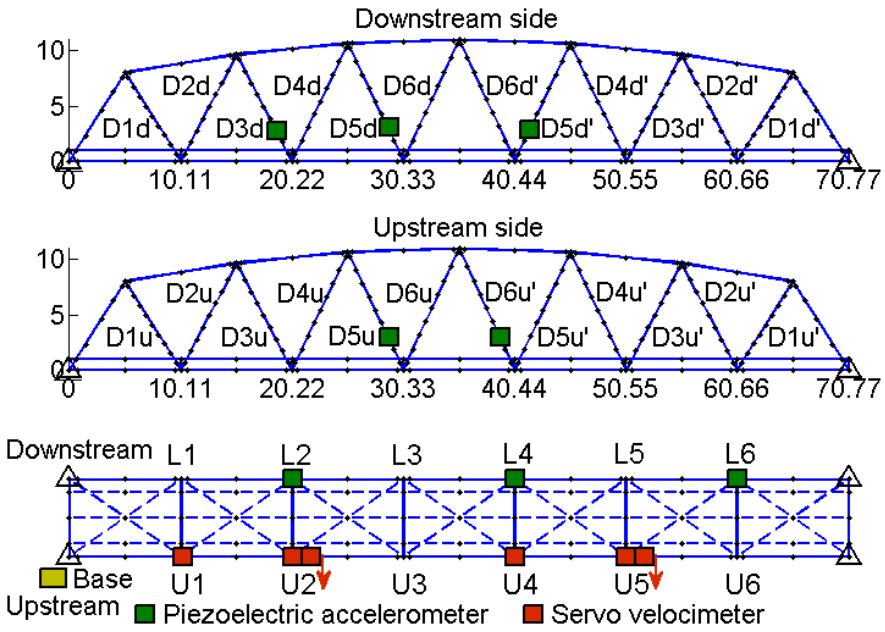

Fig. 4.3. Layout of sensors for the identification of diagonal modes

4.3.2 Identification of Loss Factors and Friction Coefficients

For the identification of equivalent loss factors and friction coefficients, it is necessary to evaluate the strain energy corresponding to each sub-structure. The strain energy of each element was calculated using updated mode shapes and updated stiffness parameters and the corresponding subsystem stiffness matrices. Then the strain energy of each sub-structure was estimated by adding the strain energies of elements belonging to that sub-structure. Fig. 4.6 shows the distribution of modal strain energy ratio of each sub-structure for first five bending modes (B1-B5), first three torsional modes (T1-T3) and 3rd diagonal mode (D3) in which the contribution of strain energy from diagonal members was dominant compared to the other diagonal modes. As seen in this figure, the bending modes have significant contribution of strain energies from upper chords, girders and diagonal members whereas the torsional modes

also have contribution of strain energies from top and bottom lateral bracing members as well in addition to those sub-structures, as expected.

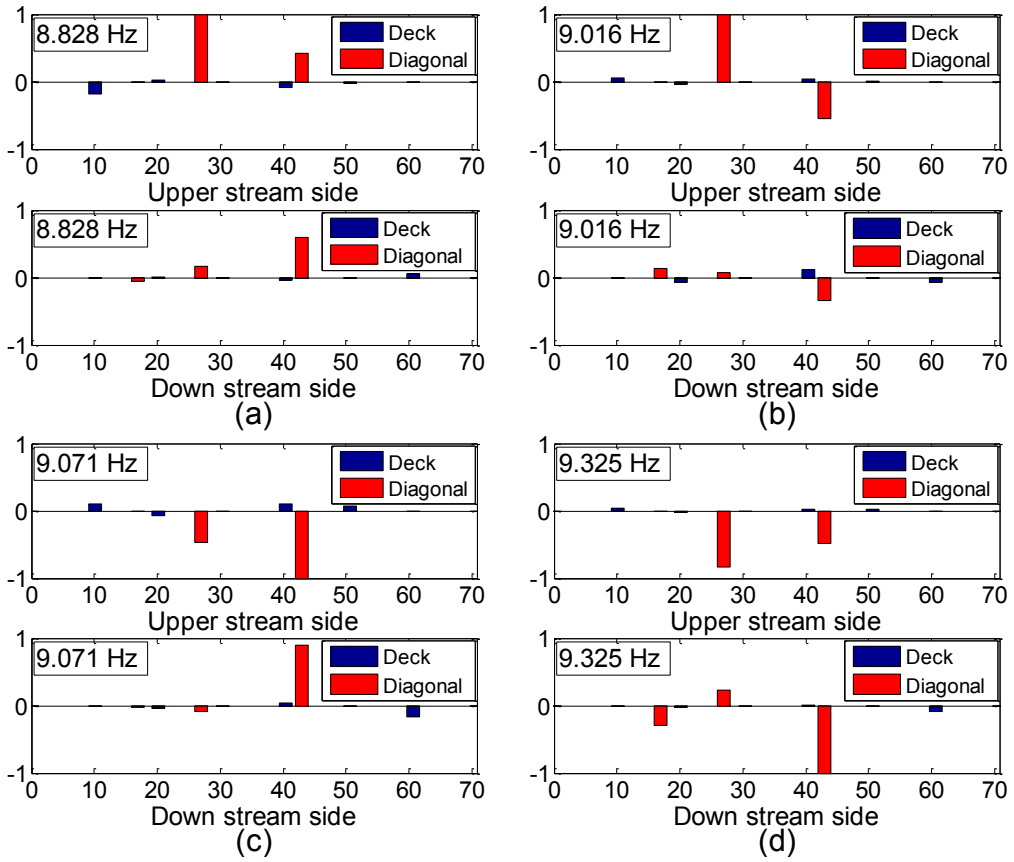

Fig. 4.4. Diagonal mode shapes identified from FV6; (a) 1st diagonal, (b) 2nd diagonal, (c) 3rd diagonal, (d) 4th diagonal

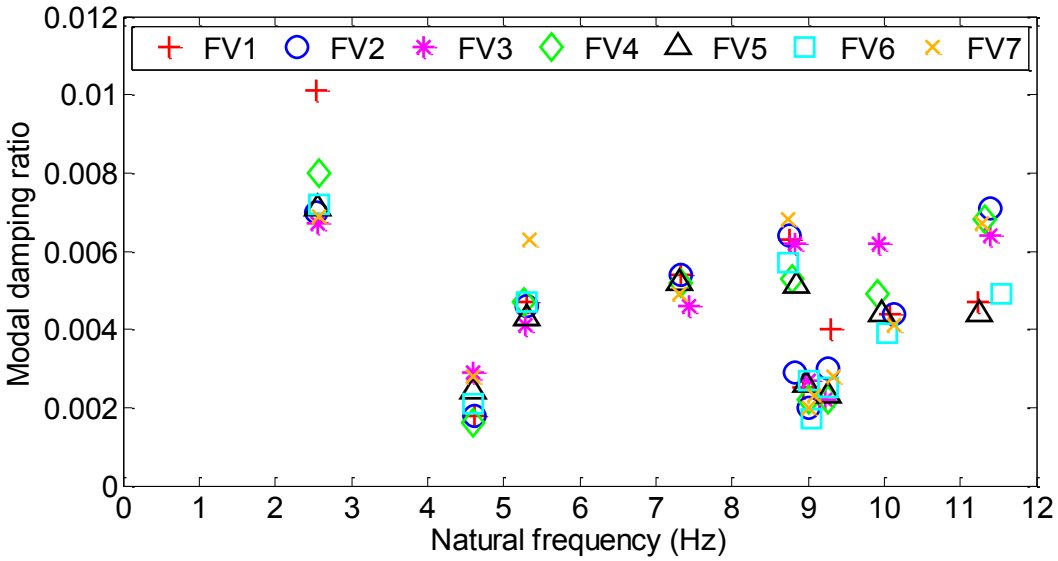

Fig. 4.5. Modal identification results for damping and corresponding natural frequency for all the FV records

Equivalent loss factors and friction coefficients were then identified following the steps described in Table 4.1. At Step 1, the equivalent loss factor of diagonal members was estimated by considering diagonal dominant mode on the assumption that the energy dissipated owing to the diagonal members only. The mean value of the estimated loss factors corresponding to different FV records was taken as the equivalent loss factor of diagonal members and used in the next step for the determination of other unknown damping parameters. At Step 2, the equivalent loss factors of girders, upper chord members, top lateral bracings and bottom lateral bracings and friction coefficient of supports were estimated by considering six global modes. Table 4.2 shows the estimated equivalent loss factors for all the FV records along with the average estimated values. Different damping parameters were estimated for different FV records owing to the fluctuation in the identified modal damping ratios. However, the reasonability of the estimated damping parameters can be judged by the fact that all estimated values are larger than the loss factor of steel which ranges from 0.0001-0.0006 [87], suggesting the assumed energy dissipation in the sub-structures.

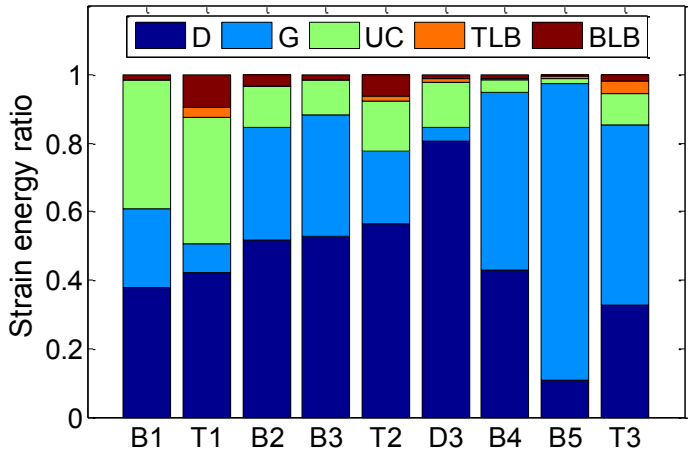

Fig. 4.6. Distribution of modal strain energy ratios

4.3.3 Evaluation of Analytical Modal Damping Ratios

After getting the equivalent loss factors, the analytical modal damping ratios were evaluated using Eq. (4.4) by substituting the loss factors and corresponding energy ratios. Fig. 4.7 shows the comparison between experimentally identified and analytically estimated modal damping ratios for different FV records. In this figure, mode numbers 1-6 correspond to the modes considered for the identification of damping parameters in Table 4.1. It can be seen that analytically evaluated modal damping ratios agree well with the experimentally identified ones for all the FV records. Fig. 4.8 shows the comparison between analytical modal damping ratios

estimated using average loss factors and friction coefficient shown in Table 4.2 and corresponding experimental damping by taking average over all the FV records. Here also, it can be seen that analytically evaluated modal damping ratios agree well with the experimentally identified ones.

Table 4.1. Steps for estimating loss factors and friction coefficient

Analysis step	Considered mode	FV record	Estimated parameter	Analysis conditions
Step 1	3rd diagonal (Dominant diagonal mode)	FV 1 to 6	η_d	Assumed that energy dissipated only from diagonal members
Step 2	1: 1st bending 2: 2nd bending 3: 3rd bending 4: 2nd torsional 5: 4th bending 6: 3rd torsional	FV 1 to 7	$\eta_{uc}, \eta_g, \eta_{tlb}, \eta_{blb}, \mu_s$	Average value of η_d from Step 1 was used NNLS was employed to get equivalent loss factors

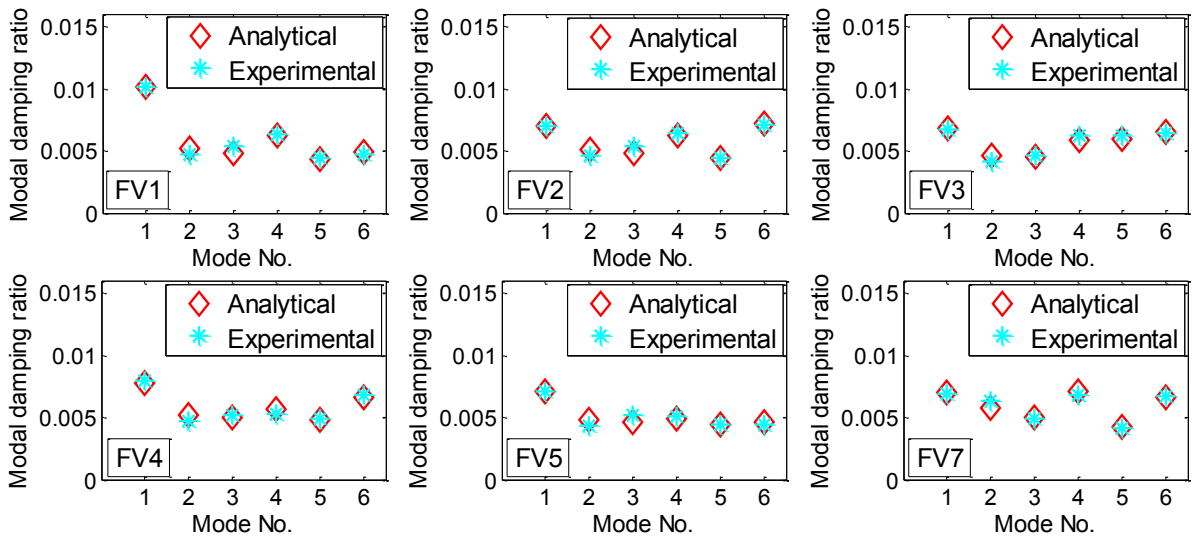

Fig. 4.7. Comparison of experimentally and analytically estimated modal damping ratios

The contribution of each sub-structure to the modal damping ratios was then estimated by using corresponding loss factor and energy ratio. Fig. 4.9 shows the contribution of damping from each sub-structure to the modal damping ratios estimated analytically with the average damping parameters shown in Table 4.2. From Fig. 4.9(a), it can be seen that there is a significant damping contribution from support for the 1st bending mode as it is expected due

to the slip of the movable support in longitudinal direction. There is also dominant damping contribution from upper chord members due to bending of these members in this mode. For other bending modes, there are significant damping contribution from upper chords, girders and diagonal members, however, the damping contribution from supports is much less than the 1st bending mode. In Fig. 4.9(b), the significant contribution of modal damping from top and bottom lateral bracings for the 1st torsional mode express the torsional effect in that mode. Similar trends can also be found in the 2nd and 3rd torsional modes as can be seen in Figs. 4.9(e) and 4.9(i). In the diagonal mode, the dominant damping contribution from diagonal members can be observed from Fig. 4.9(f).

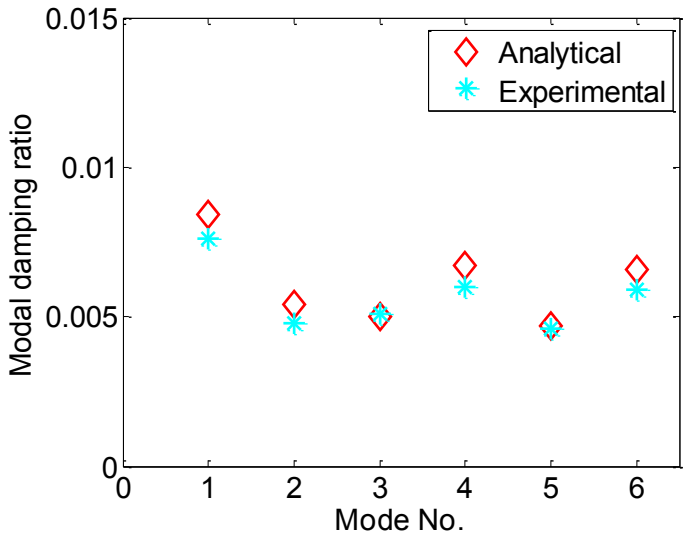

Fig. 4.8. Comparison of average experimental modal damping ratios and corresponding analytical modal damping ratios

Table 4.2. Estimated equivalent loss factors and friction coefficient for the first span

Analysis step	Para-meter	FV1	FV2	FV3	FV4	FV5	FV6	FV7	Avg.
Step 1	η_d	0.0085	0.0068	0.0073	0.0100	0.0068	0.0073	-	0.0078
Step 2	η_{uc}	0.0206	0.0245	0.0000	0.0277	0.0183	0.0136	0.0226	0.0212
	η_g	0.0085	0.0077	0.0121	0.0090	0.0088	0.0074	0.0075	0.0087
	η_{tlb}	0.0000	0.1532	0.0914	0.1041	0.0000	0.0346	0.0982	0.0963
	η_{blb}	0.0000	0.0196	0.0021	0.0000	0.0027	0.0211	0.0692	0.0229
	μ_s	0.7688	0.0025	0.7753	0.0288	0.2545	0.4476	0.0000	0.3796

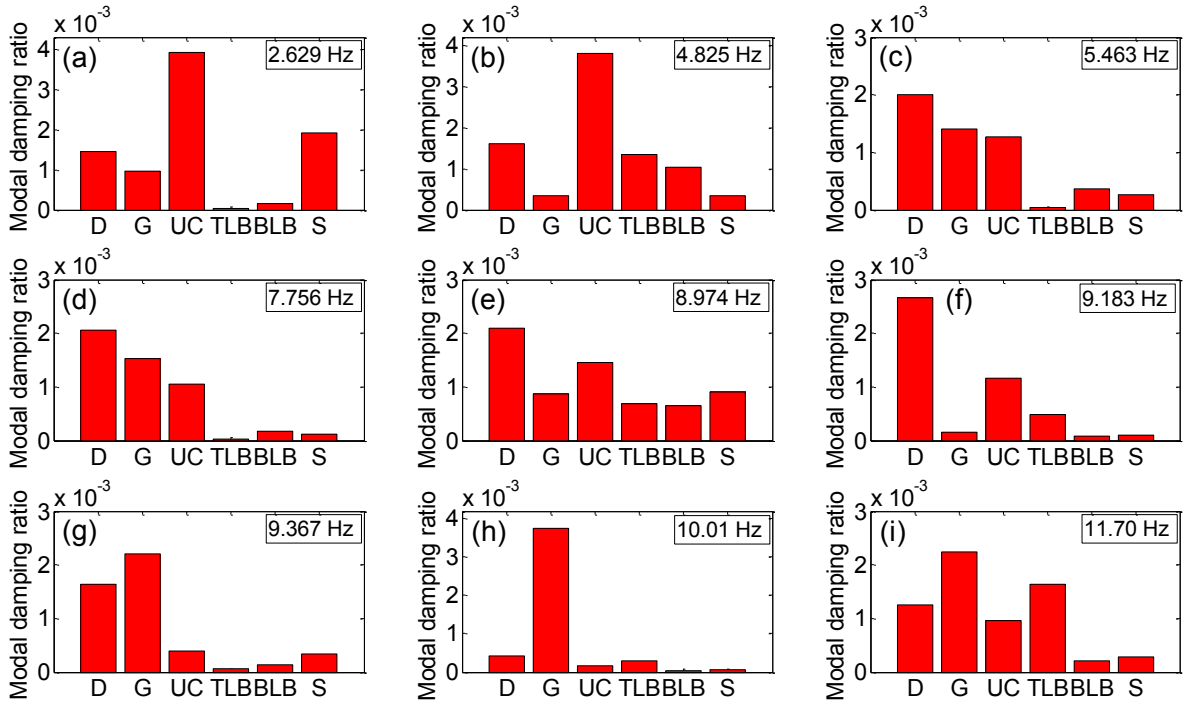

Fig. 4.9. Contribution of each damping source to modal damping ratios for: (a) 1st bending, (b) 1st torsional, (c) 2nd bending, (d) 3rd bending, (e) 2nd torsional, (f) 3rd diagonal, (g) 4th bending, (h) 5th bending and (i) 3rd torsional mode

4.3.4 Contribution of Modal Damping from Each Element

Using the same energy-based damping definition, the contribution of modal damping ratios from each element was estimated by using corresponding loss factor and modal energy ratio (MER) in Eq. (4.6). In this dissertation, the MER was defined as the ratio of modal strain energy of a structural component to the modal potential energy of the whole structure. The assumption here was that all the elements in a sub-structure had the same loss factor which was equal to the loss factor of that sub-structure. Fig. 4.10 shows the elements contributing largely to the modal damping ratio for the 1st bending mode, 1st torsional mode and 3rd diagonal mode respectively. The dissipation of energy occurs mainly from the upper chord members due to the bending in vertical direction for the 1st bending mode as can be seen from Fig. 4.10(a). In case of the 1st torsional mode, the elements from upper chords, top and bottom lateral bracings and diagonals have dominant contribution to damping as can be seen from Fig. 4.10(b). The diagonal elements which have dominant damping contribution can be observed in Fig. 4.10(c). From similar plots for other modes, one should be able to identify the elements contributing largely to the energy dissipation for a particular mode. This kind of information can be useful for the identification of damage in case of large structures, such as bridges, especially when

the problem related to low sensitivity of frequencies and mode shapes due to local damage remains a concern and model updating using these two modal parameters inadequate to trace the changes in stiffness parameters due to local damage. In such cases, increases in modal damping due to damages can be attributed to increases in damping contribution from elements which have damage. Those increases in damping contribution from damaged elements will be identified as increases in the loss factors of the elements. It should be noted that, if this is the case, the loss factors identified will differ from the actual loss factors of the elements due to errors in the stiffness parameters and the estimation of strain energy.

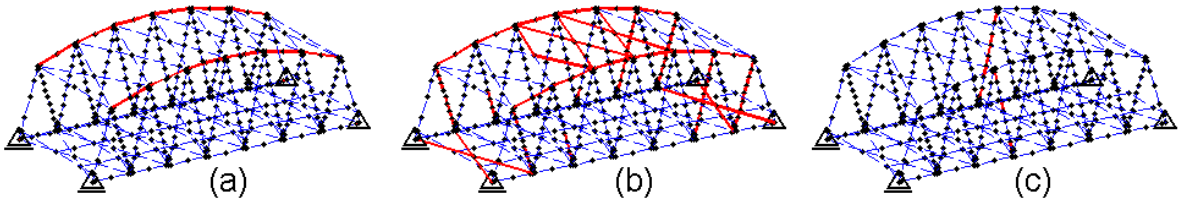

Fig. 4.10. Elements having significant analytical modal damping ratio (shown in red colour): (a) >0.3% of modal damping for 1st bending, (b) >0.1% of modal damping for 1st torsional, and (c) >1% of modal damping for 3rd diagonal mode

4.4 Conclusions

In this chapter, energy-based damping evaluation was carried out for the test structure. An equivalent viscous damping model was considered in this study for the evaluation of analytical modal damping. The updated mode shapes and the updated stiffness matrix obtained in the previous chapter were used to evaluate the modal potential energy and modal strain energy of each element of the updated FE-model. The evaluation of analytical modal damping has an advantage that the contribution of energy dissipations in sub-structures on modal damping ratios can be estimated which could be useful knowledge in the field of vibration-based SHM. For the studied truss bridge, five sub-structures were considered to investigate the contribution of modal damping from different components of the structure. The main conclusions derived from this can be summarized as:

1. Equivalent loss factors and friction coefficient were estimated using experimentally identified modal damping ratios and corresponding modal energies. It was found that the equivalent loss factors of all the sub-structures are different.
2. The analytical modal damping ratios evaluated using the proposed framework showed good agreements with the corresponding experimental ones.

3. Significant damping contribution from supports was observed for the 1st bending mode as it was expected due to the slip of the movable support in longitudinal direction. For torsional modes, significant damping contributions from top and bottom lateral bracings were observed due to torsional effect in those modes.
4. An extension of the existing framework by Dammika et al. [32] was introduced to calculate the contributions from different structural elements to modal damping ratios. The proposed framework can be used to detect local damage by observing the change in elemental modal damping ratios before and after possible damage.

CHAPTER 5

APPLICATION OF PROPOSED FRAMEWORK TO SHM WITH A SMALL NUMBER OF SENSORS

5.1 Introduction

For the application of vibration-based SHM to steel truss bridge to detect local damages, such as fatigue cracks, corrosion, and bolt loosening, a large number of sensors may be required because of the low sensitivity issue of frequencies and mode shapes to local damage. Hence, it leads to a trade-off between monitoring cost and ability of damage detection. It would be, therefore, worth to develop a method to detect damage or evaluate structural state with less number of sensors. For SHM with less number of sensors, complimentary theoretical consideration is necessary which is discussed in this chapter. A previous study by Yoshioka, et al. [28] reported that the studied bridge with damage at local diagonal member showed a significant increase in the damping of global vibration mode of the structure. The present study utilized the energy-based damping evaluation to identify the cause of the modal damping increase by observing the change in the contribution from different structural elements on the modal damping ratios.

5.2 Problem Description

A large crack at the lower end part of D5u diagonal member (see Fig. 5.1) was observed in the fourth span of the same bridge. As an emergency measure, reinforcing plates were installed inside and outside of the flange and web. Fig. 5.2 shows the damaged D5u member and its reinforced condition. Field vibration measurements of this span were carried out before and immediately after reinforcement using five accelerometers only as shown in Fig. 5.1. The three accelerometers on diagonal member were placed at quarter point of damaged D5u member to measure vibrations in three orthogonal axes. Table 5.1 shows the modal identification results by ERA for frequencies and damping that were averaged over identified parameters corresponding to nine sets of recorded data for before and after reinforcement conditions of

D5u diagonal member. It was observed that the changes in natural frequencies of the global modes due to damage are much smaller than the change in modal damping ratios. However, significant changes in both natural frequency and modal damping ratio were observed in the case of diagonal mode. It can also be observed that the frequency of the diagonal mode came very close to the frequency of the 3rd bending mode due to damage. The standard deviation (SD) of the identified modal damping ratios, shown in the parentheses, were not large so that the average values identified could be considered reliable. More details of the measurement at the fourth span and discussion on the modal parameters identified experimentally have been described in [78].

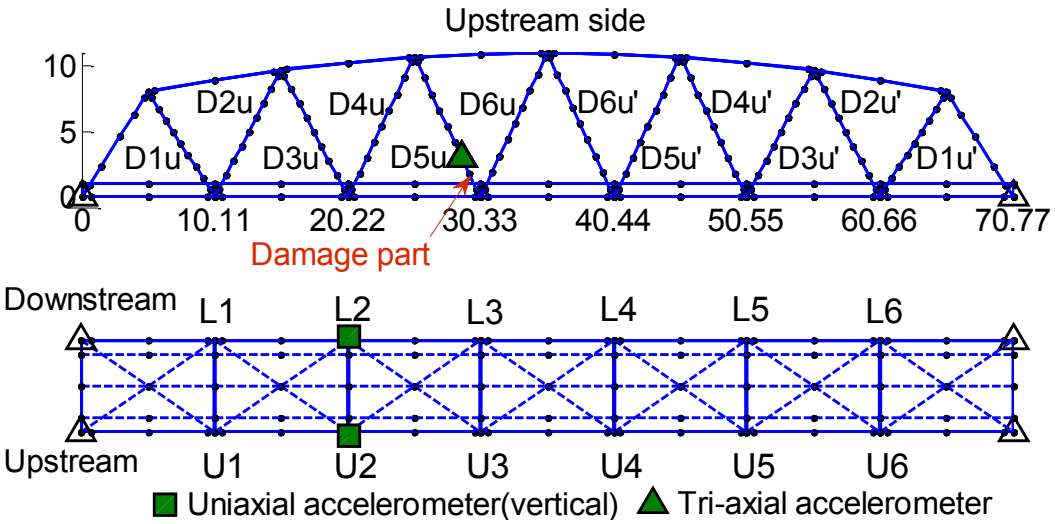

Fig. 5.1. Layout of sensors for the fourth span

Fig. 5.2. Damaged and reinforced conditions of D5u diagonal member

In order to simulate the damage in the FE-model, the sectional properties of all the elements of D5u diagonal member (Elements 436-443) were reduced to half. The frequencies of the FE-model show a reasonable agreement with the corresponding experimental identification, as observed in Table 5.1. The change in the natural frequency of diagonal mode due to damage,

which resulted in close natural frequencies for the diagonal and 3rd bending modes, can also be confirmed from the simulated damaged FE-model. Because of this closeness in frequency, dynamic coupling [78] of D5u diagonal member was observed in the 3rd bending mode as can be seen in Fig. 5.3(b). Here, it is important to note that, the proposed model updating framework was not applied here to identify the damaged stiffness parameters corresponding to the damaged D5u diagonal member because of the limitation of the number of identified modes and too less components of experimentally identified mode shapes. In a situation where the location of damage is not known, the identification of damaged stiffness parameters by the proposed FE-model updating framework requires a large array of sensors at both deck and diagonal members, leading to an increase in monitoring cost and time. In that case, identifying the change in updated stiffness parameters would be sufficient to detect damage at local level without going into the analysis of damping discussed in this section. However, in many practical situations, the model updating using only global modes identified with a limited number of sensors may not be able to trace the damaged stiffness parameters as the changes in the frequencies for the global modes due to local damage are not significant. The advantage of using the damping, as used in this study, is that the damping change in global modes affected by local damage can be identified with a small number of sensors [78].

Table 5.1. Modal identification results of frequencies and damping for the fourth span

Identified modes	Natural frequency (Hz)					Modal damping ratio		
	Experimental			FE-model		Experimental		
	Before	After	Rate	Before	After	Before(SD)	After(SD)	Rate
1st bending	2.577	2.604	-1%	2.615	2.629	0.0093 (0.0020)	0.0069 (0.0007)	35%
2nd bending	5.254	5.313	-1%	5.394	5.463	0.0072 (0.0014)	0.0061 (0.0009)	18%
3rd bending	7.143	7.295	-2%	7.604	7.756	0.0106 (0.0009)	0.0060 (0.0007)	77%
Diagonal	7.135	9.783	-27%	7.164	9.184	0.0055 (0.0008)	0.0039 (0.0017)	41%

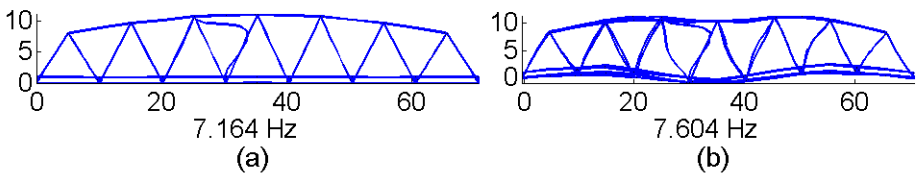

Fig. 5.3. Modes obtained from damaged FE-model of the fourth span; (a) Diagonal, (b) 3rd bending

5.3 Identification of Loss Factors for Damaged Span

To understand possible causes of the significant change in experimentally identified modal damping ratios for global modes due to damage in D5u diagonal member, the analytical modal damping ratios were evaluated for this span using the same energy-based damping model. Due to the limitation of number of identified modes shown in Table 5.1, only the loss factors of diagonal members, girders and upper chord members, which appeared to be the dominant contributors of damping in those modes as observed in Fig. 4.9, were estimated using the experimentally identified modal damping ratios at the fourth span. Loss factors of other sub-structures were assumed to be the same as those of the first span which are given in Table 4.2. At first, the analytical modal damping ratios corresponding to the after reinforcement (AR) condition were evaluated. Table 5.2 shows the analysis steps for the identification of loss factors for AR condition. The value of the equivalent loss factors of diagonal members, girders and upper chord members obtained from the above analysis were 0.0115, 0.0130 and 0.0078 respectively. For before reinforcement (BR) condition, the equivalent loss factor of damaged D5u member (η_{d5}) was estimated by considering D5u diagonal in-plane mode shown in Fig. 5.3(a). In this step, the equivalent loss factor for other diagonal members was taken as 0.0115 which is corresponding to AR condition. In the second step, the loss factors of girders, upper chord members for BR condition were taken to be the same as the AR condition as the damage was observed in D5u diagonal member only. Table 5.3 shows the identified damping parameters for the fourth span for AR and BR conditions. In case of BR condition, significant increase in equivalent loss factor of damaged D5u diagonal member was observed.

Table 5.2. Analysis steps for the identification of equivalent loss factors for AR condition

Analysis step	Considered mode	Estimated parameter	Analysis conditions
Step 1	Diagonal	η_d	Assumed that energy dissipated only from diagonal members
Step 2	1: 1st bending 2: 2nd bending 3: 3rd bending	η_{uc}, η_g	Same values of $\eta_{tlb}, \eta_{blb}, \mu_s$ from reinforced first span were used here NNLS was employed to get equivalent loss factors

Table 5.3. Damping parameters corresponding to AR and BR conditions

Damping parameters	η_{d5}	η_d	η_g	η_{uc}	η_{tlb}	η_{blb}	μ_s
AR	0.0115	0.0115	0.0130	0.0078	0.0963	0.0229	0.3796
BR	0.0172	0.0115	0.0130	0.0078	0.0963	0.0229	0.3796

5.4 Damage Detection Using Change in Analytical Modal Damping Ratios

5.4.1 Evaluation of Analytical Modal Damping Ratios for Damaged Span

The modal damping ratios of the identified global modes were then analytically evaluated using the damping parameters listed in Table 5.3 and the corresponding MER of sub-structures obtained from the FE-model. Table 5.4 shows the experimentally identified and analytically evaluated modal damping ratios for AR and BR conditions. The percentage changes in analytically evaluated modal damping ratios were also listed in the last column of Table 5.4. It can be seen that analytically evaluated modal damping ratios agree well with the corresponding experimental ones for AR condition because the damping parameters for three sub-structures were identified with the experimental data for AR condition as shown in Table 5.2. However, for BR condition, such kinds of agreements between the analytically evaluated and experimentally identified modal damping ratios were not observed.

Very small amount of changes were observed in analytically evaluated modal damping ratios of first two bending modes due to damage in D5u diagonal member, although significant amount of changes were observed in experimentally identified damping ratios of these two modes. In case of the 3rd bending mode, an increment of around 17% was observed in analytical modal damping ratio, although this change was much smaller than the change in experimental modal damping ratio.

Table 5.4. Experimentally identified and analytically evaluated modal damping ratios

Mode	Experimental AR	Analytical AR	Experimental BR	Analytical BR	% Change in Analytical ξ
1st bending	0.0069	0.0070	0.0093	0.0071	1.4%
2nd bending	0.0061	0.0061	0.0072	0.0064	4.9%
3rd bending	0.0060	0.0059	0.0106	0.0069	16.9%

For the 3rd bending mode, the modal damping contribution from each element was estimated using Eq. (15) for both AR and BR conditions. Fig. 5.4 shows the bar diagram plots of change

in elemental modal damping ratios evaluated analytically between AR and BR conditions. The changes in elemental modal damping ratios of Elements 436 to 443 that correspond to D5u diagonal member are much higher than the changes in other elements for the coupled 3rd bending mode. This result suggests that the elemental modal damping ratios can be used to detect damage at local level by observing change in elemental modal damping ratios of the coupled bending mode identified with a small number of sensors, which could lead to an effective SHM based on vibration measurement. It is worthy to note here that to identify the damaged stiffness parameters by FE-model updating a large number of sensors is required, however, with a small number of sensors one can identify the change in modal properties for lower order global modes and seek a possibility to identify damage from that information along with relevant analysis instead of updating model with data from a large array of sensors at deck and diagonal members.

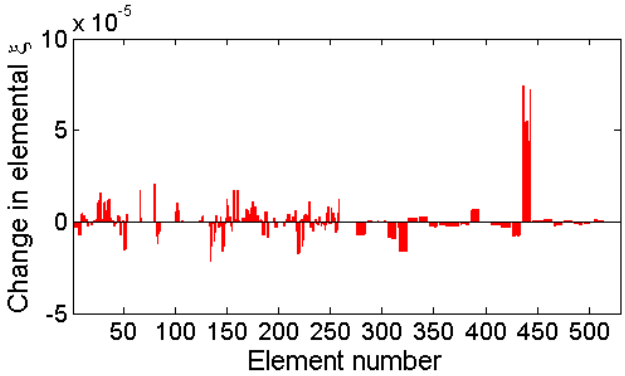

Fig.5.4. Bar diagram of change in elemental modal damping ratios for 3rd bending mode

It is understood from Eq. (4.4) that the change in modal damping ratios can only be possible if there is change either in equivalent loss factors or in MER of sub-structures or due to both. Hence to investigate further, the distribution of MER of each sub-structure in AR and BR conditions are compared in Fig. 5.5. The values of the MER of all the sub-structures for the first three bending modes are also listed in Table 5.5. From this comparison, it can be seen that the distribution of MER of diagonal members, girders and upper chord members remain almost the same for global modes due to the local damage at D5u diagonal member. On the other hand, some changes in the distribution of MER of top and bottom lateral bracings and supports were observed as can be seen from Table 5.5, although, their contributions are much smaller compared to the contributions from diagonals, girders and upper chord members. From the energy-based damping model as given in Eq. (4.4), it is understood that the modal damping ratio is proportional to the equivalent loss factors and friction coefficient for a constant MER of each sub-structure. Hence, there must be some increase in equivalent loss factor(s) of one or

several sub-structures as well due to damage at D5u diagonal member, as the experimental identification results for BR condition clearly indicated significant increase in modal damping ratios of first three bending modes. Some changes in loss factors of the sub-structures which appear not to have damage could be possible, if the modal damping ratios are found to be dependent on the amplitude of vibration which is discussed in more details in next sub-section.

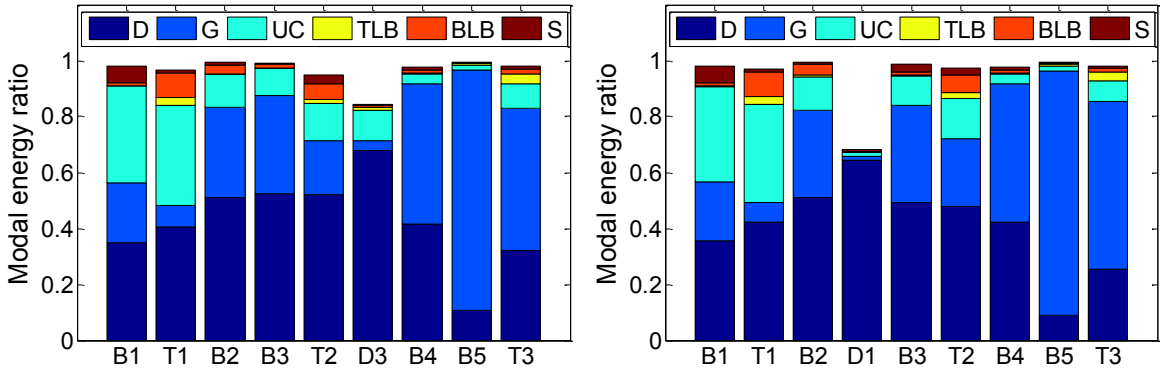

Fig. 5.5. Distribution of MER of each sub-structure; (a) AR, (b) BR

Table 5.5. The values of the MER of all the sub-structures at AR and BR conditions

Members	MER of sub-structures $(V_{n,i}/U_n)$					
	1st bending		2nd bending		3rd bending	
	AR	BR	AR	BR	AR	BR
D	0.3728	0.3791	0.5151	0.5136	0.5256	0.5054
G	0.2246	0.2230	0.3246	0.3152	0.3524	0.3583
UC	0.3693	0.3650	0.1204	0.1214	0.0995	0.1063
TLB	0.0006	0.0007	0.0009	0.0055	0.0004	0.0024
BLB	0.0129	0.0128	0.0321	0.0379	0.0148	0.0134
S	0.0633	0.0647	0.0090	0.0072	0.0042	0.0261

5.4.2 Re-analysis of Loss Factors for Damaged Span

The loss factors of sub-structures were re-identified using the experimentally identified modal damping ratios of first three bending modes for BR condition. However, due to the limitation of number of identified modes, only the loss factors of girders and upper chord members were re-estimated following the same steps as described in Table 5.2. The values of equivalent loss factors of girders and upper chords members were obtained as 0.0258 and 0.0078 respectively. Comparing these values with the corresponding values in Table 5.3, there was a significant increase in the equivalent loss factor of girders from 0.0130 to 0.0258, although the value of

the loss factor of upper chord members remains unchanged at 0.0078. Fig. 5.6 shows the comparison of experimentally identified and analytically evaluated modal damping ratios for both AR and BR conditions and the values are also listed in Table 5.6. A much better agreement between experimentally identified and analytically evaluated modal damping ratios were observed for BR condition when there was the increase in loss factor of girders along with the increase in loss factor of damaged diagonal member (see Tables 5.4 and 5.6).

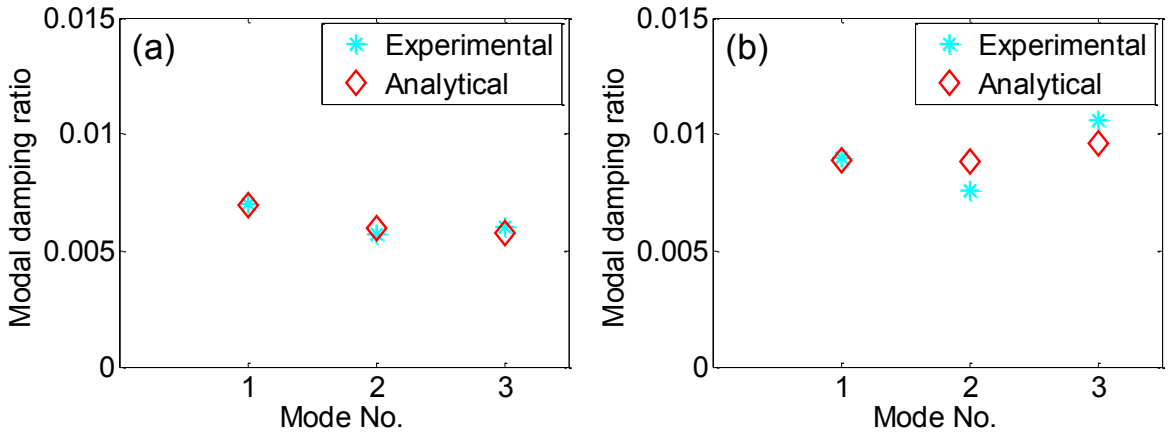

Fig. 5.6. Comparison of experimentally identified and analytically evaluated modal damping ratios; (a) AR, (b) BR

Table 5.6. Experimentally identified and analytically evaluated modal damping ratios after re-analysis of loss factors

Mode	Experimental **AR**	Analytical **AR**	Experimental **BR**	Analytical **BR**	% Change in Analytical ξ
1st bending	0.0069	0.0070	0.0093	0.0092	31.4%
2nd bending	0.0061	0.0061	0.0072	0.0078	27.9%
3rd bending	0.0060	0.0059	0.0106	0.0097	64.4%

5.4.3 Justification against Change in Loss Factors and Discussion

To investigate that much of change in the loss factor of girders, the distribution of MER of different components of girders such as cross beams (CB), stringers (St) and lower chords (LC) were studied. Table 5.7 shows the values of the MER of different components of girders for AR and BR conditions for the first three bending modes. The percentage change in the MER of each component with respect to the AR condition was also listed in the same table. Significant changes were observed in the distribution of MER of lower chords for the 2nd and 3rd bending modes due to damage at D5u diagonal member. Some changes in the distribution of MER of other components were observed as well for the 2nd and 3rd bending modes.

However, the distribution of MER of the 1st bending mode was almost unaffected by the damage.

To understand the change in the distribution of modal damping ratios of various components of girder, the distribution of MER of elements near to the damaged D5u member were studied. Fig. 5.7 shows the elements of girders near to the damaged D5u member. Table 5.8 shows the MER of elements near to the damaged D5u member for first three bending modes. The results suggest significant increase in MER for the 3rd bending mode in Element 9 and 10, which are the elements of lower chords, due to damage. For the 2nd bending mode, the MER of Elements 9 and 10 were reduced whereas the MER of Elements 1306 and 1307, which are the elements of stringers, were increased significantly. These changes at elemental level are consistent with the change in different components of girder observed in Table 5.7. On the other hand, the MER from all these elements almost remain the same for the 1st bending mode. From these results, it is clear that the damage in D5u diagonal member has some effects on the distribution of MER for the 2nd and 3rd bending modes and it is more prominent for the 3rd bending mode due to the coupling with the local motion of D5u damaged diagonal member. The change in the loss factors of girder sub-structure observed between AR and BR conditions may be attributed to the change in modal energy distribution as discussed above and the non-homogeneity in the loss factors of different components of girders. While considering the same loss factor for a non-homogeneous sub-structure such as girders due to the limitation of number of identified modes in the present study, some weighting factors can be introduced to express non-identical contributions of damping from different components of a non-homogeneous sub-structure. The selection of weighting factors could be based on the actual exposure conditions and material properties of these components in real structure. In this study, the concrete deck slab was modelled by equivalent section concept with added mass and stiffness properties to stringer beams and added stiffness to the cross beams. Thus higher weightage values can be assigned to stringers and cross beams compared to the lower chords as viscous damping of reinforced concrete is higher than the steel.

The increase in the loss factor of girders also might have attributed to the fact that the same values of loss factors and friction coefficient of the first span were used in the fourth span for top and bottom lateral bracings and supports, although it was observed that the modal damping ratios of the fourth span are different from the first span even for AR condition. Although the contributions of damping from these sub-structures were smaller individually, collectively their contribution can be significant and could affect the results as well.

Table 5.7. MER of different components of girders for AR and BR conditions

Member	MER of different components of girder								
	1st bending			2nd bending			3rd bending		
	AR	BR	%	AR	BR	%	AR	BR	%
CB	0.0275	0.0272	-0.8	0.0656	0.0661	0.7	0.1225	0.1176	-4.0
St	0.0601	0.0599	-0.3	0.0949	0.1035	9.0	0.1739	0.1704	-2.0
LC	0.1371	0.1358	-1.0	0.1640	0.1456	-11.3	0.0560	0.0702	25.4

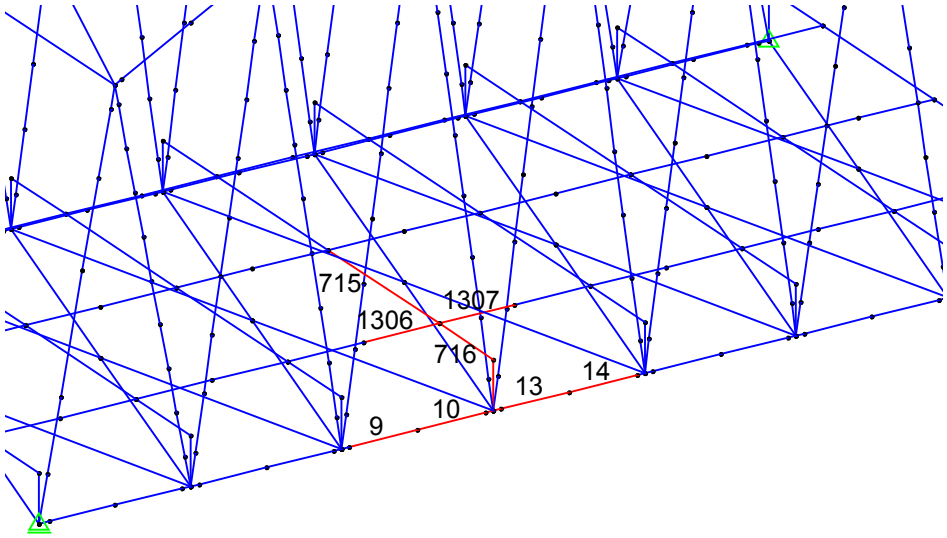

Fig.5.7. Elements of girder near to the damaged D5u diagonal member

Table 5.8. MER of elements near to the damaged D5u member

Element No.	MER of elements $(V_{n,i}/U_n)$					
	1st bending		2nd bending		3rd bending	
	AR	BR	AR	BR	AR	BR
9	6.22e-3	5.93e-3	2.84e-3	1.98e-3	8.71e-4	1.63e-3
10	6.03e-3	5.82e-3	2.84e-3	1.93e-3	9.37e-4	1.73e-3
13	7.15e-3	7.11e-3	3.03e-4	3.71e-4	3.83e-3	4.03e-3
14	7.14e-3	7.09e-3	3.11e-4	3.55e-4	3.94e-3	4.16e-3
715	1.47e-3	1.37e-3	2.04e-3	2.42e-3	9.08e-3	8.73e-3
716	1.33e-4	1.09e-4	2.24e-4	1.95e-4	1.61e-3	2.05e-3
1306	1.77e-3	1.76e-3	1.81e-3	2.62e-3	7.25e-4	6.39e-4
1307	2.11e-3	2.29e-3	8.04e-4	1.60e-3	9.83e-3	1.11e-2

Possible reasons for the increase in the loss factor of girder could include the amplitude dependence of the loss factor. Yamaguchi et al. [78] found that the modal damping ratios for the lower order modes, in particular the 1st bending mode, of the bridge studied in the present

study showed the dependence on amplitude in which the modal damping ratios tended to increase with increase in the initial modal amplitude. It was also reported in that study that the modal damping ratios for the higher order modes including the coupled bending mode did not show any clear sign of amplitude dependence. To investigate more on this, the initial modal amplitudes of vibration at measurement locations obtained from ERA were listed in Table 5.9. From this table, it can be seen that the initial modal amplitudes of girders for 1st and 2nd bending modes are much higher in BR condition compared to AR condition which might have caused the increase in the modal damping for these two modes. For the 3rd bending mode, a significantly large amplitude of D5u member was observed in BR condition. If the loss factor of D5u is amplitude-dependent, then the loss factor of D5u member for the 3rd bending mode in BR condition would be much higher compared to that for the damaged diagonal mode and this increase in the loss factor might have caused the significant increase in the modal damping ratio for the 3rd bending mode. Considering the above hypothesis, the loss factor of damaged D5u member for the 3rd bending mode was evaluated as 0.1047, keeping the loss factors of all other sub-structures same as the AR condition, which was clearly much higher than the corresponding value of 0.0172 for the damaged diagonal mode. Here, the consideration of amplitude-dependent loss factor could be reasonable as the damage discussed in this dissertation was due to cracks that could induce significant increase in frictional damping which is expected to be dependent on the amplitude of vibration. Hence, the analytical model for damping using energy-based approach could be modified considering amplitude-dependent loss factors to express the substantial change in the modal damping ratio of coupled global mode more reasonably in case of damage in diagonal member of steel truss bridges, which could be the future works in this field.

Table 5.9. Initial modal amplitudes at measurement locations for AR and BR conditions

Mode	Amp. at AR condition (m/s^2)			Amp. at BR condition (m/s^2)		
	Amp. at U2	Amp. at L2	Amp. at D5u	Amp. at U2	Amp. at L2	Amp. at D5u
1st bending	0.0058	0.0062	0.0001	0.0255	0.0270	0.0050
2nd bending	0.0126	0.0128	0.0033	0.0261	0.0246	0.0015
3rd bending	0.0053	0.0043	0.0021	0.0053	0.0083	0.1488
Diagonal	0.0008	0.0014	0.0342	0.0024	0.0011	0.0583

5.5 Conclusions

In this study, an energy-based damping model was introduced for practical and effective SHM based on vibration measurement by estimating the contribution of modal damping ratios from different structural elements utilizing the data from updated FE-model and the identification results of damping from a small number of sensors. The main conclusions of this chapter can be summarized as:

1. The results of energy-based damping evaluation implied that substantial change found experimentally in the damping for the global mode coupled with diagonal mode was caused by significant increase in the equivalent loss factor of damaged diagonal member.
2. From the investigation of damping of damaged span, it was found that the loss factors can be dependent on the amplitude of vibration. The consideration of amplitude-dependent loss factor could be reasonable as the damage discussed in this dissertation was due to cracks that could induce significant increase in frictional damping which is expected to be dependent on the amplitude of vibration.
3. It was also found that the initial modal amplitudes of girders for 1st and 2nd bending modes are much higher in BR condition compared to AR condition which might have caused the increase in the modal damping for these two modes.
4. The proposed approach may be able to detect damage at local level by investigating analytically the contribution from structural elements to the damping of global mode coupled with vibration of local member in steel truss bridges.

CHAPTER 6

SUMMARY AND FUTURE WORKS

The studies taken up in this dissertation have developed a global method for vibration-based SHM using Bayesian model updating and energy-based damping evaluation for an existing steel truss bridge. Summary and detailed discussions have been taken up at the end of relevant chapters. The purpose of this chapter is to recapitulate the main findings, unifying them and to suggest some further research directions.

6.1 Summary of the Contributions Made

Difficulties in practical application of vibration-based SHM of structures include considerable amount of uncertainties in structural modeling and vibration measurement and sensitivity issues of modal parameters due to local damage in case of large structure. This dissertation proposes an analytical framework for SHM addressing the aforementioned difficulties by combining two techniques: a Bayesian based probabilistic approach for FE-model updating that accounts for the underlying uncertainties, and an energy-based damping evaluation for detecting damage at local level. The proposed vibration-based SHM approach could be promising in detecting damage at local level when the problem related to low sensitivity of frequencies and mode shapes due to local damage remains a concern and damage detection by change in stiffness parameters using FE-model updating utilizing data from a large number of sensors is not practically feasible due to limitation of budget and time.

The first step of the proposed methodology is to develop a baseline model using Bayesian probabilistic approach. For that an initial FE-model of the studied truss bridge was developed in MATLAB for the ease and faster analysis instead of linking a finite element analysis package with MATLAB. The structural members were modelled as three-dimensional frame elements. Six DOFs are considered at each joint. In this dissertation, the Bayesian statistical framework was considered as it is capable of incorporating all types of available information, all types of

uncertainties and incomplete experimental data. An advanced Bayesian statistical framework was proposed in this dissertation by introducing a new objective function and a realistic parameterization of mass and stiffness matrices to address the difficulties associated with the practical application of Bayesian model updating. In this framework, the likelihood function for mode shapes is formulated based on the cosine of the angle between the analytical and measured mode shapes which does not require any scaling or normalization.

It is evident from practical experiences that different parts of the structure are subjected to different level of deterioration due to corrosion and fatigue depending on their exposer conditions and dynamic characteristics. Hence, it is more practical to consider stiffness parameters corresponding to each element of the FE-model. In this dissertation, a realistic and reasonable parameterization of stiffness matrix was introduced by considering four stiffness parameters for each element considering both sectional and material properties. For the parameterization of mass matrix, mass density per unit length of each section was considered as uncertain parameter. It is important to note that, the variation of mass was assumed to be much smaller compared to the stiffness due to local damage. Hence, lesser number of uncertain parameters were assigned for mass matrix. Basically, the main purpose of the parameterization of mass matrix was to make the updating results more robust to the modelling errors. The proposed updating method was validated experimentally by updating a FE-model of existing steel truss bridge. It was found that the proposed updating framework was efficient enough in updating a FE-model of existing truss bridge having large discrepancy utilizing experimental data from limited number of sensors only.

After getting the updated FE-model which is supposed to be free from all the underlying uncertainties mentioned above, the next step is to use that for structural analysis and SHM. In this dissertation, an energy-based damping model was introduced for practical and effective SHM based on vibration measurement by estimating the contribution of modal damping ratios from different structural elements utilizing the data from updated FE-model and the identification results of damping from a small number of sensors. A previous study reported that the studied bridge with damage at local diagonal member showed a significant increase in the damping of global vibration mode of the structure. The energy-based damping evaluation was utilized to identify the cause of the modal damping increase by observing the change in the contribution from different structural elements on the modal damping ratios. The results of energy-based damping evaluation implied that substantial change found experimentally in the

damping for the global mode coupled with local vibration of damaged diagonal member was caused by the significant increase in the equivalent loss factor of damaged diagonal member. The results also suggested that the elemental modal damping ratios can be used to detect damage at local level by observing the change in elemental modal damping ratios of the coupled bending mode identified with a small number of sensors, which could lead to an effective SHM based on vibration measurement.

In summary, the work conducted in this dissertation achieved the followings:

- Introduction of a new objective function by considering cosine of angle between the analytical and measured mode shapes in the likelihood function for mode shapes which does not require any normalization of mode shapes as compared to conventional Bayesian methods (Chapter 3)
- Introduction of a realistic parameterization of mass and stiffness matrices for FE-model updating (Chapter 3)
- Development of a FE-model of studied truss bridge in MATLAB for the ease and faster analysis instead of linking a finite element analysis package with MATLAB (Chapter 3)
- Extension of existing framework to calculate the contributions of modal damping ratios from different structural elements of FE-model (Chapter 4)
- Estimation of loss factors of different structural components corresponding to damaged conditions (Chapter 5)
- Introduction of a methodology to detect local damage by investigating analytically the contribution from structural elements to the damping of global mode coupled with vibration of local member in steel truss bridges (Chapter 5)

6.2 Suggestions for Further Works

The study conducted in this dissertation throws some general questions on vibration-based SHM. The followings are some important areas of research which emerge immediately from this study:

- From the experimental identification results of damaged span, it was observed that the changes in natural frequencies for global modes due to local damage were not significant. Hence, the FE-model updating using only global modes may not be able to

trace the damaged stiffness parameters. On the other hand significant changes in the modal damping ratios for global modes were observed due to local damage. Therefore, it would be worthy to develop a methodology for FE-model updating considering damping as well in addition to frequencies and mode shapes as the observed data in the objective function.

- Development of appropriate damping model to express the energy dissipation mechanism more realistically to overcome the limitation of existing framework of energy-based damping evaluation where viscous damping model was assumed for simplicity. Real structures often do not show purely viscous damping and, in case of damage, energy dissipation mechanism depends on the types of damage. Hence, further study is needed to model damping of a damaged structure more appropriately.
- In this dissertation, it was found that the loss factors can be dependent on the amplitude of vibration. The consideration of amplitude-dependent loss factor could be reasonable as the damage discussed in this dissertation was due to cracks that could induce significant increase in frictional damping which is expected to be dependent on the amplitude of vibration. Hence, the analytical model for damping using energy-based approach could be modified considering amplitude-dependent loss factors to express the substantial change in the modal damping ratio of coupled global mode more reasonably in case of damage in diagonal member of steel truss bridges.
- Development of optimal sensor placement (OSP) methodology to get sufficient information about the dynamic behaviour of a large structural system with a small number of sensors that are practically available.

CHAPTER 7

CONCLUSIONS

In this dissertation, a vibration-based SHM approach that combined two techniques was presented. A Bayesian based probabilistic approach was proposed for FE-model updating utilizing incomplete modal data (modal frequencies and partial mode shapes) and an energy-based damping evaluation was introduced for detecting damage at local level by using a small number of sensors. The main conclusions of this dissertation can be summarized as:

1. One new objective function was introduced for Bayesian model updating that does not require any scaling or normalization of mode shapes as the likelihood function for mode shapes was formulated based on cosine of the angle between the analytical and experimentally identified mode shapes.
2. A realistic parameterization of mass and stiffness matrices were introduced for FE-model updating to take into account any variation in stiffness due to local changes.
3. It was found that the proposed updating framework is efficient enough in updating a FE-model of existing truss bridge with four stiffness parameters for each element corresponding to sectional and material properties utilizing experimental data from limited number of sensors only.
4. The modal damping ratios can be analytically evaluated by using energy-based damping definition and a method to know the contribution of modal damping ratios from different structural elements of a FE-model was introduced.
5. The results of energy-based damping evaluation implied that substantial change found experimentally in the damping for the global mode coupled with diagonal mode was caused by significant increase in the equivalent loss factor of damaged diagonal member.
6. The proposed approach may be able to detect damage at local level by investigating analytically the contribution from structural elements to the damping of global mode coupled with vibration of local member in steel truss bridges.

REFERENCES

1. Fujino Y and Siringoringo DM. Structural health monitoring of bridges in Japan: an overview of the current trend, Proceedings of the 4th International Conference on FRP Composites in Civil Engineering, Zurich, 2008.

2. National Guideline. Guideline for periodic inspection of bridges, Ministry of Land, Infrastructure, Transport and Tourism, Japan, 2014. (in Japanese)

3. Nakamura M, Masri SF, Chassiakos AG, Caughey TK. A method for non-parametric damage detection through the use of neural networks. *Earthquake Engineering and Structural Dynamics* 1998; 27(9):997-1010.

4. Nair KK, Kiremidjian AS, Law KH. Time series-based damage detection and localization algorithm with application to the ASCE benchmark structure. *Journal of Sound and Vibration* 2006; **291**:349–68.

5. Salawu O. Detection of structural damage through changes in frequency: a review. *Engineering Structures* 1997; **19**(9):718-723.

6. Vanik MW, Beck JL, Au SK. Bayesian probabilistic approach to structural health monitoring. *Journal of Engineering Mechanics* 2000; **126**(7):738–45.

7. Goller B, Beck JL, Schueller GI. Evidence-based identification of weighting factors in Bayesian model updating using modal data. *Journal of Engineering Mechanics* 2012; **138**(5):430-40.

8. Soize C, Capiez-Lernout E, Ohayon R. Robust updating of uncertain computational models using experimental modal analysis. *AIAA Journal* 2008; **46**(11):2955–65.

9. Govers Y, Link M. Stochastic model updating-covariance matrix adjustment from uncertain experimental modal data. *Mechanical Systems and Signal Processing* 2010; **24**(3):696–706.

10. Simoen E, De Roeck G, Lombaert G. Dealing with uncertainty in model updating for damage assessment: a review. *Mechanical Systems and Signal Processing* 2015; **56–57**:123–49.

11. Beck JL, Katafygiotis LS. Updating models and their uncertainties. I: Bayesian statistical framework. *Journal of Engineering Mechanics* 1998; **124**(4):455-61.

12. Sohn H, Law KH. Bayesian probabilistic damage detection of a reinforced-concrete bridge column. *Earthquake Engineering and Structural Dynamics* 2000; **29**(8):1131-52.

13. Yuen KV, Au SK, Beck JL. Two-stage structural health monitoring approach for Phase I benchmark studies. *Journal of Engineering Mechanics* 2004; **130**:16–33.

14. Beck JL, Au SK, Vanik MW. Monitoring structural health using a probabilistic measure. *Computer-Aided Civil and Infrastructure Engineering* 2001; **16**:1–11.

15. Ching J, Muto M, Beck JL. Structural model updating and health monitoring with incomplete modal data using Gibbs sampler. *Computer-Aided Civil and Infrastructure Engineering* 2006; **21**(4):242–57.

16. Gardoni P, Reinschmidt KF, Kumar R. A Probabilistic Framework for Bayesian Adaptive Forecasting of Project Progress. *Computer-Aided Civil and Infrastructure Engineering* 2007; **22**(3):182-96.

17. Yuen KV, Beck JL, Katafygiotis LS. Efficient model updating and monitoring methodology using incomplete modal data without mode matching. *Structural Control and Health Monitoring* 2006; **13**(1):91–107.

18. Papadimitriou C, Papadioti DC. Component mode synthesis techniques for finite element model updating. *Computers and Structures* 2013; **126**:15–28.

19. Ching J, Beck JL. New Bayesian model updating algorithm applied to a structural health monitoring benchmark. *Structural Health Monitoring* 2004; **3**:313–32.

20. Yan WJ, Katafygiotis Lambros S. A novel Bayesian approach for structural model updating utilizing statistical modal information from multiple setups. *Structural Safety* 2015; **52**:260–71.

21. Behmanesh I, Moaveni B. Probabilistic identification of simulated damage on the Dowling Hall footbridge through Bayesian finite element model updating. *Structural Control and Health Monitoring* 2015; **22**:463–483.

22. Mustafa S, Debnath N, Dutta A. Bayesian probabilistic approach for model updating and damage detection for a large truss bridge. *International Journal of Steel Structures* 2015; **15**(2):473-85.

23. Au SK. Assembling mode shapes by least squares. *Mechanical Systems and Signal Processing* 2011; **25**(1):163–79.

24. Doebling SW, Farrar CR, Prime MB. A summary review of vibration-based damage identification methods. *Shock and Vibration Digest* 1998; **30**(2):91–105.

25. Fan W, Qiao P. Vibration-based damage identification methods: a review and comparative study. *Structural Health Monitoring* 2011; **10**:83–129.

26. Modena C, Sonda D, Zonta D. Damage localization in reinforced concrete structures by using damping measurements, Damage assessment of structures. *Proceedings of the international conference on damage assessment of structures*, *DAMAS 99* 1999; 132–141.

27. Curadelli RO, Riera JD, Ambrosini D, Amani MG. Damage detection by means of structural damping identification. *Engineering Structures* 2008; **30**(12):3497-3504.

28. Yoshioka T, Yamaguchi H, Matsumoto Y. Structural health monitoring of steel truss bridges based on modal damping changes in local and global modes. *Proceedings of 5th World Conference on Structural Control and Monitoring, International Association for Structural Control and Monitoring*: Los Angeles, 2010; **167**.

29. Kawashima K, Nagashima H, Iwasaki H. Evaluation of modal damping ratio based on strain energy proportional damping method. *Proceedings of 9th U.S.–Japan Bridge Engineering Workshop, Public Works Research Institute (PWRI)* 1994;211-26.

30. Yamaguchi H, Jayawardena L. Analytical estimation of structural damping in cable structures. *Journal of Wind Engineering and Industrial Aerodynamics* 1992; **41/44**:1961–72.

31. Yamaguchi H, Takano H, Ogasawara M, Shimosato T, Kato M, Kato H. Energy-based damping evaluation of cable-stayed bridges and application to Tsurumi Tsubasa bridge. *Structural Engineering Earthquake Engineering, JSCE* 1997; **14**(2):201s–213s.

32. Dammika AJ, Kawarai K, Yamaguchi H, Matsumoto Y, Yoshioka T. Analytical Damping Evaluation Complementary to Experimental Structural Health Monitoring of Bridges. *Journal of Bridge Engineering* 2014; **20**(7).

33. Huang Q, Gardoni P, Hurlebaus S. A probabilistic damage detection approach using vibration-based nondestructive testing. *Structural Safety* 2012; **38**:11-21.

34. Farrar CR, Doebling SW, Nix DA. Vibration-based Structural Damage Identification, *Philosophical Transactions of the Royal Society of London Series A-Mathematical Physical and Engineering Sciences* 2001; **359**:131–149.

35. Sohn H, Farrar CR, Hemez FM, Shunk DD, Stinemates DW, Nadler BR. A Review of Structural Health Monitoring Literature: 1996–2001, *Los Alamos National Laboratory*, USA, 2003.

36. Maia NMM, Silva JMM. Theoretical and Experimental Modal Analysis. England: Research Studies Press Ltd., 1997.

37. Doebling SW, Farrar CR, Prime MB, Shevitz DW. Damage Identification and Health Monitoring of Structural and Mechanical Systems from Changes in their Vibration Characteristics: A Literature Review, *Los Alamos National Laboratory report*, USA, 1996.

38. Carden EP, Fanning P. Vibration based condition monitoring: A review. *Structural Health Monitoring* 2004; **3**:355–377.

39. Hadjileontiadis LJ, Douka E, Trochidis A. Fractal dimension analysis for crack identification in beam structures. *Mechanical Systems and Signal Processing* 2005; **19**: 659–674.

40. Hadjileontiadis LJ, Douka E. Crack detection in plates using fractal dimension. *Engineering Structures* 2007; **29**:1612–1625.

41. Liew KM, Wang Q. Application of wavelet theory for crack identification in structures. *Journal of Engineering Mechanics* 1998; **124**:152–157.

42. Quek ST, Wang Q, Zhang L, Ang KK. Sensitivity analysis of crack detection in beams by wavelet technique. *International Journal of Mechanical Sciences* 2001; **43**:2899–2910.

43. Hong JC, Kim YY, Lee HC, Lee YW. Damage detection using the Lipschitz exponent estimated by the wavelet transform: applications to vibration modes of a beam. *International Journal of Solids and Structures* 2002; **39**:1803–1816.

44. Huth O, Feltrin G, Maeck J, Kilic N, Motavalli M. Damage identification using modal data: Experiences on a prestressed concrete bridge. *Journal of Structural Engineering* 2005; **131**:1898–1910.

45. Friswell MI, Mottershead JE. Finite element modal updating in structural dynamics. Dordrecht: Kluwer, 1995.

46. Fritzen CP, Bohle K. Global damage identification of the ‘‘Steelquake’’ structure using modal data. *Mechanical Systems and Signal Processing* 2003; **17**:111–117.

47. Goerl E, Link M. Damage identification using changes of eigenfrequencies and mode shapes. *Mechanical Systems and Signal Processing* 2003; **17**(1):219–226.

48. Xu GY, Zhu WD, Emory BH. Experimental and numerical investigation of structural damage detection using changes in natural frequencies. *Journal of Vibration and Acoustics* 2007; **129**:686–700.

49. Reynders E, Teughels A, Roeck GD. Finite element model updating and structural damage identification using OMAX data. *Mechanical Systems and Signal Processing* 2010; **24**:1306–1323.

50. Shang S, Yun GJ, Qiao P. Delamination identification of laminated composite plates using a continuum damage mechanics model and subset selection technique. *Smart Materials and Structures* 2010; **19**:055024(13pp).

51. Sohn H, Law KH. A Bayesian probabilistic approach for structural damage detection. *Earthquake Engineering & Structural Dynamics* 1997; **26**:1259-81.

52. Papadimitriou C, Beck JL, Katafygiotis LS. Updating robust reliability using structural test data. *Probabilistic Engineering Mechanics* 2001; **16**:103-13.

53. Fritzen CP, Jennewein D. Damage detection based on model updating methods. *Mechanical Systems and Signal Processing* 1998; **12**(1):163–186.

54. Gola MM, Soma A, Botto D. On theoretical limits of dynamic model updating using a sensitivity-based approach. *Journal of Sound and Vibration* 2001; **244**(4):583–595.

55. Papadopoulos L, Garcia E. Structural damage identification: a probabilistic approach. *AIAA Journal* 1998; **36**(11):2137–2145.

56. D’Ambrogio W, Zobel PB. Damage detection in truss structures using a direct updating technique. *Proceeding of 19th International Seminar for Modal Analysis on Tools for Noise and Vibration Analysis*, Katholieke Universiteit, Belgium, 1994; **2**:657–667.

57. Cha PD, Tuck-Lee JP. Updating structural system parameters using frequency response data. *Journal of Engineering Mechanics* 2000; **126**(12):1240–1246.

58. Marwala T, Heyns PS. Multiple-criterion method for determining structural damage. *AIAA Journal* 1998; **36**(8):1494–1501.

59. Teughels A, Maeck J, Roeck GD. Damage assessment by FE model updating using damage functions. *Computers & Structures* 2002; **80**:1869–79.

60. Brownjohn JMW, Moyo P, Omenzetter P, Lu Y. Assessment of highway bridge upgrading by dynamic testing and finite-element model updating. *Journal of Bridge Engineering* 2003; **8**(3):162–72.

61. Jaishi B, Ren WX. Structural finite element model updating using ambient vibration test results. *Journal of Structural Engineering* 2005; **131**(4):617–28.

62. Koh CG, Hong B, Liaw C-Y. Parameter identification of large structural systems in time domain. *Journal of Structural Engineering* 2000; **126**(8):957–63.

63. Katkhuad H, Martinez R, Haldar A. Health assessment at local level with unknown input excitation. *Journal of Structural Engineering* 2005; **131**(6):956–65.

64. Bu JQ, Law SS, Zhu XQ. Innovative bridge condition assessment from dynamic response of a passing vehicle. *Journal of Engineering Mechanics* 2006; **132**(12):1372–9.

65. Banan MR, Banan MR, Hjelmstad KD. Parameter estimation of structures from static response, I. Computational aspects. *Journal of Structural Engineering* 1994; **120**(11):3243–55.

66. Hjelmstad KD, Shin S. Damage detection and assessment of structures from static responses. *Journal of Engineering Mechanics* 1997; **123**(6):568–76.

67. Chen HP. Efficient methods for determining modal parameters of dynamic structures with large modifications. *Journal of Sound and Vibration* 2006; **298**:462-470.

68. Carvalho J, Datta BN, Lin W, Wang C. Symmetry preserving eigenvalue embedding in finite element model updating of vibration structures. *Journal of Sound and Vibration* 2006; **290**:839-864.

69. Yang YB, Chen YJ. A new direct method for updating structural models based on measured modal data. *Journal of Engineering Structures* 2009; **31**:32-42.

70. Udwadia FE. Methodology for optimum sensor locations for parameter identification in dynamic systems. *Journal of Engineering Mechanics*, 1994; 120 (2):368–390.

71. Meo M, Zumpano G. On the optimal sensor placement techniques for a bridge structure. Engineering Structures, 2005; 27:1488-1497.

72. Hemez FM. Uncertainty quantification and the verification and validation of computational models. *Proceeding of Damage Prognosis for Aerospace, Civil and Mechanical Systems*, Chichester, England, Hoboken, NJ: Wiley, 2004.

73. Mustafa S, Matsumoto Y. Bayesian Model Updating and Its Limitations for Detecting Local Damage of an Existing Truss Bridge. *Journal of Bridge Engineering* 2017; DOI: 10.1061/(ASCE)BE.1943-5592.0001044. (In press)

74. Dammika AJ. Experimental-analytical framework for damping change-based structural health monitoring of bridges. Ph.D Thesis, Saitama University, Japan, 2014.

75. Beck JL, Au SK, Vanik MW. A Bayesian Probabilistic Approach to Structural Health Monitoring. *Proceedings of the American Control Conference*: San Diego, California 1999; **2**:1119-1123.

76. Mustafa S, Dammika AJ, Matsumoto Y, Yamaguchi H, Yoshioka T. A Bayesian Probabilistic Approach for Finite Element Model Updating Utilizing Vibration Data Measured in an Existing Steel Truss Bridge. *Proceeding of Structural Health Monitoring of Intelligent Infrastructure*: Torino, Italy, 2015; **RS3**:114-123.

77. Yuen KV. Bayesian methods for structural dynamics and civil engineering. John Wiley & Sons; 2010.

78. Yamaguchi H, Matsumoto Y, Yoshioka T. Effects of local structural damage in a steel truss bridge on internal dynamic coupling and modal damping. *Smart Structures and Systems* 2015; **15**(3):523-41.

79. Overschee PV, Moor BD. Subspace algorithms for the stochastic identification problem. *Automatica* 1993; **29**(3):649-60.

80. Juang JN, Pappa RS. An eigensystem realization algorithm for modal parameter identification and model reduction. *Journal of Guidance, Control, and Dynamics* 1985; **8**(5):620-27.

81. Richard SP, Kenny BE, Axel S. Consistent-mode indicator for the eigensystem realization algorithm. *Journal of Guidance, Control, and Dynamics* 1993; **16**(5):852-858.

82. Ungar EE, Kerwin EM. Loss factor of viscoelastic systems in terms of energy concepts. *The Journal of the Acoustical Society of America* 1962; **34**(7):954-7.

83. Yamaguchi H, Nagahawatta HD. Damping effects of cable cross ties in cable-stayed bridges. *Journal of Wind Engineering and Industrial Aerodynamics* 1995; **54/55**:35-43.

84. Nashif AD, Jones DI, Henderson JP. Vibration damping. Wiley, New York 1985;45-50.

85. Yamaguchi H, Ito M. Mode-dependence of structural damping in cable-stayed bridges. *Journal of Wind Engineering and Industrial Aerodynamics* 1997; **72**:289-300.

86. Chen GW, Beskhyroun S, Omenzetter P. Experimental investigation into amplitude-dependent modal properties of an eleven-span motorway bridge. *Engineering Structures* 2016; **107**:80-100.

87. Zoghi M. The international handbook of FRP composites in civil engineering. CRC Press; 2014.

APPENDIX A
OPTIMAL SENSOR PLACEMENT FOR EXISTING STEEL TRUSS BRIDGE

A.1 Introduction

The problem of sensor placement is an important issue in dynamic testing of large structures, and has been investigated from different approaches, as can be seen from the abundance of literature [A1-A4], and the references therein. Especially due to the increasing interest of damage identification and SHM in last two decades, more researchers are involved in this topic and methods from various perspectives are proposed [A5,A6]. The key ideas behind these approaches are, however, similar. Most sensor placement methods aim to achieve best sensitivity changes detection of signatures indicating damage, or the best identification of structural characteristics, including the modal frequencies, mode shapes and modal damping ratios using the limited sensors that are practically available. Hence, an optimal sensor placement (OSP) configuration can minimize the number of sensors required, increase accuracy and provide a robust system. OSP is important in cases where the properties of a system, described in terms of continuous functions, need to be identified using discrete sensor information. Hence, the efficiency of vibration-based SHM techniques using a small number of sensors depend highly on the sensitivity of the acquired data to structural changes that may be obtained by placing the sensors according to the OSP strategies. The present study investigates techniques for selecting optimal sensor locations to monitor the health condition of an existing steel truss bridge by capturing sufficient information to identify structural dynamic behavior.

A.2 OSP Techniques

From the literature survey, three major groups of techniques are observed as: (1) Effective independence method (EFI), (2) Energy matrix rank optimization method, and (3) Modal approaches using various system norms (Hankel, H_∞ and H_2). In this study, different techniques from all the groups were investigated which are discussed in the following sub-sections.

A.2.1 Effective Independence Method

The aim of this method is to search the best set DOFs locations from all the candidate locations in the structure such that the linear independence of the mode shapes is maintained while containing the sufficient information about the target modal responses in the measurements. The method originates from estimation theory by sensitivity analysis of the parameters to be estimated, and then it arrives at the maximization of the Fisher information matrix (FIM) which is defined as the product of the mode shape matrix, $\boldsymbol{\Phi}$ and its transpose. The starting point of this method is the full modal matrix from a finite element model. The number of sensors is reduced from an initially large candidate set in an iterative manner by removing sensors from those DOFs which contribute least among all the candidate sensors to the linear independence of the target modes. In the end, it preserves the required necessary candidate sensors as the optimal sensor set.

The vector of the measured structural response denoted by $\boldsymbol{y}_s$ can be estimated as a combination of *N* mode shapes through the expression:

$$\boldsymbol{y}_s = \boldsymbol{\Phi q} + \boldsymbol{w} = \sum_{i=1}^{N} q_i \boldsymbol{\phi}_i + \boldsymbol{w} \tag{A.1}$$

where $\boldsymbol{\Phi}$ is the matrix of FE-model target mode shapes, $\boldsymbol{q}$ is the coefficient response vector and $\boldsymbol{w}$ is a sensor noise vector which can be assumed a stationary Gaussian white noise with zero mean and a variance of σ_0^2. The above representation of structural response is based on the concept [A7] that the response in any point of an elastic structure can be obtained in the time or frequency domain as a linear combination of mode shape values. In this way, the *i*th coefficient of $\boldsymbol{y}_s$ is a linear combination of the *i*th mode shape vectors where q_i is a multiplier coefficient that is a function either of time or frequency.

Evaluating the coefficient response vector using an efficient unbiased estimator and then, estimating the covariance of the errors results in:

$$E[(\boldsymbol{q} - \hat{\boldsymbol{q}})(\boldsymbol{q} - \hat{\boldsymbol{q}})^T] = \left[\frac{1}{\sigma_0^2}\boldsymbol{\Phi}^T\boldsymbol{\Phi}\right]^{-1} = \mathbf{FIM}^{-1} \tag{A.2}$$

where *E* denotes the expected value and $\hat{\boldsymbol{q}}$ is the efficient unbiased estimator of $\boldsymbol{q}$. Hence, the best estimation of $\boldsymbol{q}$ occurs when **FIM** is maximized, therefore the procedure for selecting the best sensor placements is to unselect candidate sensor positions such that the determinant of **FIM** is maximized. In order to achieve this, an iterative algorithm was developed by Kammer

and Brillhart [A8], which evaluates the candidate location sensor contributions employing the effective independence distribution vector, $\boldsymbol{E}_d$ given by:

$$\boldsymbol{E}_d = [\boldsymbol{\Phi\psi}]^2 \lambda^{-1}\{1\}_k \tag{A.3}$$

where $\boldsymbol{\psi}$ and λ are the eigenvectors and corresponding eigenvalues of $\mathbf{FIM}$. $\{1\}_k$ is a $k \times 1$ column vector with all elements of 1. The selection procedure is to sort the elements of the $\boldsymbol{E}_d$ coefficients, and to remove the smallest one at a time. The $\boldsymbol{E}_d$ coefficients are then updated according to the new mode shape matrix and the process is repeated iteratively until the number of remained sensors equals to a preset value.

A mass weighted version of the EFI (EFIWM) method is also studied in the literature [A9,A10]. In this case the FIM and $\boldsymbol{E}_d$ correspond to

$$\mathbf{FIM} = \boldsymbol{\Phi}^T \boldsymbol{M} \boldsymbol{\Phi} \text{ and } \boldsymbol{E}_d = \sqrt{\boldsymbol{M}}\boldsymbol{\Phi}\mathbf{FIM}^{-1}\boldsymbol{\Phi}^T\sqrt{\boldsymbol{M}} \tag{A.4}$$

where $\boldsymbol{M}$ represents the symmetric mass matrix of the initial FE-model. In this case, Guyan reduction is implemented at each iteration to reduce the mass matrix to the candidate DOFs.

A.2.2 Energy Matrix Rank Optimization

The basic idea underlying the energy matrix rank optimization (EMRO) algorithm is to achieve a sensor location configuration that maximizes the strain energy (SE) or kinetic energy (KE) of the measured mode shapes from the structure [A11,A12]. The strain energy and kinetic energy are given by

$$\mathbf{SE} = \boldsymbol{\Phi}^T \boldsymbol{K} \boldsymbol{\Phi} \text{ and } \mathbf{KE} = \boldsymbol{\Phi}^T \boldsymbol{M} \boldsymbol{\Phi} \tag{A.5}$$

where $\boldsymbol{K}$ is the stiffness matrix of the initial FE-model. This method is similar to the EFI method where the FIM is assembled using a Cholesky decomposition of the mass or stiffness matrix given by

$$\boldsymbol{K} = \boldsymbol{C}^T \boldsymbol{C} \text{ or } \boldsymbol{M} = \boldsymbol{C}^T \boldsymbol{C} \tag{A.6}$$

where $\boldsymbol{C}$ is an upper triangular matrix. Then, the FIM is assembled as

$$\mathbf{FIM} = \boldsymbol{\psi}^T \boldsymbol{\psi} \text{ where } \boldsymbol{\psi} = \boldsymbol{C\Phi} \tag{A.7}$$

The same procedure is then carried out to calculate effective independence distribution vector similar to EFI method but Guyan reduction is employed here at each step of iteration to reduce the stiffness or mass matrix to the candidate DOFs.

A.2.3 Modal Approach Using System Norms

System norms serve as a measure of intensity of its response o standard excitations and in this capacity they are used in the model reduction and in the sensor placement procedures. There are three system norms: H_2, H_∞ and Hankel norms. Given a large set of sensors, the placement problem consists of determining the locations of a smaller subset of sensors such that the system norms of the subset is as close as possible to the norms of the original set [A13]. In this study only H_2 norm was considered and hence, the following description is restricted to OSP using H_2 norm only.

Let $(\boldsymbol{A}, \boldsymbol{B}, \boldsymbol{C})$ be a system state-space representation of a linear system and let $G(\omega) = \boldsymbol{C}(j\omega I - \boldsymbol{A})^{-1}\boldsymbol{B}$ be its transfer function. The H_2 norm of the system is defined as

$$\|G\|_2^2 = \frac{1}{2\pi}\int_{-\infty}^{\infty} tr(G^*(\omega)G(\omega))d\omega \tag{A.8}$$

where $tr(G^*(\omega)G(\omega))$ is the sum of the squared magnitudes of all of the elements of $G(\omega)$. Thus, it can be interpreted as an average gain of the system, performed over all the elements of the matrix transfer function and over all frequencies. For structure in modal representation, each mode is independent of others, thus the norms of a single mode are independent as well. Considering the *i*th mode and its state-space representation $(\boldsymbol{A}_{mi}, \boldsymbol{B}_{mi}, \boldsymbol{C}_{mi})$, the H_2 norm of the *i*th mode is given by [A13-A15]

$$\|G_i\|_2 \cong \frac{\|\boldsymbol{B}_{mi}\|_2\|\boldsymbol{C}_{mi}\|_2}{2\sqrt{\xi_i\omega_i}} \tag{A.9}$$

where ξ_i and ω_i are the *i*th modal damping ratio and modal frequency respectively. The placement index σ_{2ki} that evaluates the *k*th sensor at the *i*th mode in terms of the H_2 norm is defined with respect to all the modes and all admissible R sensors

$$\sigma_{2ki} = w_{ki}\frac{\|G_{ki}\|_2}{\|G\|_2}, \qquad k = 1, \dots, R \tag{A.10}$$

where $w_{ki} \geq 0$ is the weight assigned to the kth sensor and the *i*th mode, and G_{ki} is the transfer function of the *k*th sensor and *i*th mode. Eq. (A.10) represents the sensor placement index of *k*th sensor for a single mode. For N number of target modes, the placement index for *k*th sensor with respect to H_2 norm can be expressed as

$$\sigma_{2k} = \sqrt{\sum_{i=1}^{N}\sigma_{ik}^2} \tag{A.11}$$

Hence, the vector of the sensor placement indices for all the R candidate sensors is defined as $\boldsymbol{\sigma}_s = [\sigma_{s1}, \sigma_{s2}, \ldots, \sigma_{sR}]^T$, and its kth entry is the placement index of the kth sensor for the N number of target modes which is given in Eq. (A.11). After calculating the sensor placement indices for the targeted modes and for all the candidate sensor locations, the sensors with the higher indices can be considered for the OSP.

A.3 Results of OSP for Test Structure

All the DOFs used in the FE-model cannot be measured in the real structure due to physical limitations. Therefore, the DOFs corresponding to rotations were eliminated from the full modal matrix. Similarly, not all of the mode shapes can be experimentally measured, hence first fifty modes were selected as a target modes to be optimally detected. For norm based modal approach, mass and stiffness proportional damping was considered with the assumption of monotonic increment of damping ratio with natural frequency. Damping ratio corresponding to the fundamental frequency was considered as 1%. Fundamental frequency was found from the initial FE-model as 2.067 Hz with transversely dominant mode shape. State space modal model was then constructed with mass, stiffness and damping matrices to carry out necessary computations.

Three different OSP techniques were tested on the studied steel truss bridge. Optimal sensor locations were identified for fifty numbers of target modes. Fig. A.1 shows the optimal sensor locations in vertical direction for 20 uniaxial accelerometers which were obtained by different OSP techniques. It can be seen that the optimal sensor locations for 20 vertical sensors obtained from all the methods are mostly on stringers which is matching with the expected outcome. The results obtained from the EFI, EFIWM and EMRO methods were showing good agreements with each other's because of their analytical similarities to calculate the optimal sensor locations.

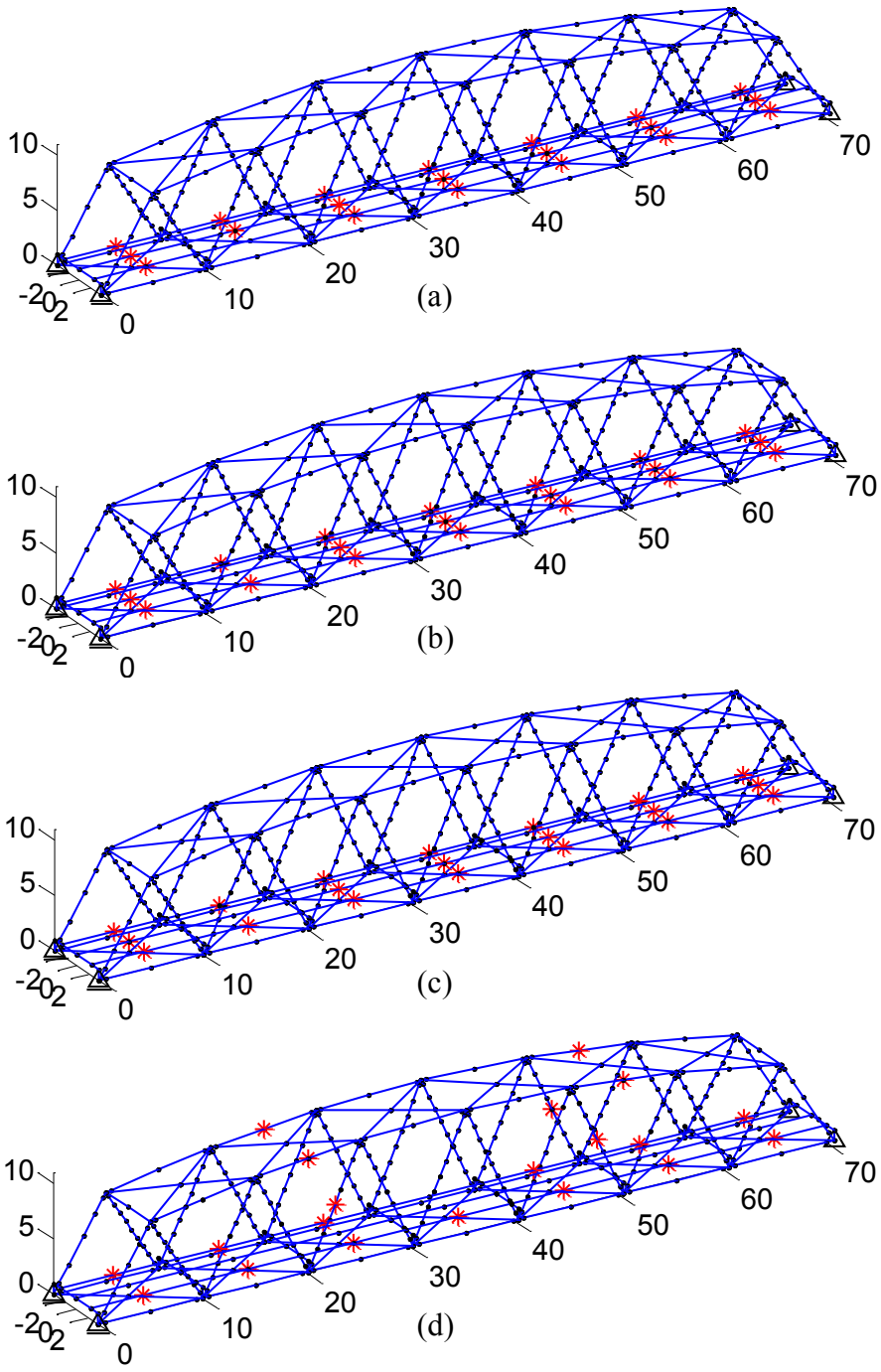

Fig. A.1. Placements of 20 vertical sensors considering fifty numbers of target modes according to: (a) EFI, (b) EFIWM, (c) EMRO and (d) H_2 norm

A.4 Conclusions

In this work, several OSP techniques for an existing steel truss bridge were studied. The sensor locations were chosen in such a way that they should be able to give relevant information in the reconstruction of modal and dynamic characteristics of the bridge under investigation. From the sensor placement results obtained by various methods it was clear that the sensors must be

placed on stringers on both sides of the bridge to identify the bending and torsional modes by placing sensors in vertical direction only. Hence, a better placement of sensors can be obtained in a scientific way rather than placing sensors based on practical judgement which is highly dependent on the experience and the knowledge of the inspector. Moreover, for the placement of a small number of sensors in case of large structure, the sensors must be placed judiciously in order to provide adequate information for the identification of the structural behavior which can be achieved by following the procedure as described in this study.

References

A1. Udwadia FE. Methodology for optimum sensor locations for parameter identification in dynamic systems. *Journal of Engineering Mechanics* 1994; **120**(2):368–390.

A2. Kammer DC. Sensor placement for on-orbit modal identification and correlation of large space structures. *Journal of Guidance, Control and Dynamics* 1991; **14**:251–259.

A3. Papadopoulos M, Garcia E. Sensor placement methodologies for dynamic testing, *AIAA Journal* 1998; **36**(2):256–263.

A4. Meo M, Zumpano G. On the optimal sensor placement techniques for a bridge structure. *Engineering Structures* 2005; **27**:1488-1497.

A5. Balageas D, Fritzen CP, Guemes A. Structural Health Monitoring, ISTE, London, UK, 2006.

A6. Li DS, Li HN, Fritzen CP. On the physical significance of the norm based sensor placement method, *Proceedings of the Third European Workshop on Structural Health Monitoring*, Granada, Spain, July 2006; 1542–1550.

A7. Ewins DJ. Modal testing: theory, practice and application. 2nd ed. Research Studies Press LTD, 2000.

A8. Kammer DC, Brillhart RD. Optimal sensor placement for modal identification using system-realization methods. *Journal of Guidance, Control and Dynamics* 1996; **19**:729–31.

A9. Garvey SD, Friswell MI, Penny JET. Evaluation of a method for automatic selection of measurement locations based on subspace-matching. *In proceeding of XIV International Modal Analysis Conference*, Michigan 1996; 1546–1552.

A10. Lollock JA, Cole TR. The effect of mass-weighting on the effective independence of mode shapes. *In proceeding of 46thAIAA/ASME/ASCE/AHS/ASC Structures, Structural Dynamics and Materials Conference*, Texas, USA, 2005; 1–8.

A11. Hemez FM, Farhat C. An energy based optimum sensor placement criterion and its application to structural damage detection. *In proceeding of XII International Modal Analysis Conference*, Hawaii, 1994; 1568–1575.

A12. Castro-Triguero R, Murugan S, Gallego R, Friswell MI. Robustness of optimal sensor placement under parametric uncertainty. *Mechanical Systems and Signal Processing* 2013; **41**:268-287.

A13. Gawronski W. Advanced Structural Dynamics and Active Control of Structures, Springer-Verlag, New York, 2004.

A14. Gawronski W. Almost-balanced structural dynamics. *Journal of Sound and Vibration* 1997; **202**(5):669–687.

A15. Debnath N, Dutta A, Deb SK. Placement of sensors in operational modal analysis for truss bridges, *Mechanical Systems and Signal Processing* 2012; **31**:196-216.

APPENDIX B

DAMAGE DETECTION BY FE-MODEL UPDATING

B.1 Application to SHM

In order to determine damage, the most probable values of the stiffness parameters from the damaged and undamaged structure and their standard deviations are used to compute the probability that a given stiffness parameter θ_l has been reduced by a certain fraction d compared to the undamaged state of the structure [6,14,17]. Based on the Gaussian approximation of stiffness parameters, the probability of damage in terms of a fractional damage level, d can be obtained as

$$P_l^{dam}(d) = P\left(\boldsymbol{\theta}_l^{pd} < (1-d)\boldsymbol{\theta}_l^{ud}\right) \approx \boldsymbol{\Phi}\left[\frac{(1-d)\boldsymbol{\theta}_l^{*ud} - \boldsymbol{\theta}_l^{*pd}}{\sqrt{(1-d)^2(\boldsymbol{\sigma}_l^{ud})^2 + (\boldsymbol{\sigma}_l^{pd})^2}}\right] \tag{B.1}$$

where $\boldsymbol{\Phi}(\cdot)$ is the cumulative distribution function of the standard Gaussian random variable, $\boldsymbol{\theta}_l^{*ud}$ and $\boldsymbol{\theta}_l^{*pd}$ denote the most probable values of the stiffness parameters for the undamaged and possibly damaged structures respectively, and $\boldsymbol{\sigma}_l^{ud}$, $\boldsymbol{\sigma}_l^{pd}$ are the corresponding standard deviations of the stiffness parameters.

The posterior uncertainty of unknown parameters can be obtained by modelling the posterior PDF of unknown parameters using a Gaussian distribution with mean at the optimal parameters and covariance matrix $\boldsymbol{\Xi}$ which is equal to the inverse of the Hessian calculated at the optimal parameters [17,20]. This covariance matrix is given by

$$\boldsymbol{\Xi}(\boldsymbol{\phi}^*, \boldsymbol{\nu}^*, \boldsymbol{\gamma}^*, \boldsymbol{\lambda}^*, \boldsymbol{\vartheta}^*, \boldsymbol{\theta}^*) = \begin{bmatrix} \boldsymbol{\Gamma}^{\phi\phi} & \boldsymbol{\Gamma}^{\phi\nu} & \boldsymbol{\Gamma}^{\phi\gamma} & \boldsymbol{\Gamma}^{\phi\lambda} & \boldsymbol{\Gamma}^{\phi\vartheta} & \boldsymbol{\Gamma}^{\phi\theta} \\ \boldsymbol{\Gamma}^{\nu\phi} & \boldsymbol{\Gamma}^{\nu\nu} & \boldsymbol{\Gamma}^{\nu\gamma} & \boldsymbol{\Gamma}^{\nu\lambda} & \boldsymbol{\Gamma}^{\nu\vartheta} & \boldsymbol{\Gamma}^{\nu\theta} \\ \boldsymbol{\Gamma}^{\gamma\phi} & \boldsymbol{\Gamma}^{\gamma\nu} & \boldsymbol{\Gamma}^{\gamma\gamma} & \boldsymbol{\Gamma}^{\gamma\lambda} & \boldsymbol{\Gamma}^{\gamma\vartheta} & \boldsymbol{\Gamma}^{\gamma\theta} \\ \boldsymbol{\Gamma}^{\lambda\phi} & \boldsymbol{\Gamma}^{\lambda\nu} & \boldsymbol{\Gamma}^{\lambda\gamma} & \boldsymbol{\Gamma}^{\lambda\lambda} & \boldsymbol{\Gamma}^{\lambda\vartheta} & \boldsymbol{\Gamma}^{\lambda\theta} \\ \boldsymbol{\Gamma}^{\vartheta\phi} & \boldsymbol{\Gamma}^{\vartheta\nu} & \boldsymbol{\Gamma}^{\vartheta\gamma} & \boldsymbol{\Gamma}^{\vartheta\lambda} & \boldsymbol{\Gamma}^{\vartheta\vartheta} & \boldsymbol{\Gamma}^{\vartheta\theta} \\ \boldsymbol{\Gamma}^{\theta\phi} & \boldsymbol{\Gamma}^{\theta\nu} & \boldsymbol{\Gamma}^{\theta\gamma} & \boldsymbol{\Gamma}^{\theta\lambda} & \boldsymbol{\Gamma}^{\theta\vartheta} & \boldsymbol{\Gamma}^{\theta\theta} \end{bmatrix}^{-1} \tag{B.2}$$

where each element of the Hankel matrix represents the double derivatives of the objective function, $\boldsymbol{\Gamma}$ given in Eq. (3.13) with respect to two vectors in the subscript. As the Hankel matrix is symmetric, only the elements in the upper or lower triangular are needed to be derived analytically. After computing the posterior covariance matrix given in above equation, the variance of each unknown parameter then can be obtained from the corresponding diagonal elements of $\boldsymbol{\Xi}$.

B.2 Damage Detection

The proposed Bayesian model updating framework in Chapter 3 can be applied to detect damage at local level. The application to SHM was carried out by considering both the data from simulated damage structure and experimental data from actual damaged span in the subsequent sub-sections [73].

B.2.1 Considering Simulated Damage

As actual damage may not be possible to be introduced in the existing bridge, the numerical model was considered for damage simulation. One element (element number 316) of D5d diagonal member was assumed to be damaged. In order to introduce damage, the sectional properties of element 316 had been reduced by 50%. The sectional properties of all other elements were kept same as the undamaged state. Modal parameters were then extracted from this damaged structure and a sample of zero-mean Gaussian noise with 1% coefficient of variation was added to the extracted modal frequencies and mode shapes from the view point of realistic measurements. With all other values same as the undamaged case, the same iterative procedure is followed to update the preliminary model having simulated damage. After updating the preliminary FE-model, the posterior uncertainty of stiffness parameters was estimated using Eq. (B2). Based on the most probable values and the standard deviation of the stiffness parameters, the probabilities of damage for all the four stiffness parameters (defined in Eq. (3.23)) corresponding to 514 frame elements were evaluated using Eq. (B.1). Figs. B.1-B.4 show the probabilities of damage of four stiffness parameters for all the elements respectively. From these figures, it can be clearly seen that element 316 has possible damage with a very high probability having an extent of damage of around 50% in all the four stiffness parameters. These plots suggest that the method is very sensitive as it has not only identified the damaged element but also the extent of damage. Therefore, the proposed updating framework has great potential to detect damage at the elemental property level without showing

any false alarm despite having complexity of the analysed structure, which is very appealing characteristic of this method. Fig. B5(a) shows the bar diagram of the percentage change in the updated stiffness parameters between the undamaged and damaged structures. Fig. B5(b) shows the same bar plot which was partly zoomed for better clarity. It can be seen that stiffness parameters corresponding to element 316 $\left(\theta_{4\times(316-1)+1}:\theta_{4\times(316-1)+4}=\theta_{1261}:\theta_{1264}\right)$ are showing higher index suggesting substantial change in the stiffness value of the concerned element compared to the other undamaged elements of the structure. However, the damage detection by simulated data is much easier compared to the realistic scenarios as in case of simulated damage, the data corresponding to the undamaged and simulated damage structures are subjected to similar levels of model errors and the variations in system properties are only due to the induced damage in the structure. Additionally, the problem related to low sensitivity of frequencies and mode shapes due to local damage remains a concern for the practical application of the methodology discussed above.

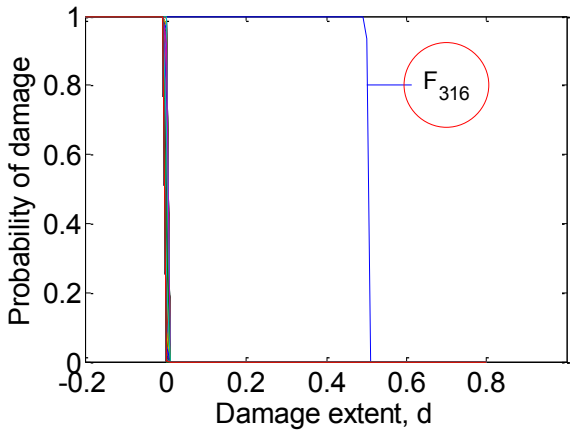

Fig. B.1. Probability of damage of axial stiffness parameters for all the elements

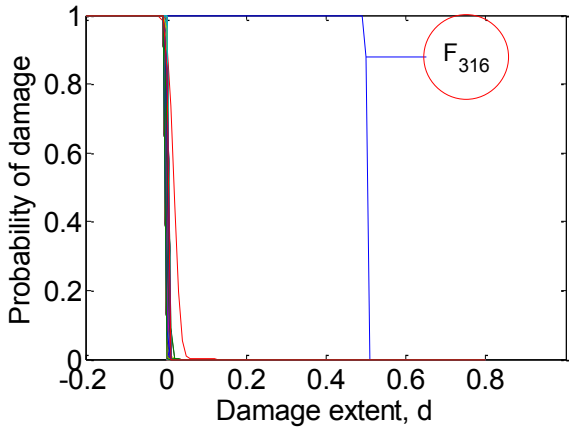

Fig. B.2. Probability of damage of bending stiffness parameters about *z*-axis for all the elements

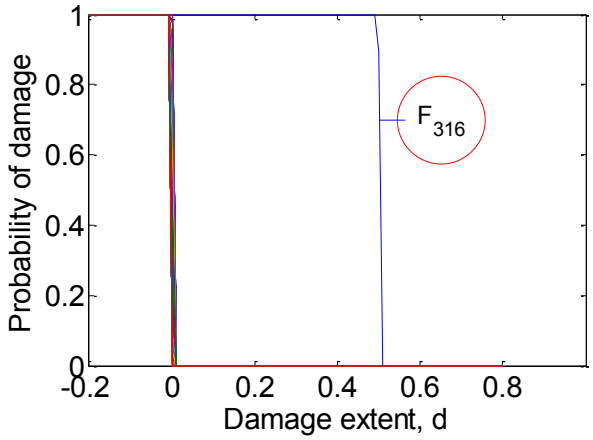

Fig. B.3. Probability of damage of bending stiffness parameters about *y*-axis for all the elements

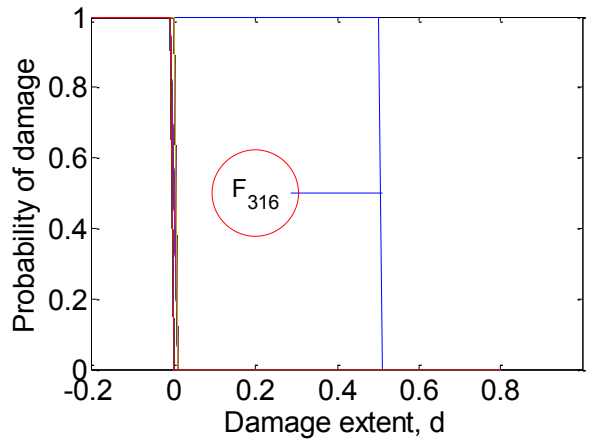

Fig. B.4. Probability of damage of torsional stiffness parameters for all the elements

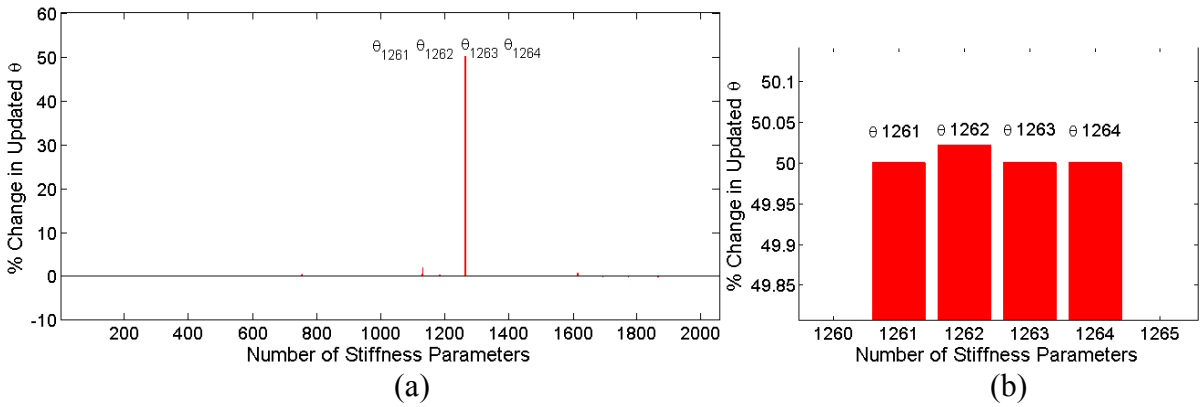

Fig. B.5. (a) Bar diagram of the percentage change in updated stiffness parameters between damaged and undamaged structures, (b) Same bar diagram which is party zoomed

B.2.2 Considering Experimental Data from Damaged Span

For the practical applicability of the proposed model updating framework to detect local damage, the identified modal data from the damaged fourth span were used to update an initial FE-model. Four global modes and one diagonal mode were identified from the recorded data at the fourth span (see Fig. 5.1) corresponding to BR condition. The natural frequencies and partial mode shape vectors of 3 components of the identified modes were used to update the initial FE-model using the proposed updating framework. The nominal stiffness values for this initial FE-model were selected from the uniform distribution over $\tilde{\boldsymbol{\theta}}$ to $1.5\tilde{\boldsymbol{\theta}}$ where $\tilde{\boldsymbol{\theta}}$ is the actual stiffness parameters of the preliminary model. Table B.1 shows the model updating results for frequencies and mode shapes after 100 iterations. It can be seen that the frequencies of the global modes of the updated FE-model are close to the corresponding experimental ones and MAC values are also improved. On the other hand, there was still some discrepancy in the frequencies of damage diagonal mode between actual structure and updated FE-model. However, the frequency of the diagonal mode of updated FE-model was found significantly lower than the corresponding frequency of the baseline model (decrease of frequency from 9.183Hz to 8.664Hz), representing the damaged structural condition of the fourth span.

Table B.1. Model updating results for frequencies and MAC values

Experimental order of Mode	Experimental f(Hz)	Initial f(Hz)	Updated f(Hz)	MAC initial	MAC Updated
1st bending	2.588	2.899	2.598	0.9766	0.9998
1st torsional	4.596	5.289	4.742	0.8147	0.9997
2nd bending	5.250	6.062	5.443	0.7629	0.9986
Diagonal	7.129	9.467	8.664	0.9982	0.9998
3rd bending	7.206	8.604	7.665	0.8216	0.9983

To determine the extent of damage and its location, the bar diagram showing the percentage change in updated stiffness parameters between possibly damaged and undamaged structures was plotted in Fig. B.6. It can be seen that stiffness parameters θ_{1762} and θ_{1766} are showing higher percentage of change in the bar plot. The damaged elements corresponding to these two stiffness parameters were shown in Fig. B.7. From this figure it can be seen that the damage elements are the ones which are connected to the node where the measurement on damaged D5u diagonal member was taken. Table B.2 shows the identification results for stiffness parameters corresponding to damaged elements. It can be seen that only the stiffness

parameters corresponding to the bending component about *z*-axis for both the elements are showing significant reduction in stiffness properties. This is because of the fact that only acceleration response data corresponding to vertical direction (*z*-direction) were used in the analysis.

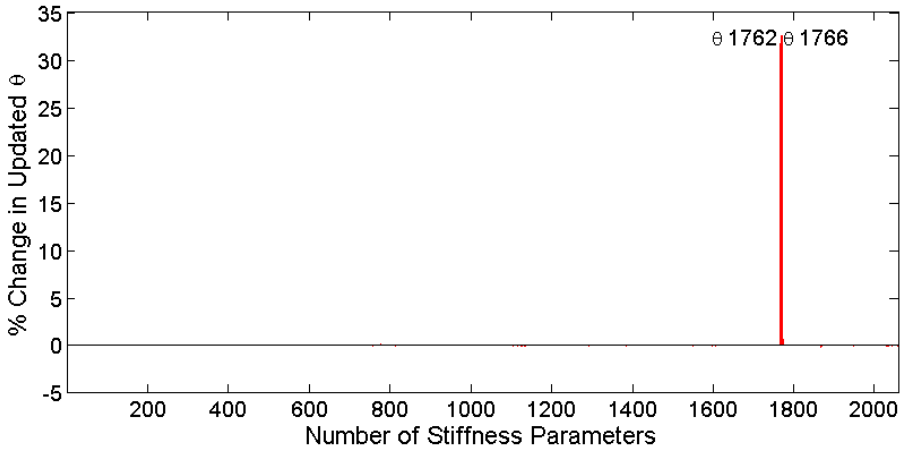

Fig. B.6. Bar diagram of the percentage change in updated stiffness parameters between damaged and undamaged structure

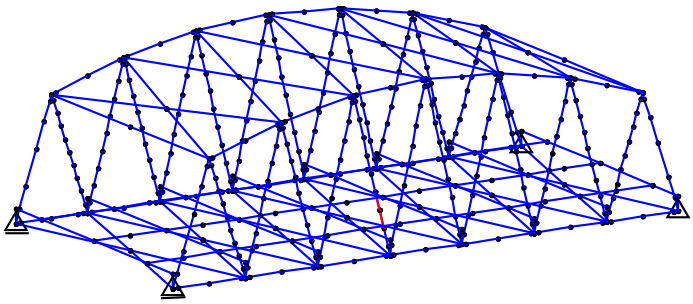

Fig. B.7. Damaged elements identified by FE-model updating using global and diagonal modes of the fourth span

Table B.2. Identified stiffness parameters for damaged and undamaged structure

Element No.	Parameter	Undamaged	Damaged	% change
441	θ_{1761}	832000 kN	832000 kN	0.0
	θ_{1762}	2400 kN-m^2	1640 kN-m^2	-31.7
	θ_{1763}	18800 kN-m^2	18800 kN-m^2	0.0
	θ_{1764}	77 kN-m^2	77 kN-m^2	0.0
442	θ_{1765}	832000 kN	832000 kN	0.0
	θ_{1766}	2400 kN-m^2	1621 kN-m^2	-32.4
	θ_{1767}	18800 kN-m^2	18800 kN-m^2	0.0
	θ_{1768}	77 kN-m^2	77 kN-m^2	0.0

The above discussion about the identification of damaged stiffness parameters using proposed model updating framework is based on prior information about the damage location in which the vibration measurement was taken on the damaged diagonal member. However, in practical cases such kind of information is not available. The objective is to identify the local damage using global vibrational characteristics of the structure which can be identified with limited number of sensors. Therefore, the model updating was performed again using only global modes and identified components of mode shapes corresponding to L2 and U2 sensor locations (see Fig. 5.1). Table B.3 shows the model updating results for frequencies and mode shapes after 100 iterations. Here also, it can be seen that the frequencies of the global modes of the updated FE-model are close to the corresponding experimental ones and MAC values are also improved. On the other hand, the frequency of the diagonal mode remains almost unaffected by the updating process. Fig. B.8 shows the bar diagram of the percentage change in updated stiffness parameters between possibly damaged and undamaged structures by considering only global modes. No damage with significant change in stiffness parameter has been detected this time as only global modes were used to perform FE-model updating. Hence, it can be concluded that the detection of local damage using proposed updating framework by utilizing global vibration characteristics can only be possible if the changes in frequencies and/or mode shapes of the global modes due to local damage are significant.

Table B.3. Model updating results for frequencies and MAC values

Experimental order of Mode	Experimental f(Hz)	Initial f(Hz)	Updated f(Hz)	MAC initial	MAC Updated
1st bending	2.588	2.899	2.598	0.9994	1.0000
1st torsional	4.596	5.289	4.744	0.9932	1.0000
2nd bending	5.250	6.062	5.443	0.9934	1.0000
Diagonal	7.129	9.467	9.204	0.9982	0.9983
3rd bending	7.206	8.604	7.721	0.9469	0.9999

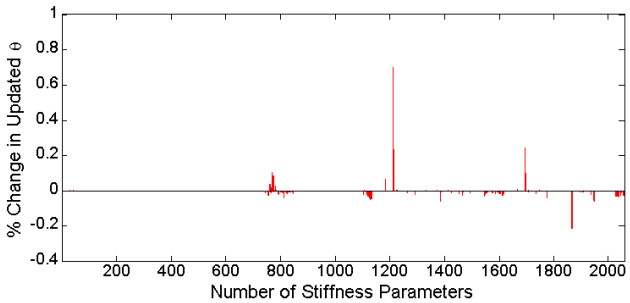

Fig. B.8. Bar diagram of the percentage change in updated stiffness parameters between damaged and undamaged structure considering only global modes

B. 3 Conclusions

In this Appendix, damage detection by the proposed model updating framework was presented by considering both the data from simulated damaged structure and experimental data from real damaged structure, having damage in one of the diagonal member, were used in the analysis. In case of simulated damage data, the proposed model updating framework successfully detected the local damage may be because of the assumption that the data corresponding to the undamaged and simulated damage structures are subjected to similar levels of model errors and the variations in system properties are only due to the induced damage in the structure. In case of experimental data from real damaged structure, the damage detection by the proposed updating framework could only be possible by considering damaged diagonal mode and the component of mode shapes measured at damaged diagonal member. However, no damage with significant change in stiffness parameter has been detected when considering only global modes to perform FE-model updating. Hence, it can be concluded that the detection of local damage using proposed updating framework by utilizing global vibration characteristics can only be possible if the changes in frequencies and/or mode shapes of the global modes due to local damage are significant.

APPENDIX C
FORMULATION AND PARAMETERIZATION OF MASS AND STIFFNESS MATRICES

A linear finite element program was developed with sufficient features for linear analysis of the truss bridge. This program was developed in MATLAB software and all necessary structural information such as joint coordinates, joint restraint assignment, element connectivity, material properties, sectional properties etc. were collected from the design drawing and engineering knowledge. The important features considered in the FE-model program are presented below.

C.1 Stiffness Formulation

The structural members were modelled as three-dimensional frame elements and six DOFs were considered at each joint resulting in 12×12 elemental stiffness matrices. Fig. C1 shows the DOFs at joint of frame element in local coordinate. The convention adopted is to label first the three translatory displacements of the first joint followed by the three rotational displacements of the same joint, then to continue with the three translatory displacements of the second joint and finally the three rotational displacements of this second joint. To differentiate rotational nodal coordinates from translational nodal coordinates, the double arrows were used for rotational nodal coordinates in Fig. C1. Local 1 axis was considered along the length of frame element with positive direction from first node to second node. For a three dimensional frame element, the local orthogonal axes will be established such that the X defines the longitudinal centroidal axis of the member and the X-Y plane will coincide with the plane of the structural system. In this case, the z axis will define the minor principal axis of the cross section while the Y axis will define the major axis of the cross section. It was assumed that the shear centre of the cross section coincides with the centroid of the cross section. The local 1-2 plane was taken to be vertical, i.e. parallel to the global Z or 3 axis. The elemental stiffness matrix in local coordinates can be expressed as

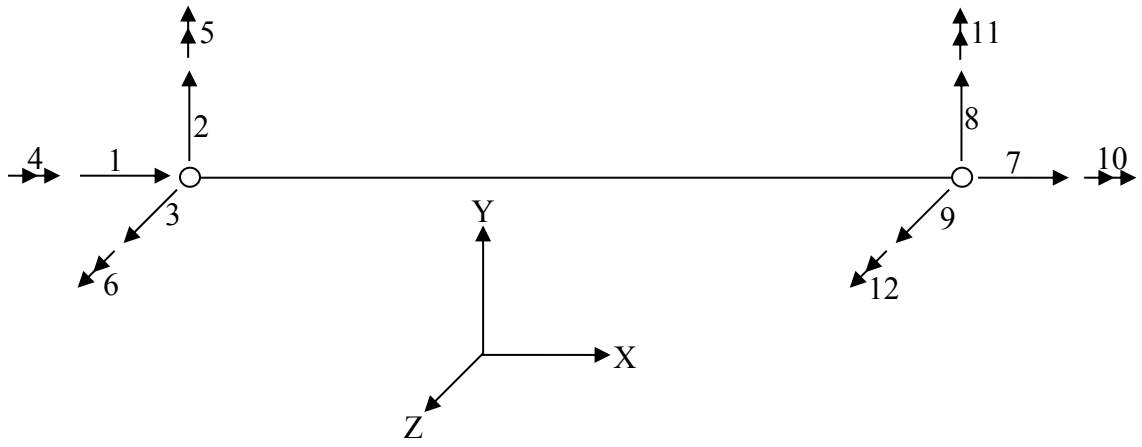

Fig. C.1 DOFs at joint of frame element in local coordinate

$$K_e = \begin{bmatrix}
\frac{AE}{L} & 0 & 0 & 0 & 0 & 0 & -\frac{AE}{L} & 0 & 0 & 0 & 0 & 0 \\
0 & \frac{12EI_z}{L^3} & 0 & 0 & 0 & \frac{6EI_z}{L^2} & 0 & -\frac{12EI_z}{L^3} & 0 & 0 & 0 & \frac{6EI_z}{L^2} \\
0 & 0 & \frac{12EI_y}{L^3} & 0 & -\frac{6EI_y}{L^2} & 0 & 0 & 0 & -\frac{12EI_y}{L^3} & 0 & -\frac{6EI_y}{L^2} & 0 \\
0 & 0 & 0 & \frac{GJ}{L} & 0 & 0 & 0 & 0 & 0 & -\frac{GJ}{L} & 0 & 0 \\
0 & 0 & -\frac{6EI_y}{L^2} & 0 & \frac{4EI_y}{L} & 0 & 0 & 0 & \frac{6EI_y}{L^2} & 0 & \frac{2EI_y}{L} & 0 \\
0 & \frac{6EI_z}{L^2} & 0 & 0 & 0 & \frac{4EI_z}{L} & 0 & -\frac{6EI_z}{L^2} & 0 & 0 & 0 & \frac{2EI_z}{L} \\
-\frac{AE}{L} & 0 & 0 & 0 & 0 & 0 & \frac{AE}{L} & 0 & 0 & 0 & 0 & 0 \\
0 & -\frac{12EI_z}{L^3} & 0 & 0 & 0 & -\frac{6EI_z}{L^2} & 0 & \frac{12EI_z}{L^3} & 0 & 0 & 0 & -\frac{6EI_z}{L^2} \\
0 & 0 & -\frac{12EI_y}{L^3} & 0 & \frac{6EI_y}{L^2} & 0 & 0 & 0 & \frac{12EI_y}{L^3} & 0 & \frac{6EI_y}{L^2} & 0 \\
0 & 0 & 0 & -\frac{GJ}{L} & 0 & 0 & 0 & 0 & 0 & \frac{GJ}{L} & 0 & 0 \\
0 & 0 & -\frac{6EI_y}{L^2} & 0 & \frac{2EI_y}{L} & 0 & 0 & 0 & \frac{6EI_y}{L^2} & 0 & \frac{4EI_y}{L} & 0 \\
0 & \frac{6EI_z}{L^2} & 0 & 0 & 0 & \frac{2EI_z}{L} & 0 & -\frac{6EI_z}{L^2} & 0 & 0 & 0 & \frac{4EI_z}{L}
\end{bmatrix} \quad \text{(C.1)}$$

where I_y and I_z are, respectively, the cross-sectional moments of inertia with respect to the principal axes labelled as y and z and L, A, and J are the length, cross-sectional area, and torsional constant of the frame element respectively.

C.2 Mass Formulation

The lumped mass matrix was used for the dynamic analysis of the truss bridge. The lumped mass matrix for the uniform beam segment of a three-dimensional frame element is simply a

diagonal matrix in which the coefficients corresponding to translatory displacements are equal to one-half of the total inertia of the frame element while coefficients corresponding to rotations were assumed to be zero. The elemental mass matrix in local coordinates can be expressed as

$$\boldsymbol{M_e} = \frac{\rho_m AL}{2}\begin{bmatrix} 1 & 0 & 0 & 0 & 0 & 0 & 0 & 0 & 0 & 0 & 0 & 0 \\ 0 & 1 & 0 & 0 & 0 & 0 & 0 & 0 & 0 & 0 & 0 & 0 \\ 0 & 0 & 1 & 0 & 0 & 0 & 0 & 0 & 0 & 0 & 0 & 0 \\ 0 & 0 & 0 & 0 & 0 & 0 & 0 & 0 & 0 & 0 & 0 & 0 \\ 0 & 0 & 0 & 0 & 0 & 0 & 0 & 0 & 0 & 0 & 0 & 0 \\ 0 & 0 & 0 & 0 & 0 & 0 & 0 & 0 & 0 & 0 & 0 & 0 \\ 0 & 0 & 0 & 0 & 0 & 0 & 1 & 0 & 0 & 0 & 0 & 0 \\ 0 & 0 & 0 & 0 & 0 & 0 & 0 & 1 & 0 & 0 & 0 & 0 \\ 0 & 0 & 0 & 0 & 0 & 0 & 0 & 0 & 1 & 0 & 0 & 0 \\ 0 & 0 & 0 & 0 & 0 & 0 & 0 & 0 & 0 & 0 & 0 & 0 \\ 0 & 0 & 0 & 0 & 0 & 0 & 0 & 0 & 0 & 0 & 0 & 0 \\ 0 & 0 & 0 & 0 & 0 & 0 & 0 & 0 & 0 & 0 & 0 & 0 \end{bmatrix} \tag{C.2}$$

where ρ_m, A and L are the mass density of material, the cross-sectional area and the length of the frame element respectively.

C.3 Transformation of Coordinates

The stiffness and mass matrices given by Eqs. (C.1) and (C.2) respectively are referred to local coordinates axes of the frame element. To obtain the stiffness and mass matrices of the structure, it is necessary first to transform these matrices to the same reference systems, the global system of coordinates. If v_1, v_2 and v_3 are the unit vectors along the local coordinates 1, 2 and 3 respectively and (l_1, m_1, n_1), (l_2, m_2, n_2) and (l_3, m_3, n_3) represents their direction cosines with the global coordinates respectively, then the transformer matrix, $\boldsymbol{T}$ to compute the global stiffness and mass matrices is given by

$$\boldsymbol{T} = \begin{bmatrix} R & 0 & 0 & 0 \\ 0 & R & 0 & 0 \\ 0 & 0 & R & 0 \\ 0 & 0 & 0 & R \end{bmatrix} \tag{C.3}$$

where $\boldsymbol{R}$ is the block matrix which is given by

$$\boldsymbol{R} = \begin{bmatrix} l_1 & m_1 & n_1 \\ l_2 & m_2 & n_2 \\ l_3 & m_3 & n_3 \end{bmatrix} \tag{C.4}$$

The global stiffness and mass matrices of each frame element then can be computed as

$$\boldsymbol{K_{ge}} = \boldsymbol{T}^T \boldsymbol{K}_e \boldsymbol{T} \qquad \text{and} \qquad \boldsymbol{M_{ge}} = \boldsymbol{T}^T \boldsymbol{M_e} \boldsymbol{T} \tag{C.5}$$

C.4 Parameterization of Stiffness and Mass Matrices

As mentioned earlier in Chapter 3, four stiffness parameters were considered for the parameterization of stiffness matrix for each element considering both sectional and material properties. The subsystem stiffness matrices at local coordinates corresponding to four stiffness parameters are given by

$$\boldsymbol{K_{l,1}} = \begin{bmatrix} 1/L & 0 & 0 & 0 & 0 & 0 & -1/L & 0 & 0 & 0 & 0 & 0 \\ 0 & 0 & 0 & 0 & 0 & 0 & 0 & 0 & 0 & 0 & 0 & 0 \\ 0 & 0 & 0 & 0 & 0 & 0 & 0 & 0 & 0 & 0 & 0 & 0 \\ 0 & 0 & 0 & 0 & 0 & 0 & 0 & 0 & 0 & 0 & 0 & 0 \\ 0 & 0 & 0 & 0 & 0 & 0 & 0 & 0 & 0 & 0 & 0 & 0 \\ 0 & 0 & 0 & 0 & 0 & 0 & 0 & 0 & 0 & 0 & 0 & 0 \\ -1/L & 0 & 0 & 0 & 0 & 0 & 1/L & 0 & 0 & 0 & 0 & 0 \\ 0 & 0 & 0 & 0 & 0 & 0 & 0 & 0 & 0 & 0 & 0 & 0 \\ 0 & 0 & 0 & 0 & 0 & 0 & 0 & 0 & 0 & 0 & 0 & 0 \\ 0 & 0 & 0 & 0 & 0 & 0 & 0 & 0 & 0 & 0 & 0 & 0 \\ 0 & 0 & 0 & 0 & 0 & 0 & 0 & 0 & 0 & 0 & 0 & 0 \\ 0 & 0 & 0 & 0 & 0 & 0 & 0 & 0 & 0 & 0 & 0 & 0 \end{bmatrix} \tag{C.6}$$

$$\boldsymbol{K_{l,2}} = \begin{bmatrix} 0 & 0 & 0 & 0 & 0 & 0 & 0 & 0 & 0 & 0 & 0 & 0 \\ 0 & 12/L^3 & 0 & 0 & 0 & 6/L^2 & 0 & -12/L^3 & 0 & 0 & 0 & 6/L^2 \\ 0 & 0 & 0 & 0 & 0 & 0 & 0 & 0 & 0 & 0 & 0 & 0 \\ 0 & 0 & 0 & 0 & 0 & 0 & 0 & 0 & 0 & 0 & 0 & 0 \\ 0 & 0 & 0 & 0 & 0 & 0 & 0 & 0 & 0 & 0 & 0 & 0 \\ 0 & 6/L^2 & 0 & 0 & 0 & 4/L & 0 & -6/L^2 & 0 & 0 & 0 & 2/L \\ 0 & 0 & 0 & 0 & 0 & 0 & 0 & 0 & 0 & 0 & 0 & 0 \\ 0 & -12/L^3 & 0 & 0 & 0 & -6/L^2 & 0 & 12/L^3 & 0 & 0 & 0 & -6/L^2 \\ 0 & 0 & 0 & 0 & 0 & 0 & 0 & 0 & 0 & 0 & 0 & 0 \\ 0 & 0 & 0 & 0 & 0 & 0 & 0 & 0 & 0 & 0 & 0 & 0 \\ 0 & 0 & 0 & 0 & 0 & 0 & 0 & 0 & 0 & 0 & 0 & 0 \\ 0 & 6/L^2 & 0 & 0 & 0 & 2/L & 0 & -6/L^2 & 0 & 0 & 0 & 4/L \end{bmatrix} \tag{C.7}$$

$$\boldsymbol{K_{l,3}} = \begin{bmatrix} 0 & 0 & 0 & 0 & 0 & 0 & 0 & 0 & 0 & 0 & 0 & 0 \\ 0 & 0 & 0 & 0 & 0 & 0 & 0 & 0 & 0 & 0 & 0 & 0 \\ 0 & 0 & 12/L^3 & 0 & -6/L^2 & 0 & 0 & 0 & -12/L^3 & 0 & -6/L^2 & 0 \\ 0 & 0 & 0 & 0 & 0 & 0 & 0 & 0 & 0 & 0 & 0 & 0 \\ 0 & 0 & -6/L^2 & 0 & 4/L & 0 & 0 & 0 & 6/L^2 & 0 & 2/L & 0 \\ 0 & 0 & 0 & 0 & 0 & 0 & 0 & 0 & 0 & 0 & 0 & 0 \\ 0 & 0 & 0 & 0 & 0 & 0 & 0 & 0 & 0 & 0 & 0 & 0 \\ 0 & 0 & 0 & 0 & 0 & 0 & 0 & 0 & 0 & 0 & 0 & 0 \\ 0 & 0 & -12/L^3 & 0 & 6/L^2 & 0 & 0 & 0 & 12/L^3 & 0 & 6/L^2 & 0 \\ 0 & 0 & 0 & 0 & 0 & 0 & 0 & 0 & 0 & 0 & 0 & 0 \\ 0 & 0 & -6/L^2 & 0 & 0 & 0 & 0 & 0 & 0 & 0 & 0 & 0 \\ 0 & 0 & 0 & 0 & 0 & 0 & 0 & 0 & 0 & 0 & 0 & 0 \end{bmatrix} \tag{C.8}$$

$$\boldsymbol{K_{l,4}} = \begin{bmatrix} 0 & 0 & 0 & 0 & 0 & 0 & 0 & 0 & 0 & 0 & 0 & 0 \\ 0 & 0 & 0 & 0 & 0 & 0 & 0 & 0 & 0 & 0 & 0 & 0 \\ 0 & 0 & 0 & 0 & 0 & 0 & 0 & 0 & 0 & 0 & 0 & 0 \\ 0 & 0 & 0 & 1/L & 0 & 0 & 0 & 0 & 0 & -1/L & 0 & 0 \\ 0 & 0 & 0 & 0 & 0 & 0 & 0 & 0 & 0 & 0 & 0 & 0 \\ 0 & 0 & 0 & 0 & 0 & 0 & 0 & 0 & 0 & 0 & 0 & 0 \\ 0 & 0 & 0 & 0 & 0 & 0 & 0 & 0 & 0 & 0 & 0 & 0 \\ 0 & 0 & 0 & 0 & 0 & 0 & 0 & 0 & 0 & 0 & 0 & 0 \\ 0 & 0 & 0 & 0 & 0 & 0 & 0 & 0 & 0 & 0 & 0 & 0 \\ 0 & 0 & 0 & -1/L & 0 & 0 & 0 & 0 & 0 & 1/L & 0 & 0 \\ 0 & 0 & 0 & 0 & 0 & 0 & 0 & 0 & 0 & 0 & 0 & 0 \\ 0 & 0 & 0 & 0 & 0 & 0 & 0 & 0 & 0 & 0 & 0 & 0 \end{bmatrix} \quad \text{(C.9)}$$

Using the transformation matrix $\boldsymbol{T}$, the above subsystem stiffness matrices can be transformed in to the global coordinate system as

$$\boldsymbol{K_{gl,1}} = \boldsymbol{T}^T\boldsymbol{K}_{l,1}\boldsymbol{T},\ \boldsymbol{K_{gl,2}} = \boldsymbol{T}^T\boldsymbol{K}_{l,2}\boldsymbol{T},\ \boldsymbol{K_{gl,3}} = \boldsymbol{T}^T\boldsymbol{K}_{l,3}\boldsymbol{T},\ \text{and}\ \boldsymbol{K_{gl,4}} = \boldsymbol{T}^T\boldsymbol{K}_{l,4}\boldsymbol{T} \quad \text{(C.10)}$$

where $\boldsymbol{K_{gl,1}}$, $\boldsymbol{K_{gl,2}}$, $\boldsymbol{K_{gl,3}}$, and $\boldsymbol{K_{gl,4}}$ are the global subsystem stiffness matrices for the lth element.

For the parameterization of mass matrix mass density per unit length of each section was considered as an uncertain parameter. Hence, the subsystem mass matrix at local coordinate for the lth element having sectional properties of the rth section is given by

$$\boldsymbol{M_{r,l}} = \frac{L}{2}\begin{bmatrix} 1 & 0 & 0 & 0 & 0 & 0 & 0 & 0 & 0 & 0 & 0 & 0 \\ 0 & 1 & 0 & 0 & 0 & 0 & 0 & 0 & 0 & 0 & 0 & 0 \\ 0 & 0 & 1 & 0 & 0 & 0 & 0 & 0 & 0 & 0 & 0 & 0 \\ 0 & 0 & 0 & 0 & 0 & 0 & 0 & 0 & 0 & 0 & 0 & 0 \\ 0 & 0 & 0 & 0 & 0 & 0 & 0 & 0 & 0 & 0 & 0 & 0 \\ 0 & 0 & 0 & 0 & 0 & 0 & 0 & 0 & 0 & 0 & 0 & 0 \\ 0 & 0 & 0 & 0 & 0 & 0 & 1 & 0 & 0 & 0 & 0 & 0 \\ 0 & 0 & 0 & 0 & 0 & 0 & 0 & 1 & 0 & 0 & 0 & 0 \\ 0 & 0 & 0 & 0 & 0 & 0 & 0 & 0 & 1 & 0 & 0 & 0 \\ 0 & 0 & 0 & 0 & 0 & 0 & 0 & 0 & 0 & 0 & 0 & 0 \\ 0 & 0 & 0 & 0 & 0 & 0 & 0 & 0 & 0 & 0 & 0 & 0 \\ 0 & 0 & 0 & 0 & 0 & 0 & 0 & 0 & 0 & 0 & 0 & 0 \end{bmatrix} \quad \text{(C.11)}$$

Similarly, the global subsystem mass matrix can be obtained as

$$\boldsymbol{M_{g,l}} = \boldsymbol{T}^T\boldsymbol{M}_{r,l}\boldsymbol{T} \quad \text{(C.12)}$$